

Aus der ABTEILUNG GENVEKTOREN
des HELMHOLTZ ZENTRUM MÜNCHEN
Direktor: Prof. Dr. med. vet. Wolfgang Hammerschmidt

Quantitation of SARS-CoV-2 Neutralizing Antibodies Using Virus-Like Particles



DISSERTATION

zum Erwerb des Doktorgrades der Naturwissenschaften
an der MEDIZINISCHEN FAKULTÄT der
LUDWIG-MAXIMILIANS-UNIVERSITÄT MÜNCHEN

vorgelegt von
Johannes Rößler
aus
München

Jahr
2022

Mit Genehmigung der Medizinischen Fakultät der
Ludwig-Maximilians-Universität München

Betreuer: Prof. Dr. rer. nat. Reinhard Zeidler

Zweitgutachter: Prof. Dr. rer. nat. Karl-Klaus Conzelmann

Dekan: Prof. Dr. med. Thomas Gudermann

Tag der mündlichen Prüfung: 13. März 2023

Für meine Eltern

'... I am still confused - but on a higher level.'

ENRICO FERMI

Table of Contents

Abstract	iii
Zusammenfassung	v
List of Publications	vii
List of Abbreviations	viii
1 Introduction	1
1.1 SARS-CoV-2	1
1.2 Virus Neutralization Tests	7
1.3 Objectives and Outlook	8
2 Results	9
2.1 Monoclonal Spike Antibodies	9
2.1.1 Immunization and Antibody Generation	10
2.1.2 Antibody Characterization	12
2.1.3 Spike Detection in Biological Samples	15
2.2 Pseudotyped Virus Neutralization Test	18
2.3 Virus-Like Particles	20
2.3.1 Manufacturing of VLPs	20
2.3.2 Electron Microscopy of VLPs	21
2.3.3 Molecular Characterization of VLPs	22
2.3.4 Particle Analysis of VLPs	24
2.4 Virus-free Fusion Assay	27
2.4.1 Spike EVs with β -Lactamase Readout	27
2.4.2 VLPs with Nanoluciferase Readout	31
2.5 VLP Neutralization Test	36
2.5.1 Serum Analysis	36
2.5.2 Correlation of VLPNT and cVNT	37
2.5.3 Test Adaptation to Variants of Concern	40
2.5.4 Neutralizing Monoclonal Antibodies	40
2.6 Cell-free Fusion Assay	42
2.7 Cell-free VLP Neutralization Test	49
2.7.1 Neutralizing Monoclonal Antibodies	49
2.7.2 Serum Analysis	49
2.7.3 Correlation of cfVLPNT to cVNT and VLPNT	52
3 Discussion	55
3.1 Monoclonal Spike Antibodies	55
3.2 VLP Neutralization Test	59
3.3 Cell-free VLP Neutralization Test	63
4 Conclusion	67

5	Experimental Procedures	69
5.1	Materials	69
5.2	Methods	74
5.2.1	Plasmid Production in Prokaryots	74
5.2.2	Eukaryotic Cell Lines and Cell Culture	74
5.2.3	Flow Cytometry	75
5.2.4	Anti-Spike Antibody Generation	75
5.2.5	Antibody Production	76
5.2.6	Antibody Sequencing	76
5.2.7	Transient Transfection	77
5.2.8	Retroviral Transduction	77
5.2.9	Pseudotyped Virus Neutralization Test	78
5.2.10	Generation of VLPs and Engineered EVs	78
5.2.11	Purification of VLPs and Engineered EVs	79
5.2.12	Western Blot	79
5.2.13	ELISA	80
5.2.14	NTA	81
5.2.15	Nano Flow Technology	81
5.2.16	Negative Stain Electron Microscopy	81
5.2.17	Cryo-Electron Microscopy	81
5.2.18	EV Fusion Assay with BlaM Readout	82
5.2.19	Confocal Fluorescence Microscopy	82
5.2.20	VLPNT with Nanouciferase Readout	83
5.2.21	Cell-free VLPNT	84
5.2.22	Virus Stock Preparation	84
5.2.23	SARS-CoV-2 Virus Neutralization	84
5.2.24	Statistical Analysis	85
5.3	Patients and Specimens	85
5.4	Contributions	87
	Bibliography	88
	Appendix	99
	List of Figures	107
	List of Tables	108
	Danksagung	109
	Eidesstattliche Versicherung	111
	Lebenslauf	113

Abstract

Neutralizing antibodies specifically block the infection of cells by viruses, such as the severe acute respiratory syndrome coronavirus 2 (SARS-CoV-2). Their concentration in the sera of convalescents and vaccinees is therefore a good correlate of protection from COVID-19, the disease caused by this virus. Yet, titers in clinical samples are difficult to assess with conventional virus neutralization tests (cVNTs), as they are often cumbersome and work with the pathogen requires precautions of biological safety level 3. Alternative tests mostly rely on viral vectors with the spike protein (S) as the only structural component of the original virus and are therefore biologically distant.

To overcome these issues, this work describes the development of a safe, virus-free, and rapid *in vitro* diagnostic test, that is based on engineered but authentic virus-like particles (VLPs). The VLPs share all structural features of SARS-CoV-2 except for the viral RNA genome and are thus incapable of replication or reprogramming cells. As they enter susceptible cells via the viral fusion protein S and the respective host cell receptor ACE2, as well as a genuine processing by the protease TMPRSS2, they are nearly ideal functional mimics of the virus and a good model to study viral entry. The VLPs can be traced upon uptake, as they are equipped with an activator peptide that enables immediate enzymatic readout. Neutralizing antibodies induced by infection or vaccination, but also from recombinant sources, interfere with this process and can be reliably quantified within few hours. When tested with a set of COVID-19 patient serum samples, results from this VLP neutralization test (VLPNT) showed excellent sensitivity and specificity and correlated very well with a cVNT using fully infectious SARS-CoV-2. The test was also adapted to variants of concern and demonstrated a reduced neutralizing capacity of sera from vaccinees against B.1.617.2 Delta and B.1.1.529 BA.1 Omicron, as expected.

Despite its many advantages, this serologic test requires living cells as VLP recipients. However, it was identified for the first time that VLPs also efficiently fuse with ACE2 bearing extracellular vesicles, following the same tropism. This process was characterized, and the finding utilized to demonstrate the proof-of-concept for a second, novel, virus neutralization tests that does not depend on living cells. Similarly, this assay quantitated neutralizing antibodies and correlated with the cVNT but requires further optimization. Additionally, several S specific neutralizing monoclonal antibodies were generated from immunizations, characterized, and used as reference and molecular tools for this work.

Zusammenfassung

Neutralisierende Antikörper sind Proteine des adaptiven Immunsystems, die spezifisch die Infektion von Zellen mit Viren wie SARS-CoV-2 (severe acute respiratory syndrome coronavirus 2) verhindern können. Ihre Serumkonzentration im Blut von genesenen und geimpften ist deshalb ein geeignetes Maß für den Schutz vor COVID-19, der durch das Virus verursachten Krankheit. Titer in klinischen Proben sind mit konventionellen Virusneutralisationstests (cVNTs) jedoch schwierig zu bestimmen, da diese oft aufwändig sind und der Umgang mit dem Erreger Sicherheitsvorkehrungen der biologischen Schutzstufe 3 erfordert. Alternativen bedienen sich meist viraler Vektoren, die lediglich das Spike Protein (S) als einzige Komponente des eigentlichen Virus tragen und daher biologisch nur bedingt ähnlich sind.

Die vorliegende Dissertation beschreibt die Entwicklung eines sicheren, virusfreien und schnellen *in vitro* diagnostischen Tests, der auf modifizierten, aber authentischen virusähnlichen Partikeln (VLPs) basiert. Die VLPs enthalten alle strukturellen Merkmale von SARS-CoV-2, mit Ausnahme des viralen RNA-Genoms, weswegen sie nicht in der Lage sind sich zu replizieren oder Zellen umzuprogrammieren. Da sie über das virale Fusionsprotein S und den Rezeptor der Wirtszelle ACE2 in suszeptible Zellen eindringen, nachdem sie von der Protease TMPRSS2 prozessiert wurden, sind sie annähernd ideale funktionelle Abbilder des Virus und ein geeignetes Modell, um dessen Eintritt zu erforschen. Bei ihrer Aufnahme können die VLPs nachverfolgt werden, da sie mit einem Peptid und Aktivator ausgestattet sind, das ein sofortiges enzymatisches Auslesen ermöglicht. Neutralisierende Antikörper, induziert durch Infektion oder Impfung, aber auch aus rekombinanten Quellen, verhindern diesen Prozess und lassen sich daher innerhalb weniger Stunden verlässlich quantifizieren. Ergebnisse mit Serumproben von COVID-19 Patienten belegten die hervorragende Sensitivität und Spezifität des VLP Neutralisationstest (VLPNT) und zeigten eine sehr gute Korrelation mit einem cVNT mit infektiösem Virus. Der Test wurde auch an Virusvarianten angepasst und wies, wie erwartet, eine verringerte Neutralisationskapazität von Seren geimpfter gegenüber B.1.617.2 Delta und B.1.1.529 BA.1 Omikron nach.

Trotz seiner vielen Vorteile, benötigt dieser serologische Test lebende Zellen als Akzeptoren für die VLPs. Es konnte jedoch erstmals festgestellt werden, dass VLPs auch effizient mit ACE2 tragenden extrazellulären Vesikeln fusionieren, wobei sie dem gleichen Tropismus folgen. Dieser Prozess wurde charakterisiert und genutzt, um die Machbarkeit eines zweiten neuen Neutralisationstest zu demonstrieren, der ohne lebende Zellen auskommt. Dieser Test korrelierte ebenfalls mit dem cVNT, bedarf jedoch weiterer Optimierung. Im Rahmen dieser Arbeit wurden außerdem mehrere S-spezifische neutralisierende monoklonale Antikörper durch Immunisierungen generiert, charakterisiert und als molekulare Hilfsmittel eingesetzt.

List of Publications

Parts of this dissertation have been presented or published as follows:

18-21 July 2021

Conference

International Graduate School for Infection Research of the German Center for Infection Research, DZIF and the Helmholtz Center for Infection Research, HZI; **SARS-CoV-2 neutralizing monoclonal anti-Spike antibodies** (Poster)

1 October 2021

Conference

Symposium of the Department of Otorhinolaryngology, LMU University Hospital; **A novel assay for the quantification of SARS-CoV-2 neutralizing antibodies** (Talk)

31 December 2021

Preprint

J. Roessler, D. Pich, M. Albanese, P. R. Wratil, V. Krähling, J. C. Hellmuth, C. Scherer, M. von Bergwelt-Baildon, S. Becker, O. T. Keppler, A. Brisson, R. Zeidler, W. Hammerschmidt, **Quantitation of SARS-CoV-2 neutralizing antibodies with a virus-free, authentic test.** *medRxiv*, 2021.12.29.21268487 (2021).

14 April 2022

Journal article

J. Roessler, D. Pich, M. Albanese, P. R. Wratil, V. Krähling, J. C. Hellmuth, C. Scherer, M. von Bergwelt-Baildon, S. Becker, O. T. Keppler, A. Brisson, R. Zeidler, W. Hammerschmidt, **Quantitation of SARS-CoV-2 neutralizing antibodies with a virus-free, authentic test.** *PNAS Nexus*, 1, pgac045 (2022).

In part, data, results and figures are shared between this dissertation and the publications listed above. The open access articles are distributed under the terms of the Creative Commons Attribution license, CC BY, which permits unrestricted reuse, distribution, and reproduction in any medium, provided the original work is properly cited.

All experiments shown in this dissertation were personally designed, executed, and analyzed, unless stated otherwise.

List of Abbreviations

(+)ssRNA	Positive sense, single-stranded RNA
%	Percent
°C	Degree Celsius
ΔvFP	Without viral fusion protein
× g	Gravitational force equivalent
Ab	Antibody
ACE2	Angiotensin-converting enzyme 2
ADAM17	A disintegrin and metalloprotease 17
ADCC	Antibody dependent cellular cytotoxicity
ADCP	Antibody dependent cellular phagocytosis
ADE	Antibody dependent enhancement
ANOVA	Analysis of variance
APC	Antigen presenting cell
aq.	Aqueous solution
ARDS	Acute respiratory distress syndrome
BCA	Bicinchoninic acid assay
BlaM	β -lactamase
BSA	Bovine serum albumin
BSL	Biosafety level
BTI	Breakthrough infection
c	Concentration
C1q	Complement component 1q
C _H	Heavy-chain constant region
C _L	Light-chain constant region
CAS RN	Chemical abstracts service registry number
CDC	Complement-dependent cytotoxicity
cDNA	Complementary DNA
CDR	Complementarity-determining region
cfVLPNT	Cell-free VLP neutralization test
CI	Confidence interval
CID	Cell line identifier
CLSI	Clinical Laboratory Standards Institute
CMV	Cytomegalovirus
CN	Concordant negative
conc.	Concentrated
COVID-19	Coronavirus disease 2019
CP	Concordant positive
CPE	Cytopathic effect
cryo-EM	Cryo-electron microscopy
ct	Threshold cycle
CTSL	Cathepsin L
CTV	CellTrace Violet
CV	Coefficient of variation
cVNT	Conventional virus neutralization test

D	Aspartic acid
D	Discrepant
Da	Dalton
DAPI	4',6-diamidino-2-phenylindole
DC	Dendritic cell
dd	Double distilled
DEPC	Diethyl pyrocarbonate
DMEM	Dulbecco's modified Eagle's medium
DMSO	Dimethyl sulfoxide
DNA	Deoxyribonucleic acid
dNTP	Deoxynucleoside triphosphate
dsRNA	Double-stranded RNA
DTT	Dithiothreitol
E	Envelope protein
<i>E. coli</i>	<i>Escherichia coli</i>
e.g.	<i>exempli gratia</i>
EBV	Epstein-Barr virus
ECD	Extracellular domain
ELISA	Enzyme-linked immunosorbent assay
EM	Electron microscopy
EMA	European Medicines Agency
env	Envelope and fusion protein
ER	Endoplasmic reticulum
ERGIC	ER - Golgi intermediate compartment
EV	Extracellular vesicle
FBS	Fetal bovine serum
FC	Flow cytometry
Fc	Fragment crystallizable region
FDA	U.S. Food and Drug Administration
FL	Full-length
FN	False negative
FP	False positive
Fp	Fusion peptide
FRET	Fluorescence resonance energy transfer
FRNT	Focus reduction neutralization test
FSC	Forward scatter
G	Glycine
g	Gram
gag	Group-specific antigen
GFP	Green fluorescent protein
GMO	Genetically modified organism
GMT	Geometric mean titer
h	Human
HEK293	Human embryonic kidney 293 cells
HEK293T	HEK293 cells expressing SV40 large T antigen
HIV	Human immunodeficiency virus
HR	Heptad repeat
HRP	Horseradish peroxidase
IC ₅₀	Half maximal inhibitory concentration
ID	Identifier
IgG	Immunoglobulin G

IU	International units
IVD	<i>In vitro</i> diagnostic product
k	Kilo
K _D	Dissociation constant
kb	Kilo base pair
L	Liter
LOD	Limit of detection
log ₁₀	Decadic logarithm
LSCM	Laser scanning confocal microscopy
LTR	Long terminal repeat
Luc	Luciferase
M	Membrane protein
M	mol L ⁻¹
m	Meter
m	Milli
mAb	Monoclonal antibody
MERS-CoV	Middle East respiratory syndrome coronavirus
MFI	Mean fluorescence intensity
min	Minute
MLV	Murine leukemia virus
MMP	Matrix metalloprotease
MNA	Microneutralization assay
mol	Mole
MPSV	Myeloproliferative sarcoma virus
mRNA	Messenger RNA
N	Nucleoprotein
n	Nano
n	Sample size
n.a.	Not available
na	Not available
NAb	Neutralizing antibody
NIBSC	UK National Institute for Biological Standards and Control
NK	Natural killer cell
nLuc	Nanoluciferase
NM	<i>N</i> -myristoly
NmAb	Neutralizing monoclonal antibody
non-red.	Non-reducing
NPV	Negative predictive value
ns	Not significant
nsEM	Negative stain electron microscopy
nsp	Non-structural protein
NTA	Nanoparticle tracking analysis
NTD	N-terminal domain
o/n	Over night
OAT	Organic anion transporter
OD	Optical density
ORF	Open reading frame
p	P-value
PAGE	Polyacrylamide gel electrophoresis
PBS	Phosphate buffered saline
PBST	PBS, 0.05% Tween-20

pcAb	Polyclonal antibody
PCR	Polymerase chain reaction
Pen	Penicillin
PFA	Paraformaldehyde
PFU	Plaque-forming units
pol	Polymerase
PPV	Positive predictive value
PRNT	Plaque reduction neutralization test
PRNT ₅₀	50% plaque reduction neutralization titer
pVNT	Pseudotyped virus neutralization test
r	Pearson correlation coefficient
RACE	Rapid amplification of cDNA ends
RBD	Receptor binding domain
RBM	Receptor binding motif
rec.	Recombinant
red.	Reducing
REGN	Regeneron
RLU	Relative light units
RM	Repeated measures
RNA	Ribonucleic acid
rpm	Revolutions per minute
RSV	Respiratory syncytial virus
RT	Room temperature
RT-PCR	Reverse transcription polymerase chain reaction
RT-qPCR	Reverse transcription quantitative real-time PCR
S	Spike protein
S _p O ₂	Peripheral oxygen saturation
SARS-CoV	Severe acute respiratory syndrome coronavirus
SARS-CoV-2	Severe acute respiratory syndrome coronavirus 2
SD	Standard deviation
SDS	Sodium dodecyl sulfate
SP	Signal peptide
SSC	Side scatter
Strep	Streptomycin
SV40	Simian vacuolating virus 40
sVNT	Surrogate virus neutralization test
TAg	Large T antigen
TBS	Tris-buffered saline
TBST	Tris-buffered saline, 0.1% Tween-20
TdT	Terminal deoxynucleotidyl transferase
TEM	Transmission electron microscopy
TM	Transmembrane domain
TMPRSS2	Transmembrane protease serine 2
TN	True negative
TP	True positive
Tris	Tris(hydroxymethyl)aminomethane
V	Volt
V _H	Heavy-chain variable region
V _L	Light-chain variable region
vFP	Viral fusion protein
VLP	Virus-like particle

VLPN ₅₀	50% VLP neutralization titer
VLPNT	VLP neutralization test
VNT	Virus neutralization test
VNT ₁₀₀	100% virus neutralization titer
VOC	Variant of concern
vRNA	Viral RNA
VSV	Vesicular stomatitis virus
VSV-G	VSV glycoprotein G
w/o	Without
w/v	Weight per volume
WB	Western blot
WHO	World Health Organization

1 Introduction

1.1 SARS-CoV-2

Until a few years ago, coronaviruses were mostly associated with mild diseases in humans, causing common cold symptoms, only. However, this changed with the emergence of the severe acute respiratory syndrome coronavirus (SARS-CoV) in 2002 and the Middle East respiratory syndrome coronavirus (MERS-CoV) in 2012, which cause fatal illness and led to outbreaks mostly in China and the Arabian Peninsula, respectively.^[1,2] Then, in December 2019 a novel respiratory infectious disease led to an outbreak of severe cases of pneumonia in the city of Wuhan in China,^[3] which marked the beginning of the ongoing pandemic, caused by the severe acute respiratory syndrome coronavirus 2 (SARS-CoV-2). This pathogen is a virulent member of the *Coronaviridae* family, shares 79% genome sequence identity with SARS-CoV and 50% with MERS-CoV, and likely originated from a wildlife reservoir in bats, but spreads easily among humans via droplets and aerosols. The direct detection of the pathogen is classically performed via nucleic acid- or protein antigen testing from nasopharyngeal and oropharyngeal swabs.^[1,4] As of September 2022, the associated coronavirus disease 2019 (COVID-19) was confirmed in more than 600 million cases worldwide and accounts for almost 6.5 million deaths.*

Structure

SARS-CoV-2 is an enveloped ribonucleic acid (RNA) virus from the *Betacoronavirus* genera. Its genome of positive sense, single-stranded RNA ((+)ssRNA) comprises almost 30 kb and is therefore among the largest of RNA viruses. It encodes several open reading frames (ORFs) that translate into multiple proteins, including a large replicase polyprotein (ORF1a/ORF1b), four structural proteins, spike (S), envelope (E), membrane (M) and nucleoprotein (N, also known as nucleocapsid), and several accessory non-structural proteins (nsps).^[1,4] SARS-CoV-2 forms virions of spherical shape and approximately ~100 nm diameter, which consist of viral RNA (vRNA), S, M, N and E (Figure 1A). The N protein mediates the packaging of the genome into the lumen of virions by binding to the vRNA and the formation of a ribonucleoprotein complex. It is the most abundant structural protein in infected cells and therefore an important target for diagnostics by antigen detection. The M protein is a transmembrane protein in the envelope of a virion, which plays a major role during assembly and maintains the virion's size and shape. It is the most abundant structural protein in a virion. The E protein is the smallest of all structural proteins and apart from

*WHO dashboard, <https://covid19.who.int>

its localization in the envelope of a virion, it is found in the endoplasmic reticulum (ER) and the Golgi complex of infected host cells, where it facilitates formation of virus particles.^[1,5]

Spike, the viral fusion protein (vFP) of SARS-CoV-2 is a highly glycosylated type I transmembrane protein and with 1273 amino acids the largest of the structural proteins. It encompasses the two domains S1 and S2, which are separated by an arginine rich, multibasic, S1/S2 site, a cleavage motif for furin and furin-like proteases (Figure 1B and Figure 2A). While S1 contains the N-terminal domain (NTD) and the receptor binding domain (RBD), S2 bears the fusion peptide (Fp), two heptad repeats (HRs), mediating membrane proximity and fusion, and the transmembrane domain (TM).^[6] After proteolytic processing at the S1/S2 site, which commonly occurs during egress from a virus producing cell, S1 and S2 remain non-covalently associated.^[7] Yet, this primes S for an additional second cleavage at the S2' site within the S2 domain, which facilitates presentation of the Fp and promotes membrane insertion.^[8,9] While furin cleavage at S1/S2 seems to be dispensable for infection,^[10] it decisively enhances the accessibility of S2' for serine proteases such as trypsin or transmembrane protease serine 2 (TMPRSS2).^[9] As S is a viral class I fusion protein, it assembles in homotrimers of three protomers, which each consist of a S1 domain on top of a S2 unit (Figure 2B). Each of these complexes then forms one of the characteristic spikes, protruding from the viral envelope. To make the receptor binding motif (RBM) within the RBD accessible for the host cell receptor, S in its pre-fusion conformation can undergo conformational changes to expose one RBD of the complex in 'up' orientation, instead of the inaccessible 'down' state.^[1,11,12]

Infection and Replication

The viral infection initially depends on the presence of a respective cellular receptor. For SARS-CoV-2, S mediates the attachment to angiotensin-converting enzyme 2 (ACE2) on the host cell. Although ACE2 is seized by SARS-CoV-2, as well as SARS-CoV, its primary physiological role is to control vasoconstriction and blood pressure. Depending on the host cell, binding of S to the receptor triggers two possible routes of uptake and processing at the S2' site (Figure 1C): Either, fusion takes place at the plasma membrane upon proteolytic cleavage by the cell surface protease TMPRSS2, or occurs after endocytosis and subsequent cleavage by endosomal cathepsin L (CTSL).^[9,13] In detail, ACE2 binding causes conformational changes in S, leading to the disengagement of the S1 unit and dissociation from the trimeric S2 stem, exposing the S2' site. There, cleavage exposes the Fp and induces further rearrangements and the formation of a stable elongated structure, which mediates insertion into the target membrane, membrane approximation and ultimately fusion.^[14] The release of the cargo into the cytoplasm then leads to further downstream steps to turn the cell into a virus factory. Uncoating of the vRNA initiates the primary translation of ORF1a and ORF1b, which are co-translationally processed to nsps that form the viral replication and transcription complex. Protected from cellular sensors of the innate immune system, the (+)ssRNA genome is replicated via double-stranded RNA (dsRNA) intermediates, within perinuclear double-membrane vesicles. Simultaneously, transcription of subgenomic messen-

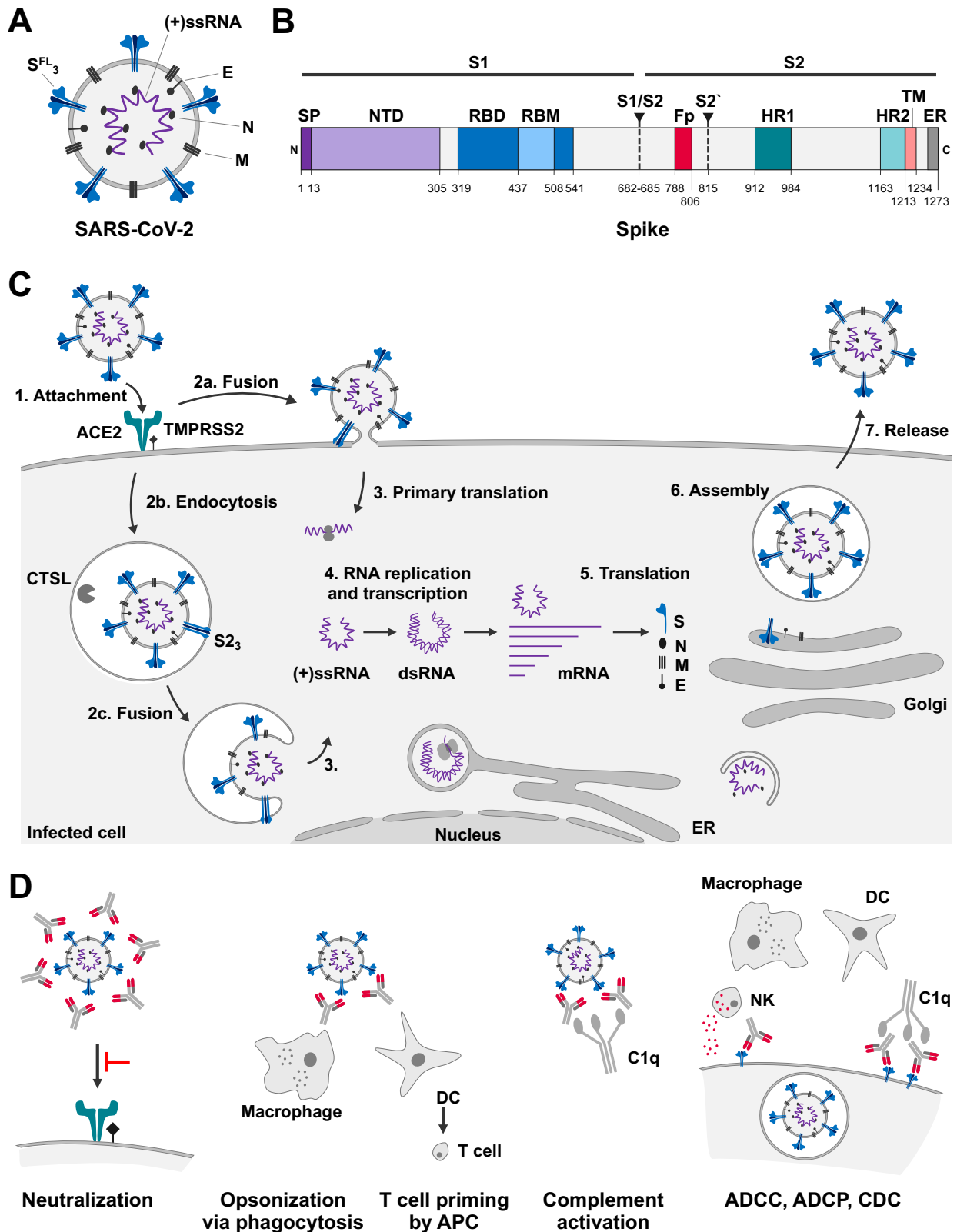


Figure 1. SARS-CoV-2, structure, replication cycle and immune response.

(A) Structure of a SARS-CoV-2 virion bearing the proteins S, M, N and E, as well as the (+)ssRNA genome. (B) Schematic map of the spike protein and its two subunits S1 and S2, with: signal peptide (SP), N-terminal domain (NTD), receptor binding domain (RBD), receptor binding motif (RBM), fusion peptide (Fp), heptad repeats (HR1 and 2), transmembrane domain (TM), endoplasmic reticulum (ER) retention tag and the protease cleavage sites S1/S2 and S2'.

(C) For infection of a permissive cell, S in the envelope of a virion mediates attachment (step 1) to the host cell receptor ACE2, triggering either proteolytic processing by TMPRSS2 and direct fusion at the plasma membrane (step 2a) or endocytosis (step 2b), cleavage by cathepsin L (CTSL) and subsequent fusion with the endosomal membrane (step 2c). After uncoating, primary translation from the (+)ssRNA genome (step 3) takes place and the resulting polyproteins are processed to non-structural proteins (nsps), forming ...

Figure 1. continued from previous page.

...the replicase–transcriptase complex in perinuclear double-membrane vesicles. Therein, the viral genome is replicated via double-stranded RNA (dsRNA) intermediates and mRNAs transcribed (step 4). Translated structural proteins (step 5) are then translocated through endoplasmic reticulum (ER) and Golgi and assembled with the viral RNA to new virions (step 6), to be secreted from the infected cell (step 7).

(D) Antibodies can mediate immune response in the context of viral infection, by neutralization of virion-receptor interaction, preventing initial infection or clearing virions directly via antigen presenting cells (APCs) such as macrophages and dendritic cells (DCs) or lysis via complement component 1q (C1q). Additionally, virus infected cells can be targeted via complement-dependent cytotoxicity (CDC), antibody dependent cellular phagocytosis (ADCP) or antibody dependent cellular cytotoxicity (ADCC) by natural killer cells (NKs).

ger RNAs (mRNAs) enables translation of accessory proteins that alter interaction with the host cell, but also the production of structural proteins, which are translocated into the ER membranes and further processed within the Golgi. Next, virus particles are assembled from newly synthesized and N protein coated RNA genome, encapsulated by a lipid bilayer with S, M and E proteins. Eventually, the novel viral particles are released by exocytosis, completing the replication cycle of SARS-CoV-2.^[15]

Variants of Concern

Throughout the course of the pandemic, the SARS-CoV-2 genome is constantly subject to change, with several mutations especially in the S gene that led to enhanced viral infectivity and spread. The first major mutation that spread all around the world in spring 2020, was the single amino acid mutation D614G. It caused higher viral loads and a global spread of the B.1 lineage (S:D614G), displacing the original Wuhan-2019 strain within few weeks.^[17] Meanwhile, other strains such as B.1.1.7, the Alpha variant of concern (VOC) also led to enhanced transmissibility,^[18] which is probably due to the N501Y mutation in S that enhances affinity to ACE2.^[19] Subsequently, the Delta-VOC B.1.617.2 evolved, which was more transmissible and posed a twofold higher risk to become hospitalized.^[20–22] In November 2021, the Omicron-VOC, B.1.1.529 BA.1, emerged with more than 30 substitutions, 6 deletions and 3 insertions in the S protein and rapidly became the predominant variant but caused milder clinical courses overall.^[23,24] As of September 2022, multiple sub-lineages of Omicron such as BA.2, BA.4 and BA.5 emerged and displaced each other since then, demonstrating the ongoing process of genome alterations.

COVID-19

Aside from few asymptomatic or subclinical infections, COVID-19 can vary from weak symptoms to mild or severe pneumonia with dyspnea, to critical clinical courses, which require external ventilation and intensive care. While most of the patients experience fever, fatigue, dry cough and occasionally olfactory and taste disorders, patients of older age (>60 years) and with serious pre-existing diseases have a greater risk of developing acute respiratory distress syndrome (ARDS) and fatal courses.^[4] For SARS-CoV pneumocytes and macrophages in lower lung tissues were the primary targets. In contrast, SARS-CoV-2 replicates abundantly in epithelia of the upper respiratory tract,^[15] where it causes neutrophil and

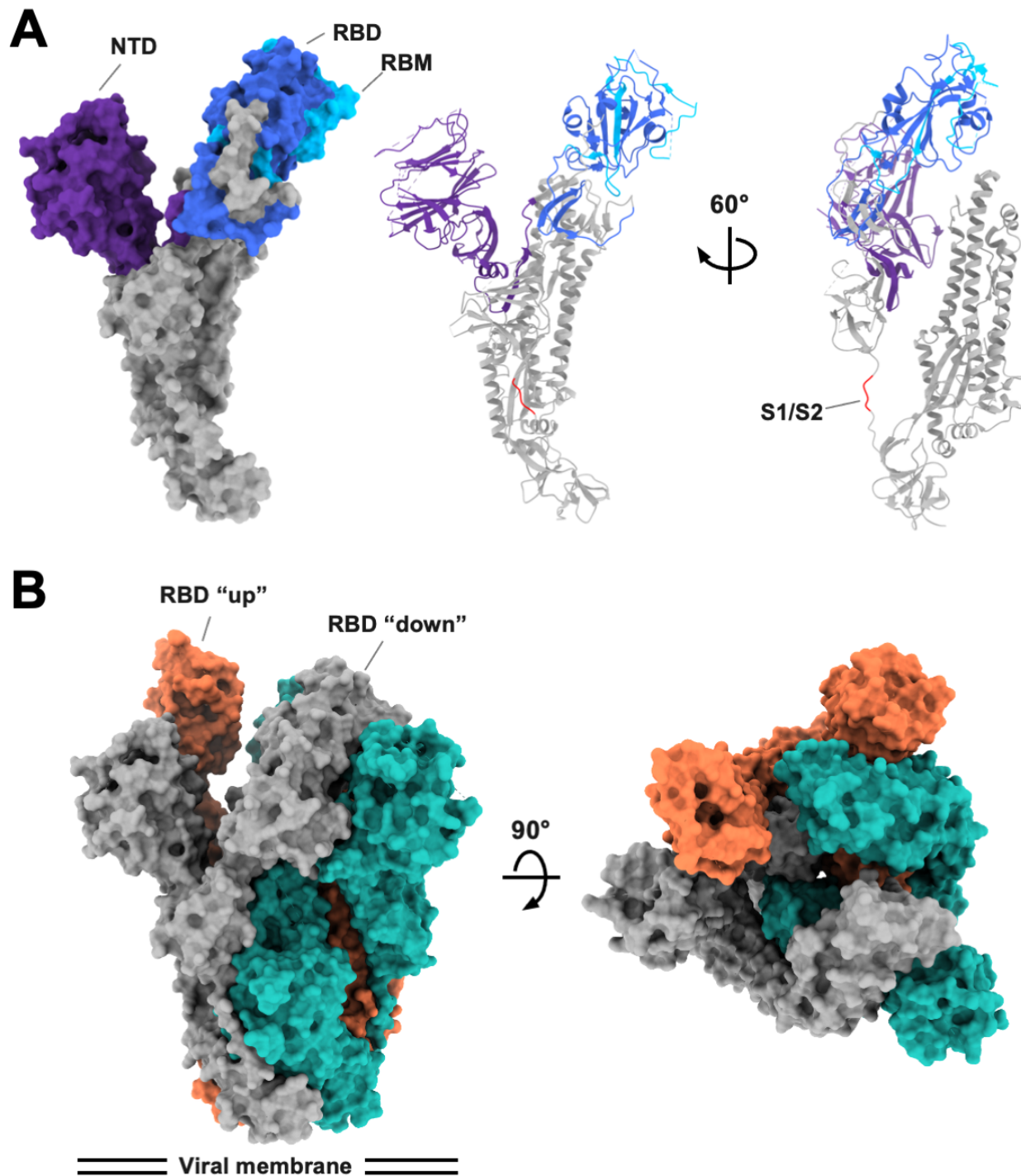


Figure 2. Molecular structure of the spike protein, based on the model PDB: 6WPT.^[16]

(A) Illustrations of a single S protomer with either molecular surface or secondary structure indicated. N-terminal domain (NTD), receptor binding domain (RBD) and receptor binding motif (RBM) of the viral glycoprotein of SARS-CoV-2 are indicated and colored individually. The S1/S2 cleavage site separates the two single subunits and is highlighted in red. The S2 subunit comprises coiled coil structures of multiple α -helices, as shown in the model on the right. All models show truncated S protein, which lack the trans-membrane domain.

(B) Three of the S protomers, here colored in grey (panel A), green and orange, assemble into homotrimers and form the characteristic spikes, protruding from the viral membrane. Each S can undergo structural changes and expose the RBD either in a receptor accessible 'up', or an inacceptable 'down' conformation. While the model on the left shows the lateral view, the one on the right shows its top view, to display the triangular symmetry.

monocyte extravasation into bronchi, cytokine storms and tissue damage from widespread inflammation.^[25] Standard therapy is thus the use of immunomodulatory corticosteroids such as dexamethasone, which act antiinflammatory and immunosuppressive.^[26,27] Despite an approval for few antiviral drugs, the use of e.g., remdesivir, a ribonucleotide analogue and inhibitor of the viral RNA polymerase, and lopinavir/ritonavir, an inhibitory therapy against viral proteases, were shown to be ineffective against COVID-19 and partially cause disproportionate adverse effects.^[28,29] Paxlovid, another inhibitor of the viral protease is a more promising candidate with potential efficacy, but has to be evaluated further.^[27]

Vaccination

As vaccines are commonly the most promising strategy for the prophylaxis of viral infectious diseases, a global research effort led among others to the development of two mRNA vaccines, BNT162b2 by BioNTech/Pfizer and mRNA-1273 by Moderna, as well as a chimpanzee adenovector ChAdOx1 vaccine (AZD1222) by AstraZeneca, which are licensed by the U.S. Food and Drug Administration (FDA) and European Medicines Agency (EMA). For infections with the Alpha- and Delta-VOCs, these vaccines significantly reduced the risk of symptomatic COVID-19, effectively attenuated disease severity and reduced the mortality rate.^[22,30,31] However, they did not confer sterile immunity as breakthrough infections (BTIs) occurred even in fully vaccinated individuals.^[32,33] A third dose or ‘booster’ of COVID-19 vaccines further reduced the risk for BTI and severe illness and was therefore introduced into the vaccination schemes.^[34] Vaccine efficacy was maintained at lower level against Omicron,^[35] yet this variant marked the emergence of an independent SARS-CoV-2 serotype, characterized by strong immune escape and reduced cross-neutralization of antibodies induced by previous variants.^[36]

Immune Response

Besides the innate immunity, the adaptive immune system can grant protection from SARS-CoV-2. Thereof, the cellular part of the response supports broad and durable immune protection by CD8⁺ T cells targeting the nucleoprotein but also with spike specific CD4⁺ T cells.^[37,38] The humoral immunity is mostly mediated by S specific antibodies, which can have several effector functions (Figure 1D): Certain antibodies can directly block the infectivity of the virus and are therefore called neutralizing antibodies (NAbs). Alternative modes of action of anti-S antibodies are the opsonization of virions by phagocytosis, which can imply the priming of T cells in the case of antigen presenting cells (APCs), the elimination of virions by complement components, as well as antibody dependent cellular cytotoxicity (ADCC), antibody dependent cellular phagocytosis (ADCP) and complement-dependent cytotoxicity (CDC).^[25]

NAbs, induced by infection or vaccination, or applied in the form of monoclonal antibodies (mAbs), have the potential to establish immunity to SARS-CoV-2 and to protect from severe COVID-19.^[39] As such, their concentration is generally accepted as a correlate of protection.

In concordance, high NAb titers were shown to be directly associated with a reduced risk of symptomatic infections and are thus predictive for the protection from COVID-19.^[40–42] Noteworthy, also anti-S immunoglobulin G (IgG) and anti-RBD IgG antibodies, which do not necessarily inhibit viral infection *in vitro*, showed acceptable correlation with protection, yet NAb titers were found to correlate best.^[41]

1.2 Virus Neutralization Tests

The quantitation of NAbS in clinical or recombinant samples is commonly performed with virus neutralization tests (VNTs). Yet, their results can be difficult to assess, as the sheer diversity of tests makes standardization and validation problematic.^[43] The undisputed ‘gold standard’ for quantitating NAbS are conventional virus neutralization tests (cVNTs), which are based on replication competent virus that as such guarantees correct virion composition and a genuine infection process. The cVNTs can be subdivided into three different types of assays:^[44]

- i. In multi-cycle assays, NAbS constantly interfere with viral infection and spread over several rounds of replication. As the amount of generated viral antigen is monitored within a defined period post infection, a reduction indicates inhibition of propagation and thus neutralization.
- ii. A cVNT based on limiting dilution uses the initial inactivation of the inoculum by NAbS and the prevention of viral cytopathic effect (CPE) to cause a binary outcome of either ‘infection’ or ‘no infection’ among the replicates. Importantly, this method is highly depended on the amount of inoculum, as almost complete initial neutralization is required to protect only half of the replicates.
- iii. Plaque reduction neutralization tests (PRNTs) are based on single infected cells, which give rise to a single ‘plaque’, a localized CPE in monolayers of immobilized gel-embedded cells. As viral spread is locally restricted to the neighboring cells, replication only causes the outcome that can be visually inspected by microscopy and trained personnel. Therefore, the neutralization of initial infections is directly quantified.

The cVNTs and in particular PRNTs depend on qualified cell lines that form unambiguous CPEs upon infection and furthermore require visual enumeration. As CPE often poses a problem, viral antigens can also be detected via immunostaining. Consequently, cVNTs are difficult to standardize between different laboratories, commonly take several days until readout and involve the handling of infectious virus, which in case of SARS-CoV-2 requires containment measures of a biosafety level (BSL)-3 facility. Thus, several alternatives to measure NAb concentration have been developed.

Surrogate virus neutralization tests (sVNTs) are based on the interaction of isolated domains of the vFP with the respective entry receptor, immobilized on an artificial surface. Therefore, they do not require living cells or infectious virus. Yet, in the case of SARS-CoV-2

they do not specifically quantitate NABs but antibodies that interfere with the RBD-ACE2 interaction, which is why they display rather weak correlation to cVNTs.^[45–47]

Given these apparent limitations, pseudotyped virus neutralization tests (pVNTs) have been developed, which often rely on replication deficient viral vectors, pseudotyped with the vFP of interest. Their readout is based e.g., on the genomic integration of a transferred gene, transcription, and *de novo* translation of a phenotypic reporter protein. Consequently, pVNTs require two to three days and a BSL-2 laboratory. These tests often use retro-, lenti- or rhabdoviral scaffolds, which then carry S as the only SARS-CoV-2 derived component in their envelope. Although pVNTs are widely used, the assembly, morphogenesis, structure, and composition of such particles significantly differs from that of coronaviruses.^[44]

A comprehensive summary of the many versions and characteristics of different multi- or single-cycled cVNTs and pVNTs to analyze SARS-CoV-2 NABs has recently been published by Khoury *et al.*^[44]

1.3 Objectives and Outlook

Given the clinical relevance of NABs and the limitations of existing VNTs, the aim of this project was to develop a virus- and genetically modified organism (GMO)-free diagnostic VNT that is safe and quick but still quantifies SARS-CoV-2 NABs comparable to a cVNT. Therefore, a protocol was established to produce authentic virus-like particles (VLPs), which are equipped with an activator peptide to trace them. These VLPs were then thoroughly examined structurally and functionally with multiple methods to validate their biochemical, physical and biological characteristics in comparison to infectious SARS-CoV-2. The documented results attest that SARS-CoV-2 VLPs enter target cells via ACE2, undergo membrane fusion and deliver their luminal protein cargo into the cytosol, thus mimicking all steps of infection of the pathogen prior to viral transcription.^[48] NABs that provide protective immunity from SARS-CoV-2 can be quantitated with this test, as they were shown to also prevent ‘infection’ with the SARS-CoV-2 VLPs. Results with a set of double-blinded COVID-19 patient serum samples showed a very high and convincing correlation between the novel virus-free test and a cVNT with infectious virus. Additionally, it was demonstrated that the test can be adapted to VOCs such as the B.1.617.2 Delta- and B.1.1.529 BA.1 Omicron variants.^[48] As the test meets important requirements for quality, reproducibility, and rapidness, it could be a valuable tool for vaccine and therapeutic antibody development, high-throughput screenings of viral entry inhibitors and the evaluation of SARS-CoV-2 mutants that may emerge in the future. Furthermore, the generation of S specific antibodies, as well as an advancement of the VLP based VNT are presented in this work.

2 Results

2.1 Monoclonal Spike Antibodies

Due to their exceptional specificity and affinity, antibodies are an essential tool for research in molecular biology, microbiology and in particular for applications in diagnostics and therapy of infectious diseases. Thus, superior antibodies especially recognizing the spike protein of SARS-CoV-2, were urgently needed in the beginning of the COVID-19 pandemic and essential for this work. To avoid adverse effects of cross-reactivity, use of a mAb which only binds to one epitope is often advantageous, also in terms of availability and reproducibility. For the generation of antibodies, various techniques are available: While polyclonal antibodies (pcAbs) can be isolated from animal plasma upon immunization with the desired antigen, they vary from batch to batch and have no clear composition. Monovalent mAbs, can also be derived from immunized animals, but by hybridoma technique or alternatively from e.g. convalescent humans and B cell sorting. Another, fully animal-free, approach to a mAb is the use of *in vitro* phage display, from a recombinant library of scaffolds and subsequent directed evolution for affinity by mutation and selection.^[49] Yet, the use of animal immunizations can still be favorable for complex antigens, like membrane proteins and viruses, as the technique tolerates a higher background of irrelevant antigens and somatic hypermutation *in vivo* often leads to superior antibodies.^[50]

Crucial to any type of immunization is the quality of the presented antigen. Due to the complex structure of membrane proteins, antigens such as vFPs are difficult to administer in their native conformation, ensuring the correct folding and post-translational modifications. Extracellular vesicles (EVs) are small cell derived particles of ~ 100 nm diameter and an encapsulated lumen with a variety of biomolecules, surrounded by an envelope of lipid bilayer and various proteins. Depending on their biogenesis, they differ in size and composition, but can be categorized in microvesicles, which bud from the plasma membrane, and exosomes, which are of endosomal origin. EVs fulfill many different functions and depending on their route of egress, cell surface proteins are naturally incorporated into their membrane.^[51] In the past, EVs were shown to be suitable for vaccination approaches, as they can induce immunity to foreign antigens presented on them.^[52,53] Furthermore, tumor derived EVs have been used for animal immunizations, to generate mAbs by hybridoma technique,^[54] but EVs can also be modified to carry viral glycoproteins.^[55]

Besides anti-S binding antibodies for protein detection methods, particularly a neutralizing monoclonal antibody (NmAb) inhibiting SARS-CoV-2 infection *in vitro*, was required as reference for the novel VNT. To generate such a set of tools, animals were immunized,

mAbs established, characterized, screened for neutralization and used for further applications (Figure 3A, B).

2.1.1 Immunization and Antibody Generation

In order to present the antigen for immunizations in a native state, EVs were engineered to carry the S protein of SARS-CoV-2. Therefore, a constitutively S(B.1) expressing HEK293 cell line was established by transfection with a respective plasmid, selection via a resistance gene and flow cytometric sorting according to cell surface expression levels. Even though 100% of these cells were found to be S⁺ in flow cytometry with a commercial anti-S2 antibody, cells were additionally transiently transfected with the same plasmid, to increase the amount of S in EV preparations, used for immunizations. EVs were then harvested from conditioned medium by differential centrifugation, concentrated by ultracentrifugation and analyzed together with lysates of cells and controls by western blot (WB) with commercial antibodies specific for S1 and S2 subunits of spike (Figure 3D). Bands corresponding to the single subunits, as well as full-length (FL) protein, S^{FL} and complexes of higher order, e.g. S^{FL}₃, were detected in S⁺ cell lysates and EV preparations, while control samples did not show any signals. Additionally, a blot incubated with human serum of a convalescent COVID-19 patient and anti-human IgG secondary antibody gave similar results, indicating that the patient was seropositive as expected. Yet, serum from this patient did not show a clear band for S1 in the WB. Therefore, it presumably did not contain many anti-S1 reactive IgG antibodies. Still, S⁺ EV preparations were thereby confirmed to contain adequate quality of native S antigen.

Next, rats were immunized with two injections of S⁺ EVs in a prime-boost scheme. In total, three immunizations, COVEV1-3, were conducted with two animals per experiment, one with and one without addition of Freund's incomplete adjuvant. For hybridoma technique, splenic B cells were isolated, immortalized by fusion with myeloma cells and single cell plated (Figure 3A). Secreted antibodies in the respective supernatants were then screened via an enzyme-linked immunosorbent assay (ELISA) for the presence of rat IgG and via flow cytometry for anti-S specificity on a 1:1 mix of S⁺ HEK293 cells and parental S⁻ HEK293 cells (Figure 3B). While non-binding or HEK293-specific antibodies are not able to differentiate the two cell types, S-specific antibodies will result in a positive and a negative cell population (Figure 3C). Afterwards, selected clones were expanded and subjected to single cell cloning to obtain monoclonality. Results from the three immunizations varied drastically: COVEV1 yielded two specific mAbs 43A11 and 55E10, while COVEV3 gave access to several hundred IgG⁺ supernatants specific for S. For unknown reasons, COVEV2 immunization resulted in no S specific hybridoma. However, addition or absence of Freund's incomplete adjuvant did not clearly alter the ratio of S-specific to total clones in this explicit experiment, which were 59 and 67% per animal respectively. From the COVEV3 immunization, four antibodies, 5D1, 5B9, 35B12 and 42E2 were selected and recloned, according to their neutralization and epitope characteristics, determined by a VNT and by WB. Purified mAb preparations were

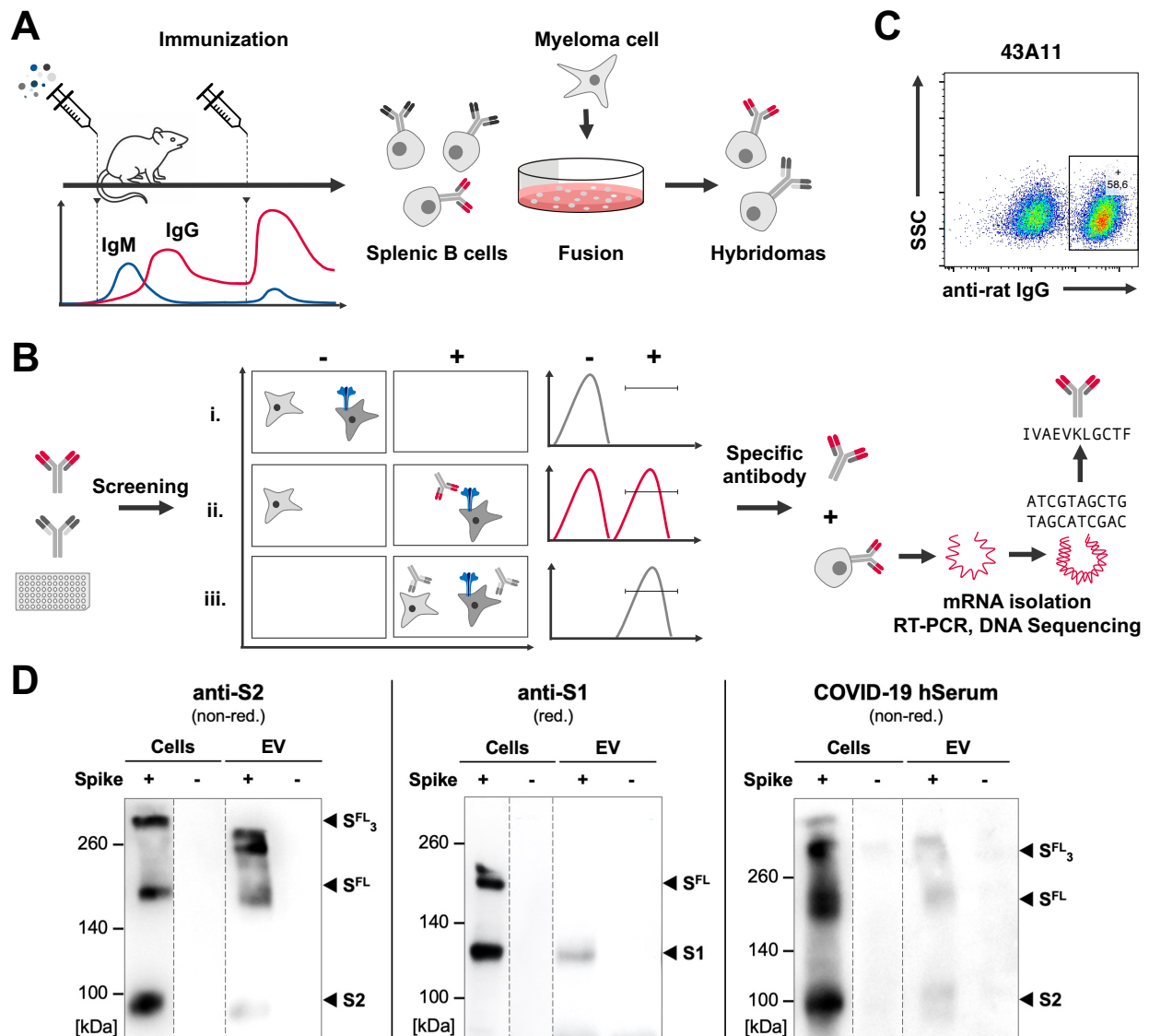


Figure 3. Anti-spike antibody generation.

(A) S specific monoclonal antibodies (mAbs) were generated via the immunization of rats with S⁺ extracellular vesicles (EVs) in a prime-boost scheme. Upon seroconversion, splenic B cells were harvested and immortalized to hybridoma cells, before plating as single cell clones.

(B) The resulting, secreted antibody supernatants were screened via flow cytometry for their S specificity, using a 1:1 mix of S^{+/-} cells, giving three possible outcomes: i. non-binding mAb, ii. S specific mAb and iii. non-specific mAb. Amino acid sequences of specific mAbs were then obtained from mRNA of the respective hybridoma clone.

(C) The mAb 43A11 successfully discriminated S⁺ from S⁻ cells during the flow cytometry screening with anti-rat IgG, giving the characteristic pattern ii. of a specific antibody.

(D) Antigen authenticity of S⁺ EVs, used for animal immunizations, was validated prior to injection. Therefore, lysates of S^{+/-} cells and EVs were analyzed by reducing (red.) and non-red. western blot (WB), using commercial S specific antibodies, as well as human serum of a convalescent COVID-19 patient as primary antibodies. Besides the S domains S1 and S2, full-length (FL) S molecules (S^{FL}) and S trimers (S^{FL}₃) were found in the respective samples.

then obtained from a core facility which also conducted hybridoma technology, cultivated clones and performed protein chromatography.

2.1.2 Antibody Characterization

The six in-house generated anti-S mAbs were then characterized in detail, as basis for all subsequent applications. The subclass of the rat antibodies was determined via flow cytometry, by incubating S⁺ HEK293 cells first with the respective novel antibody, followed by a rat IgG subclass specific secondary mAb of mouse species and finally with a mouse specific, fluorescently labeled antibody. While 43A11, 55E10, 5D1, 5B9 and 42E2 were shown to be subclass IgG2b, 35B12 was found to be an IgG2a antibody.

The avidity is the binding strength of an antigen-antibody complex. It is a composite of the paratope-epitope affinity, the antibody's valency and the number of binding sites on the antigen. To compare the binding affinities of the anti-S mAbs quantitatively, they were titrated by flow cytometry on the S(B.1)⁺ HEK293 cell line with a constant concentration of labeled secondary antibody. According to a one-site specific binding model, the dissociation constant (K_D) was calculated for each antibody from the measured mean fluorescence intensity (MFI). Resulting K_D ranged from 1.0 to 5.0 nM, indicating that all six anti-S mAbs are of high affinity (Figure 4A). While 43A11 was found to be the mAb with the lowest K_D , 42E2, 5B9 and 35B12 notably displayed a greater maximal MFI. Thus, these three mAbs resulted in higher rates of occupancy and are likely to bind epitopes that were more abundant on S⁺ cells. To put these affinities into perspective, also two recombinant human mAbs, REGN10987, imdevimab, and REGN10933, casirivimab, which have been approved under emergency use authorization for the treatment of COVID-19 by the FDA,^[39,56,57] were analyzed likewise, yet with a labeled anti-human IgG secondary antibody. The K_D of REGN10987 and REGN10933, were calculated as 1.1 and 1.0 nM respectively, which is in range of published values.^[58,59] Accordingly, the affinities of the COVEV antibodies are comparable to those of recent therapeutic mAbs. With the emerging mutations in the S gene of SARS-CoV-2, many epitopes altered drastically, causing multiple mAbs to become obsolete. To test the affinity of the COVEV mAbs to one of the novel VOC, HEK293 cells were transiently transfected to express S(B.1.1.529 BA.1) and used for titration by flow cytometry as described. Remarkably, of six novel mAbs, three (43A11, 55E10 and 5D1) lost binding entirely, while the other three displayed residual binding or retained their affinity (Figure 4A). 42E2, the antibody with the second strongest affinity for S(B.1) and 5B9 showed large reduction of maximal MFI and 7 to 2× increased K_D for S(B.1.1.529), respectively. Only 35B12 largely retained its binding capacity and seemed to have slightly lower K_D for the VOC tested. In short, all antibodies from the immunizations bind S(B.1) with great affinity, yet only 35B12 preserved affinity for B.1.1.529.

Precise localization of antibody epitopes would classically be performed by screening peptide pools, in case of linear epitopes, or by x-ray crystallography, cryo-electron microscopy (cryo-EM), cross-linking- or hydrogen-deuterium exchange mass spectrometry for conforma-

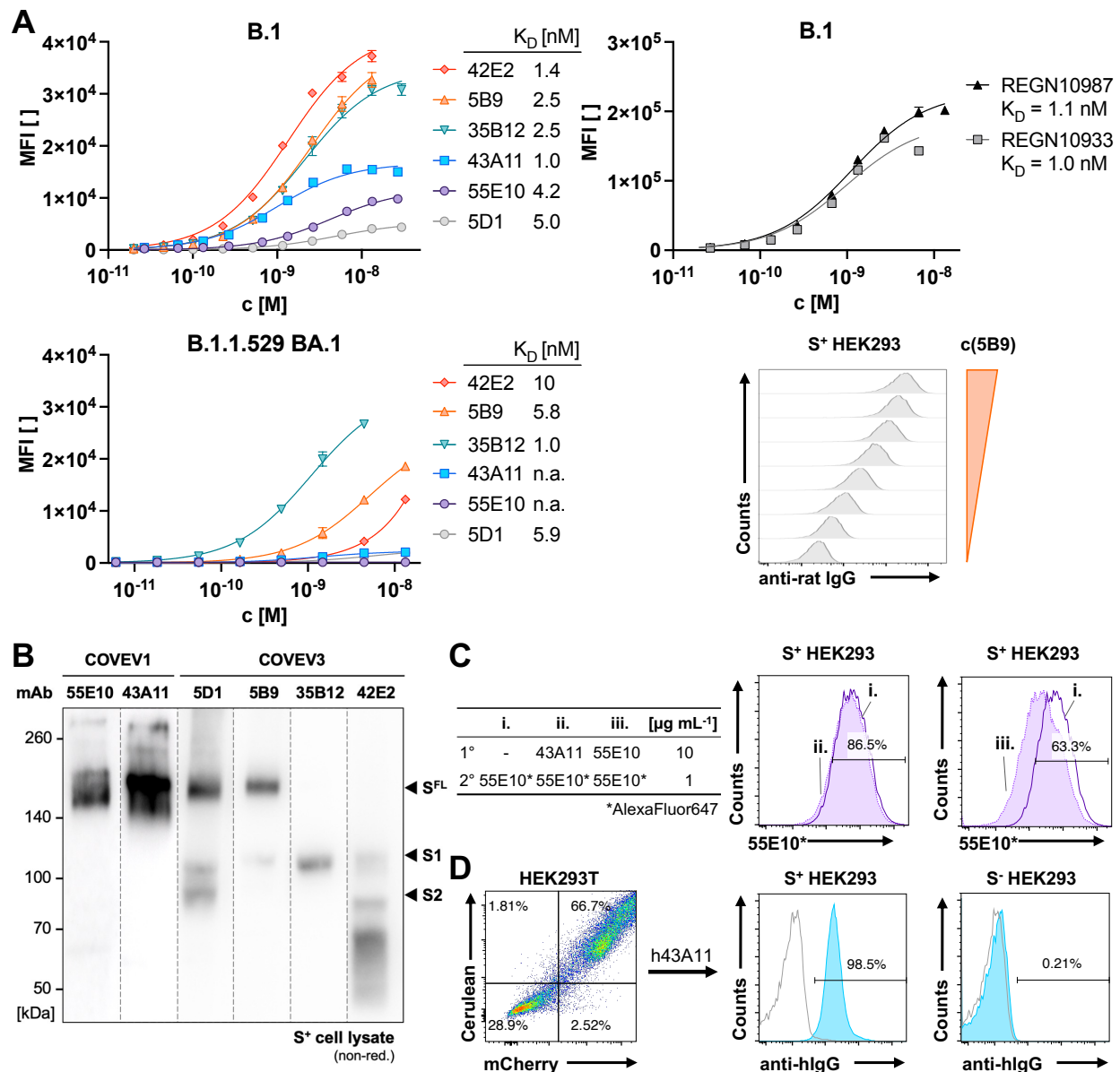


Figure 4. Anti-spike antibody characterization.

(A) Binding affinities of six anti-S, rat IgG, mAbs were determined by titration and flow cytometry on a S(B.1)⁺ cell line or cells expressing S(B.1.1.529 BA.1). Additionally, two recombinant anti-S, human IgG, mAbs, REGN10987 and REGN10933 were analyzed. Mean fluorescence intensity (MFI) of a fluorescently labeled anti-rat IgG or anti-human IgG antibody, was measured in triplicates for every single dilution of primary anti-S antibody. For each antibody, the dissociation constant (K_D) was calculated according to a one-site specific binding model from the MFI shifts. In the lower right panel, individual cytometric results of one set of replicates from 5B9 is exemplary depicted with decreasing primary antibody concentration (c).

(B) Epitope bearing domains of the six COVEV antibodies were evaluated by WB on S protein from cell lysates and the respective antibody as primary.

(C) In a competition experiment, epitope orthogonality of 43A11 and 55E10 was demonstrated by flow cytometry. Pre-incubation of S⁺ cells with 10 \times excess of 43A11 (ii.) did not reduce binding of fluorescently (*) labeled 55E10 without prior pre-incubation (i.), while pre-incubation with 10 \times excess of unlabeled 55E10 (iii.), reduced MFI by 48%. Thus, both antibodies do not compete for an identical epitope.

(D) Recombinant, human chimeric 43A11 was obtained by expression of two plasmids (bearing heavy chain + mCerulean and light chain + mCherry) in HEK293T cells, yielding 67% co-transfected cells according to flow cytometry. Secreted antibody was harvested and evaluated for S^{+/-} cell binding by flow cytometry (blue graph) with a labeled anti-human IgG antibody and compared to secondary antibody only (hollow grey line). Thereby amino acid sequence integrity and S specificity were confirmed.

tional epitopes.^[60] As those techniques are rather cost and time intensive, the epitopes of the COVEV mAbs were solely narrowed down to S subunits by WB analysis. Therefore, lysate from S(B.1)⁺ cells was loaded on the gel as sample, separated according to the respective protein size and analyzed with different primary mAbs, before developing the blot with an anti-rat, horseradish peroxidase (HRP) coupled antibody. As described earlier (Figure 3D), the S⁺ sample contains both subunits S1 and S2, as well as S^{FL} and S^{FL}₃ complex. Depending on the specificity of the COVEV antibody, bands corresponding to one or more of them were detected (Figure 4B). In detail, for all mAbs signals were only found under non-reducing conditions, while reducing disulfide bonds and boiling the sample resulted in the disappearance of signals on the blots. Thus, the COVEV mAbs are likely to recognize conformational epitopes, which are no longer intact upon complete denaturation and disruption of Cys-Cys bonds. Interestingly, the antibodies 55E10 and 43A11 exclusively recognize S^{FL} and S^{FL}₃, but not the single subunits, S1 and S2. Hence, both mAbs seem to bind epitopes at the interacting surfaces of non-dissociated S1 and S2 or alternatively, epitopes close to the unprocessed protease cleavage sites. With 5D1, a complex pattern of bands was detected, which yet contained S2 and S^{FL}. For 5B9, both S1 and S^{FL} bands were observed, unlike 35B12 which only resulted in a S1 band. Nevertheless, both mAbs clearly seem to bind epitopes in S1. Ultimately, 42E2 also showed a complex pattern of S1 and smaller bands which could e.g. correspond to degraded RBD fragments.

For 43A11 and 55E10, the antibodies obtained from the first immunization, epitopes were further investigated. As both selectively bind S^{FL} and showed equal profiles in the WB, a competition about the identical epitope could not be excluded. To clarify this, the S(B.1)⁺ cell line was pre-incubated at excess with one antibody, washed and afterwards incubated with the other, fluorophore conjugated, mAb in shortfall (Figure 4C). The resulting fluorescence intensity was quantified by flow cytometry and compared to controls: i. Reference MFI for this experiment without any interference were cells without prior pre-incubation, but stained with the labeled secondary (2°) antibody, 55E10. ii. Cells were pre-incubated with an excess of unlabeled primary antibody (1°), 43A11, before staining with the labeled 55E10. iii. Cells were pre-incubated with an excess of unlabeled 55E10, before staining with the labeled identical antibody 55E10. In case both mAbs do compete for the identical epitope, sites would be occupied and therefore MFI(ii.) < MFI(i.). In case both mAbs bind to different epitopes, MFI(ii.) would be unaltered by pre-incubation, compared to MFI(i.). To control the effect, successful self-displacement can be achieved by pre-incubation with the unlabeled 2° antibody itself, resulting in MFI(iii.) < MFI(i.). As shown in Figure 4C, 43A11 pre-incubation did not reduce MFI, yet pre-incubation with 55E10 did. The vice versa experiment with 43A11 as labeled 2° antibody likewise resulted in no reduction of MFI for pre-incubation with 55E10, but self-displacement by pre-incubation with 43A11. Therefore, both mAbs were concluded to bind orthogonal conformational epitopes in S^{FL}.

For three of the antibodies essential to this work, also the amino acid sequences were determined from cellular mRNA (Figure 3B). For that purpose, RNA was isolated from the respective hybridoma clone, complementary DNA (cDNA) synthesized by reverse transcrip-

tase and amplified by polymerase chain reaction (PCR), with mRNA onset and gene specific primers for heavy-chain constant region (C_H)1 or light-chain constant region (C_L). Next, cDNA was sent for sequencing and the resulting nucleotide sequence scanned for ORFs. Corresponding residues were computationally annotated to a rat IgG backbone and analyzed for the three paratope forming complementarity-determining regions (CDRs) per chain. Protein sequences of 43A11, 55E10 and 35B12 heavy-chain variable region (V_H) and light-chain variable region (V_L) can be found in Supplementary Table S1 with CDRs indicated. To verify the integrity of the sequences, human chimeras of the mAbs were cloned, recombinantly expressed and analyzed for specific binding to S in flow cytometry (Figure 4D). Therefore, DNA fragments were generated by commercial total synthesis that code V_H and V_L domains of the rat mAb, fused to a backbone of human IgG C_H 1-3 or C_L domains respectively. According to the World Health Organization (WHO) nomenclature,^[61] such a chimeric (-xi-), monoclonal (-mab) antibody for a viral (-vi-) target would be termed with the suffix '-viximab'.* Heavy- and light chain ORFs of the human chimeric antibody were cloned into separate plasmids, each bearing a second ORF for the fluorescent proteins mCerulean and mCherry respectively. By transient co-transfection in HEK293T cells both chains are independently translated but self assemble to a fully functional mAb, which is secreted. Flow cytometry revealed that 67% of the cells were successfully co-transfected with both plasmids, while transfection with only one of the plasmids was barely observed. Human chimeric mAb, e.g. h43A11 was harvested 72 h post-transfection and incubated with $S^{+/-}$ HEK293 cells. Staining with a labeled anti-human fragment crystallizable region (Fc) antibody and flow cytometric analysis confirmed the presence of S specific human IgG in the supernatant (Figure 4D). For h55E10 and h35B12 similar results were obtained, thus antibody sequences (Supplementary Table S1) were successfully approved.

2.1.3 Spike Detection in Biological Samples

For the sensitive detection of S protein in biological samples, a sandwich ELISA was developed using the two anti-S mAbs 43A11 and 55E10. Instead of binding the sample itself to a surface, this method uses an immobilized antibody to capture the analyte. Thus, the antigen can be specifically enriched, before another soluble antibody is added for detection. As the antigen is bound in-between two antibodies, non-overlapping epitopes are an important prerequisite for this technique, in order to not displace each other from the antigen. In detail, 55E10 was coated to a microtiter plate as capture antibody, before blocking the remaining free binding sites with protein. Next, the sample was incubated and unbound matrix cleared by washing. Upon addition of HRP coupled 43A11 and substrate, absorbance (OD) was quantified in a photometer at 450 nm, which allowed for the quantification of S in the specimen. One question which was addressed with this method was to quantify potential S protein in COVID-19 patient plasma samples, found by nanoscale flow cytometry.^[62] Free S protein or S^+ EV in the blood would have important implications for the biogenesis of

*WHO/EMP/RHT/TSN/2019.1

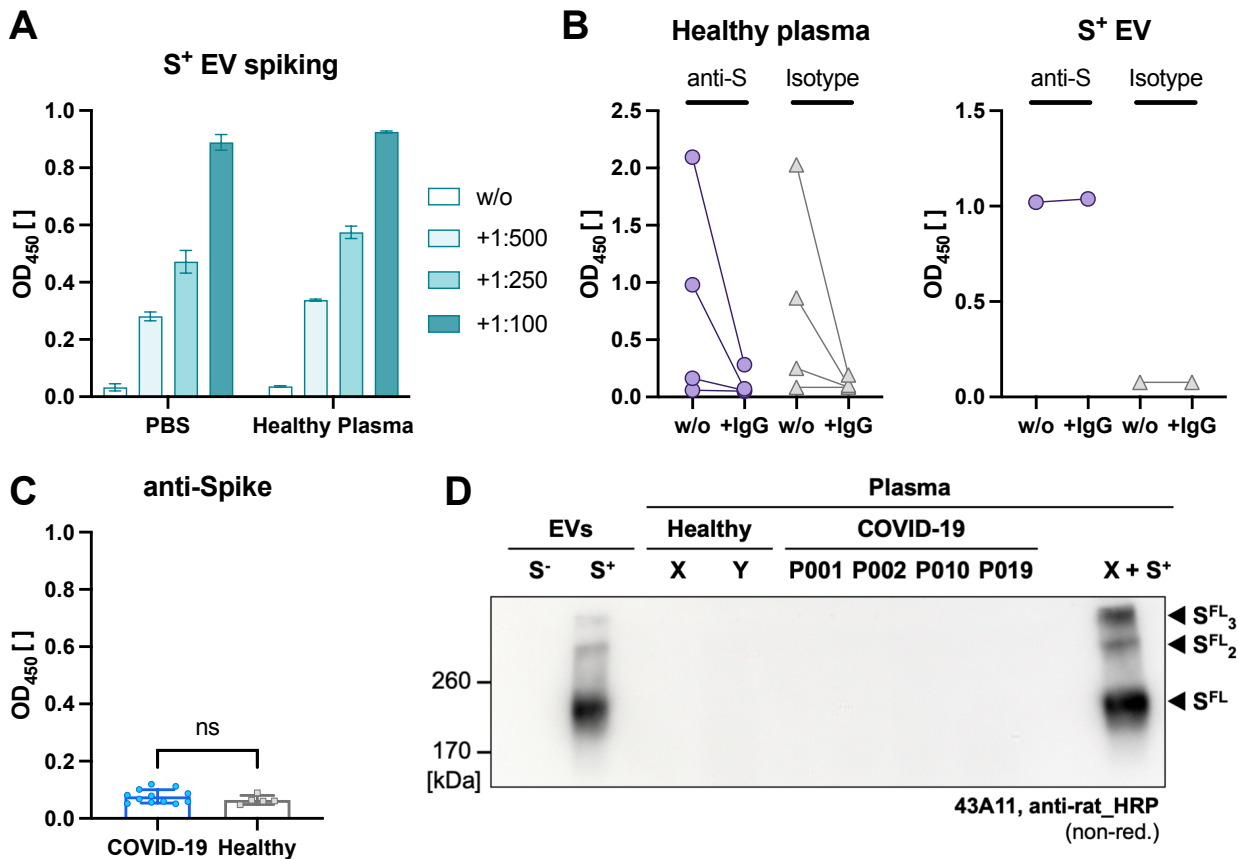


Figure 5. Evaluation of spike protein in plasma samples.

(A) Using 43A11 and 55E10 a sensitive sandwich ELISA was developed, to quantify S in biological samples. Spiking of S⁺ EVs to PBS or plasma from a healthy donor in a standard addition was reliably quantified.

(B) Yet, plasma of some healthy donors (3 of the 4 specimens shown) exhibited elevated non-specific signal in the ELISA, as a non-binding isotype capture antibody yielded similar optical densities (ODs). Pre-incubation of plasma samples with non-binding rat antibody (+IgG), successfully quenched all non-specific signal, while specific signals of samples spiked with S⁺ EVs remained unaffected.

(C) The optimized anti-S ELISA was used to evaluate plasma samples from 12 COVID-19 and 5 healthy donors for their S content. Therefore, all plasma specimens were supplemented with scavenger antibody, prior to sample incubation with the capture antibody. Yet, no significant difference was found for both cohorts. Result of a t-test is indicated: ns, not significant ($p > 0.05$).

(D) Human plasma samples, from healthy and COVID-19 donors were furthermore evaluated by WB with 43A11 anti-S antibody. S signals could only be detected in samples, with S⁺ EVs spiked in.

SARS-CoV-2 and the neutralization of virions, as they could intercept NAbs. To address this, the anti-S ELISA was first challenged with concentrated S⁺ EV positive control, spiked into phosphate buffered saline (PBS) buffer and plasma of a healthy donor at increasing concentrations (Figure 5A). In both sample types, increasing amounts of S⁺ EV were associated with higher OD values, thus the ELISA was shown to quantify S protein. Next, human plasma was titrated and found to be tolerated in the ELISA up to a dilution of 1:10 without causing interfering OD background. When tested with a larger set of healthy donors, a relevant portion of plasma samples displayed strongly elevated baseline values of ≥ 0.2 . This signal was found to be unspecific, as a non-binding isotype control capture antibody resulted in similar optical density (OD) values. Hence, a portion of donors seemed to contain interfering components in their plasma, e.g. antibodies that cross-bind capture and detection antibodies, without the necessity for their common true antigen, S. In case such anti-rat antibodies or anti-foreign specie antibodies would be present in some samples, non-specific signal could be explained. To test this, plasma from three donors with high background and from one donor without background were pre-incubated with a non-binding rat mAb isotype as decoy, prior to sample loading on the capture antibody (Figure 5B). Without (w/o) addition of this scavenger antibody, three of the signals showed non-specific background as expected for anti-S and isotype capture antibodies equally. Pre-incubation with scavenger (+IgG) mAb however reduced unspecific signal drastically, while specific signal of a S⁺ EV sample remained unaltered. Thus, an effective quenching method for such assay interference was found, which did not affect specific sample quantification in the samples tested. With the addition of quenching antibody, S quantification via the sandwich ELISA was shown to be sufficiently robust for complex plasma samples. Therefore, plasma from 12 COVID-19 patients with acute SARS-CoV-2 infection at the University Hospital Rechts der Isar (MRI), Technical University of Munich (TUM) and 5 healthy donors were analyzed (Figure 5C). Results did not show considerably increased values for any specimen and means of the COVID-19 and healthy cohort did not show significant difference in a t-test ($p > 0.05$). Thus, the analyzed plasma from COVID-19 patients did not contain quantifiable amounts of S protein, according to the applied method. Additionally, 4 of the COVID-19 and 2 of the healthy samples were analyzed by WB, along a S⁺ EV positive control and a healthy donor sample spiked with S⁺ EVs (Figure 5D). Using the antibody 43A11, signals specific for S^{FL} and its complexes could as well only be found in the positive control lanes. Consequently, in the analyzed plasma samples from COVID-19 patients, no evidence for S protein could be found by conventional methods as ELISA or WB. These results are in conflict with results from collaborators at MRI and TUM, who found S on plasma derived EVs, by nanoscale flow cytometry with the 43A11 antibody.

2.2 Pseudotyped Virus Neutralization Test

A common method to determine the neutralization capacity of an antibody is the pVNT, which does not require work with the full virus, as described. To test the anti-S antibodies 43A11 and 55E10 for SARS-CoV-2 *in vitro* neutralization, a pVNT was established with an appropriate cell line. African green monkey derived Vero cells are naturally permissive for SARS-CoV, as their endogenous ACE2 is homologous and cross-binding to S.^[63] As overexpression of the human analogue improves pVNT performance further,^[64] Vero cells were transduced to constitutively express hACE2 and analyzed by anti-ACE2 WB. Next, S-pseudotyped, replication incompetent retrovirus was produced in HEK293T cells by co-transfection of S as vFP, the respective structural protein components, reverse transcriptase, integrase and a vector encoding green fluorescent protein (GFP). After 48 h, viral stocks were harvested and used to infect hACE2⁺ Vero cells, which were then cultivated for another 48 h. Expression of GFP reporter gene was analyzed by flow cytometry and fluorescence microscopy, yielding about 80% infected cells on average, upon treatment with PBS as control (Figure 6A). Pre-incubation of the inoculum with serum of a COVID-19 vaccinee however inhibited infection entirely. When analyzed in this pVNT, both anti-S mAbs 43A11 and 55E10 did not display effective neutralization, compared to an IgG isotype control, neither as single antibodies, nor synergistically in the form of an equimolar cocktail of both (Figure 6B). Hence, 43A11 and 55E10 were found to be non-neutralizing anti-S mAbs and ineligible as controls for any VNT, despite their high affinity for S^{FL}. Yet, in principle the applied test is capable of determining neutralization quantitatively, as pre-incubation with sera of a COVID-19 vaccinee (BNT162b2) and a COVID-19 convalescent patient efficiently reduced the fraction of infected cells in a dose dependent manner, whereas serum from a healthy and immunologically naive individual did not show an effect (Figure 6B). To characterize the pVNT and S-pseudotyped retroviral particles further, hACE2⁺ Vero cells were pre-incubated with chloroquine, before they were inoculated with the viral stock. Chloroquine deacidifies endosomes and inactivates the endosomal, pH-dependent, cysteine protease CTSL, which primes S for SARS-CoV-2 entry in certain cell lines *in vitro*.^[13,48,65,66] Drug treatment efficiently inhibited infection with a half maximal inhibitory concentration (IC₅₀) of 1.5 μ M (Figure 6B), thus entry of S-pseudotyped retroviral particles into Vero cells was found to be dependent on endosomal processing of S.

In general and as demonstrated, pVNTs allow to quantitate NAbs with SARS-CoV-2 specificity, but require several days, also for *de novo* expression of the reporter gene and depend on qualified S-pseudotyped virus stocks with reproducible vector content and infectivity. In this setup, the test additionally required a flow cytometer with high throughput sampler module and the respective sample preparation, to analyze the ratio of GFP⁺ cells. Despite its automation, also the readout was therefore quite time-consuming and labor-intensive. Furthermore pseudotyped particles are biologically distant from the original infectious virus, as they do not necessarily originate from a suitable permissive cell and exploit distinct routes of egress.^[67]

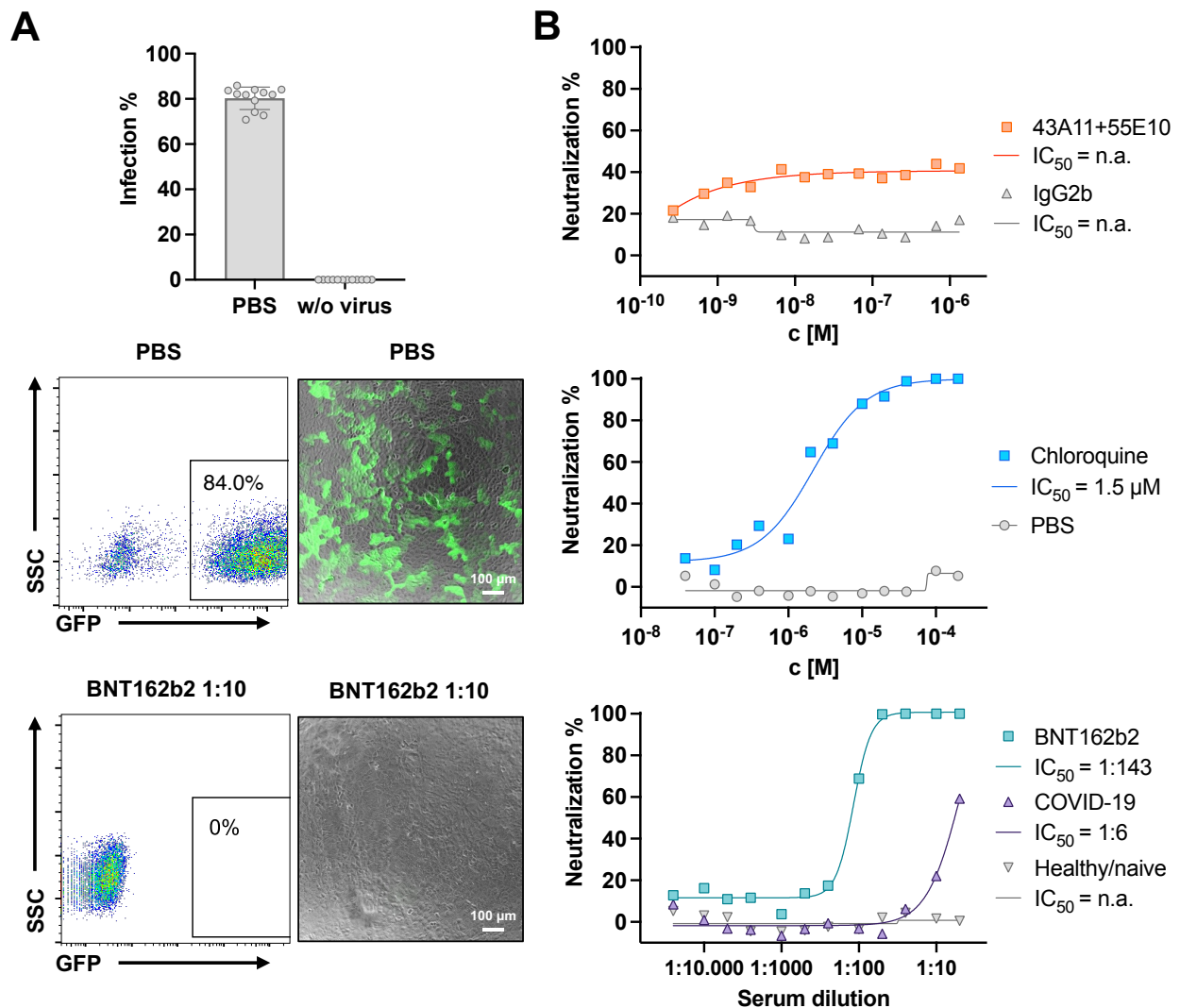


Figure 6. Pseudotyped virus neutralization test (pVNT).

S pseudotyped, replication deficient retrovirus, based on a MLV vector encoding GFP was used for infection of Vero cells expressing hACE2 and the evaluation of NABs. Quantitative readout relies on *de novo* expression of retrovirally transduced GFP gene in susceptible cells and analysis of fluorescence by flow cytometry.

(A) Cells of 12 biological replicates were analyzed for GFP expression 48 h post infection by flow cytometry and fluorescence microscopy, yielding about 80% GFP⁺ cells (top and middle charts). Pre-incubation of the inoculum with a 1:10 dilution of human serum from a BNT162b2 vaccinated individual for 30 min efficiently blocked infection (bottom charts). Merged fluorescence and brightfield microscopy images are shown with white scale bars indicating 100 μm length.

(B) Next, mAbs, human sera and a chemical compound were titrated with fixed doses of S pseudotyped retroviral inoculum. In this pVNT, a mAb cocktail of 43A11 and 55E10 did not display efficient neutralization against SARS-CoV-2, along a control of isotype (IgG2b) mAb (top chart). Chloroquine, an inhibitor of endocytosis, efficiently blocked infection of hACE2⁺ Vero cells with pseudotyped vector particles, upon pre-incubation of cells, even in low concentration (c) of the drug (middle chart). Sera of a BNT162b2 vaccinee or a COVID-19 convalescent patient displayed strong neutralization, while serum of a healthy, naive donor had no neutralizing effect (bottom chart). Half maximal inhibitory concentration (IC₅₀) was calculated, or indicated as not applicable (n.a.). Parts of this figure and its legend were adapted from Roessler *et al.* 2022,^[48] under CC BY 4.0.

2.3 Virus-Like Particles

As work with infectious SARS-CoV-2 is limited to BSL-3 containment laboratories, surrogates are urgently needed for scientific research. S-pseudotyped particles used for pVNTs are admittedly non-replicating and resemble SARS-CoV-2 with respect to the vFP but other than that are particles of e.g. retroviruses. Thus, in this study engineered EVs, hybrids of virus and host cell, were used to present the vFP natively on vesicular structures. Those S⁺ EVs were then used for immunizations up to this point. While uninfected cells naturally and constantly shed EVs, infected cells are reprogrammed to turn into virus factories. Because of their origin and their egress via preexisting pathways, virions of enveloped viruses share many similarities with EVs in terms of size, structure, lipid composition and proteins. Yet, both differ fundamentally by the fact that EVs do not replicate. In an infected host cell however, the boundaries between a replication competent enveloped virus, a defective non-replicating virus particle and EVs of purely host components become rather blurry.^[68]

Another class of particle and authentic mimic are VLPs, which consist of all structural proteins of a virus, but lack the nsps and the viral genome. Because the genetic information for the virus per se is not incorporated, they are non-replicating and per definition non-infectious, even though they are capable of entering a susceptible cell. For SARS-CoV-2, formation of VLPs has been described in a self-assembling mechanism from the four structural proteins only.^[69,70] In contrast to S-pseudotyped particles, which bear SARS-CoV-2, host and e.g. retrovirus components, VLPs entirely consist of the SARS-CoV-2 proteins S, M, N and E, as well as host components. Another key difference between both is that VLPs acquire their S protein from the ER - Golgi intermediate compartment (ERGIC), instead of the plasma membrane.^[71] Therefore, VLPs represent SARS-CoV-2 more faithfully than pseudotyped surrogates. While S was found to be dispensable for assembly, but incorporated if present,^[72] coexpression of S, M, N and E was shown to be the most efficient combination to induce VLP secretion.^[73] VLPs have been described also for other viruses, such as human immunodeficiency virus (HIV),^[74,75] Epstein-Barr virus (EBV)^[76] and influenza.^[77] Due to their morphological resemblance and antigen composition, VLPs are considered a safe alternative to study viruses and have been suggested as potential vaccine candidates.^[78]

2.3.1 Manufacturing of VLPs

SARS-CoV-2 VLPs, here termed S⁺ VLP, were generated in HEK293T cells by transient co-transfection of four expression plasmids, encoding all structural proteins of the virus, M, N, E (all Wuhan-2019) and S (Wuhan-2019 D614G B.1, or where indicated, B.1.617.2, B.1.1.529 BA.1), in defined stoichiometry. To trace the S⁺ VLP, an additional, fifth, plasmid was co-transfected to express a chimeric reporter protein consisting of the human tetraspanin CD63 and, at its carboxy terminus, the activator peptide HiBiT of split-nano-luciferase (CD63~HiBiT). Large quantities of assembled S⁺ VLPs were present in the cell culture medium, three days after transfection.^[48] S⁺ VLP were harvested from the supernatant by

differential centrifugation to eliminate cells and debris, and generally used without further processing. Additional purification and concentration were applied if needed and as indicated, before S⁺ VLP were characterized in detail.

2.3.2 Electron Microscopy of VLPs

Because of their small size, viruses can in general not be visualized by light microscopy. Their detection and structural elucidation did therefore decisively benefit by the invention of electron microscopy (EM) and its application in structural biology. Until today, this technique is indispensable for basic research but also for rapid virus diagnostics during unexpected epidemics of unknown pathogens.^[79] To investigate the morphology of S⁺ VLP, transmission electron microscopy (TEM) was performed with negative stained samples of particles purified by density gradient ultracentrifugation (Figure 7A). The depicted image shows a particle of approximately 60 nm diameter with the characteristic contours of a coronavirus. The shape of the particle has high similarity with early images of avian coronavirus VLPs,^[80] but also negative stained EM images of SARS-CoV-2 virions.^[81]

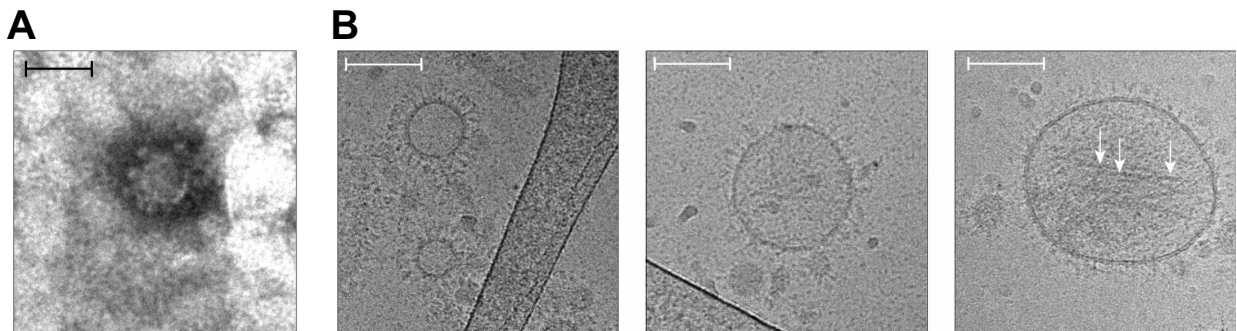


Figure 7. Electron microscopy (EM) images of SARS-CoV-2 VLPs.

(A) EM image of a negative stained S⁺ VLP, with the morphological characteristics of a coronavirus. Black scale bar indicates 50 nm.

(B) The images show different S⁺ VLPs of approximately 60 to 150 nm in diameter recorded by cryo-EM. The particles bear the characteristic corona of radial, dense spike-like proteins protruding from the envelopes' intact lipid bilayer, which are characteristic for trimers of the viral glycoprotein of coronaviruses, S, as observed for SARS-CoV-2 virions. The particle in the right panel shows elongated structures (white arrows), which might correspond to S protein protrusions lying down on the surface. White scale bars indicate 100 nm. Parts of this figure and its legend were adapted from Roessler *et al.* 2022,^[48] under CC BY 4.0.

While negative staining requires drying of heavy metal salts around particles for contrast filling and shows their two-dimensional projection, cryo-EM images native biological structures by phase contrast upon cryopreservation. Investigated objects can thus be recorded in their intact shape with greater resolution. Consequently, cryo-EM of S⁺ VLP was performed, which revealed spherically shaped vesicles of 60 to 150 nm diameter, with an intact membrane of lipid bilayer (Figure 7B). The S⁺ VLPs displayed a characteristic corona of dense, needle-like radial proteins protruding perpendicularly from the membrane, just like SARS-CoV-2 virions.^[48,82–84] Each of these structures consists of a slim stem with a spacious head on their distal end, suggesting that the protrusions correspond to the viral glycoprotein S of SARS-CoV-2.^[48] This assumption is supported by their shape and dimension of 25 nm

length and 7 nm stem width, as well as the fact that the protrusions were not detected on S⁻ EVs. On certain spike bearing particles, additional elongated structures were observed (white arrows in Figure 7B), which could correspond to S molecules laid down on the surface of the vesicle. Those might likely be caused by surface tension effects upon plunging the sample in cryogen. A reduction of the liquid film's height by evaporation could cause partial air contact of the particle's envelope and thus flattening and redistribution of the surface components, while spikes in the periphery would still be surrounded by the liquid phase and thus retain their integrity. Alternatively, the elongated structures could also correspond to fibrous proteins within the lumen of the vesicle. While SARS-CoV-2 virions contain the ~30 kb RNA genome in complex with ribonucleoprotein N, S⁺ VLPs seemingly do not comprise a similar luminal mass (Figure 7B), probably because of the absence of the vRNA genome. For virions, the large RNA molecule in complex with N could act as spatial sizing factor, explaining the variability of diameter observed in preparations of S⁺ VLP. Other than that, the S⁺ VLPs seem to mimic SARS-CoV-2 virions structurally (Figure 7).^[48]

2.3.3 Molecular Characterization of VLPs

Spike, the vFP of SARS-CoV-2, mediates attachment to ACE2, as well as fusion with the target cell. It is a glycosylated transmembrane protein of two subunits S1 and S2 and assembles in homotrimers. Because of its central role in viral infection, the correct conformation of S is critical for the tropism and fusogenicity of both SARS-CoV-2 virions and S⁺ VLPs. To ensure this, S⁺ VLP and a SARS-CoV-2 virus stock from infected Vero E6 cells, heat inactivated at 56°C for 15 min, were analyzed by WB alongside a negative control of EVs. For detection, two commercially available, subunit specific antibodies anti-S1 (pAb) and anti-S2 (mAb) were used under both reducing and non-reducing conditions to visualize bands corresponding to S1, S2 and bands of higher order, containing those subunits (Figure 8A, B). In parallel, the novel, in-house generated high affinity mAb 43A11, which exclusively recognizes non-dissociated S (but not the single S1 or S2 domains; Figure 4B) was used to detect S^{FL} and its complexes under non-reducing conditions (Figure 8C). The analysis confirmed the presence of S1 and S2 subunits, S^{FL}, trimers of S^{FL} (S^{FL}₃ or S₂₃S₁₃) and other additional S complexes in S⁺ VLP preparations. Proteolytic cleavage by furin and subsequent partial dissociation of single S1 subunits from the S₂₃S₁₃ complex during viral egress,^[10,85] but also dimeric S^{FL} complexes,^[86] might explain certain additional bands of higher order. Upon furin cleavage, subunits S1 and S2 remain non-covalently associated,^[7] as the 14 disulfide bonds in S are forming Cys-Cys bridges within domains but not between the two subunits.^[87] Thus, a reducing agent on its own is unlikely to alter the amount of dissociated subunit. In S⁺ VLP preparations from HEK293T cells, a significant portion of S seems to be efficiently cleaved and dissociated, presumably by host furin, as the anti-S2 blot shows a strong band for single S2 (Figure 8A). As the anti-S1 blot required heat treatment of the loaded sample at 95°C for 5 min in addition to the reduction agent, parts of the single S1 band likely originate from disintegrated complexes of S and therefore overrepresent the

amount of dissociated S. Yet, the residual faint S^{FL} band in the anti-S1 blot on the other hand could correspond to uncleaved, non-dissociated S (Figure 8B). Despite the proteolytic priming of S^+ VLPs, the majority of S was shown to remain largely complexed in single and higher order S^{FL} conformations. The blot with 43A11 clearly confirmed the presence of S^{FL} , S^{FL}_2 and S^{FL}_3 in S^+ VLP preparations (Figure 8C). The SARS-CoV-2 virus stock in comparison, showed a similar S composition, but the S2 specific antibody only detected the trimer S^{FL}_3 , whereas the S1 antibody detected both S^{FL} and S1. Passaging SARS-CoV-2 repeatedly on Vero E6 cells was reported to lead to a loss of the furin cleavage site,^[88] which could explain the equal fractions of uncleaved S^{FL} and S1 (Figure 8B, right panel) and the absence of single S2 domain in the virus stock in Figure 8A. Analysis with the mAb 43A11 found that SARS-CoV-2 contains S^{FL} not only as distinct trimer but also as monomer, which was barely observed in the anti-S2 blot. Thus, preparations of S^+ VLP and SARS-CoV-2 virus were concluded to be similar according to WB analyses but differ with respect to the fraction of furin cleaved S.^[48]

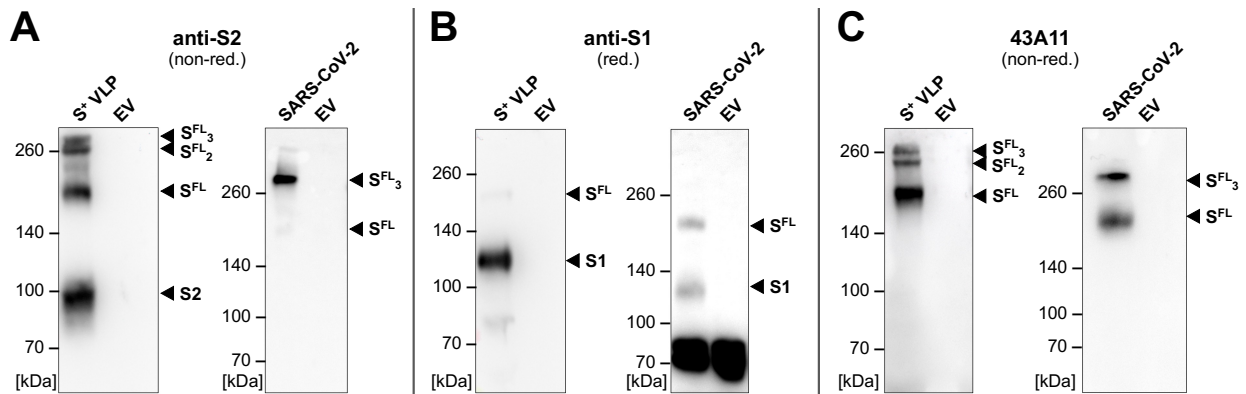


Figure 8. Western blot (WB) of protein lysates from S^+ VLPs and SARS-CoV-2.

Blots of S^+ VLPs and EVs produced in or spontaneously released from HEK293T cells, and SARS-CoV-2 virus stock from infected Vero E6 cells are shown. Antibodies are directed against the S1 or S2 subunits or recognize the intact, full-length (FL) spike molecule S^{FL} . The analyses confirm S protein in various states in S^+ VLPs and SARS-CoV-2 virus preparations but not in negative control EVs.

(A, B) S2 and S1 specific monoclonal respective polyclonal antibodies detect both S domains in preparations of S^+ VLPs as well as S^{FL} protein (left panels of A and B). The S2 domain specific antibody also detects trimeric S^{FL} (S^{FL}_3) and S complexes of higher order under non-reducing (non-red.) conditions. In SARS-CoV-2 virus stock (right panels of A and B) the antibodies detect S^{FL} protein and the S1 domain in panels A and B but not the S2 domain.

(C) Mono- and trimeric S^{FL} protein complexes in S^+ VLPs (left panel) and SARS-CoV-2 virus stock (right panel) detected with 43A11, a mAb that recognizes S^{FL} exclusively. This figure and its legend were adapted from Roessler *et al.* 2022,^[48] under CC BY 4.0.

Next, the spike specific sandwich ELISA with the two in-house generated anti-S mAbs 43A11 and 55E10, which recognize orthogonal non-overlapping epitopes, was used to quantify the S content of S^+ VLP and the heat inactivated SARS-CoV-2 virus isolate. As external reference and for the calibration of the assay, a commercially available recombinant S protein was employed to assess the absolute amount of S. Soluble, truncated ‘extra-viral-’ or commonly ‘extracellular domain (ECD)’ of S was used for this purpose, resulting in the calibration curve shown in Figure 9A. Within the linear range of OD values ($0.7 \leq OD \leq 1.7$, $r^2 > 0.99$), accurate S quantification of samples could then be performed by linear regression. The detection limit of this assay, here defined as $3 \times$ the standard deviation over the mean

blank value, was estimated to correspond to 3 ng mL^{-1} recombinant S protein. The assay sensitively detected concentrated and unconcentrated S⁺ VLP in a titration of samples (Figure 9B) and thus was found to be highly specific when probed with control EVs consisting of M, N and E but without the viral fusion protein S (ΔvFP EVs). In S⁺ VLP preparations and heat inactivated SARS-CoV-2 virus stock (RT-qPCR, ct value 15.3) $626 \pm 20 \text{ ng mL}^{-1}$ and $149 \pm 6 \text{ ng mL}^{-1}$ S protein, respectively, were found according to the applied protein standard (Figure 9C).

2.3.4 Particle Analysis of VLPs

Next, the number of particles in the samples was quantified via nanoparticle tracking analysis (NTA). While transfection of HEK293T cells with an expression plasmid encoding S and a mock plasmid yielded $5.0 \times 10^9 \text{ mL}^{-1}$ S⁺ EV particles, comparable transfections of equal DNA amount with plasmids encoding M, N, E and S, yielded $9.1 \times 10^{10} \text{ mL}^{-1}$ S⁺ VLP (Figure 9D). Therefore, co-expression of M, N, E together with S increased the number of particles drastically and led to 18-times more particles in the supernatant, compared to S⁺ EVs. This suggests that S⁺ VLP consisting of M, N, E and S evolve via a self-assembling mechanism and egress without the need of non-structural viral proteins, as described for SARS-CoV VLPs.^[70] In the inactivated SARS-CoV-2 virus stock, $7.2 \times 10^9 \text{ mL}^{-1}$ particles were counted. The total particle numbers included $1.5 \times 10^9 \text{ mL}^{-1}$ bovine EVs from fetal bovine serum (FBS) contained in the cell culture medium. Bovine EVs therefore corresponded to 2% and 30% of total particles in S⁺ VLP and S⁺ EV preparations, respectively.^[48]

While the characterization via WB, ELISA and NTA analyzed the S⁺ VLP preparations as a composite, quantitative data on a single particle level were missing. Therefore, a nano flow technique was developed, to assess the fraction of S⁺ particles among all particles released from HEK293T cells. For this method, particles were purified from cell culture supernatants and incubated with the dye CellTraceViolet (CTV; Thermo Fisher Sci.), which exhibits fluorescence only upon membrane penetration and enzymatic ester hydrolysis in the lumen of intact vesicles.^[89] Subsequently, particles were stained with fluorescently labeled anti-S mAb 43A11 and analyzed using a cytometer (CytoFLEX, Beckman Coulter).^[48] To distinguish instrument noise from intact vesicular particles, events were pre-gated for CTV⁺ and SSC-H and the fraction of S⁺ particles assessed eventually (Figure 10A). Particles obtained after transient transfection of HEK293T cells with plasmids encoding S, M, N and E, constituted 37.5% S⁺ particles of all CTV⁺ particles, i.e. S⁺ VLP. The inactivated SARS-CoV-2 stock contained about 10% S⁺ particles, i.e. SARS-CoV-2 virions (Figure 10B). In the case of this sample, thermal treatment for the purpose of inactivation might have lowered the esterase activities in both virions and contaminating EVs, which might explain the rather low fraction of CTV⁺ particles measured in this stock (0.11% of all events). The S⁺ VLPs preparations were found to contain on average 626 ng S protein (Figure 9C) and 9.1×10^{10} physical particles per mL (Figure 9D) of which 37.5% carried spike (Figure 10B). Assuming even distribution of S molecules per S⁺ particle and the given molecular weight

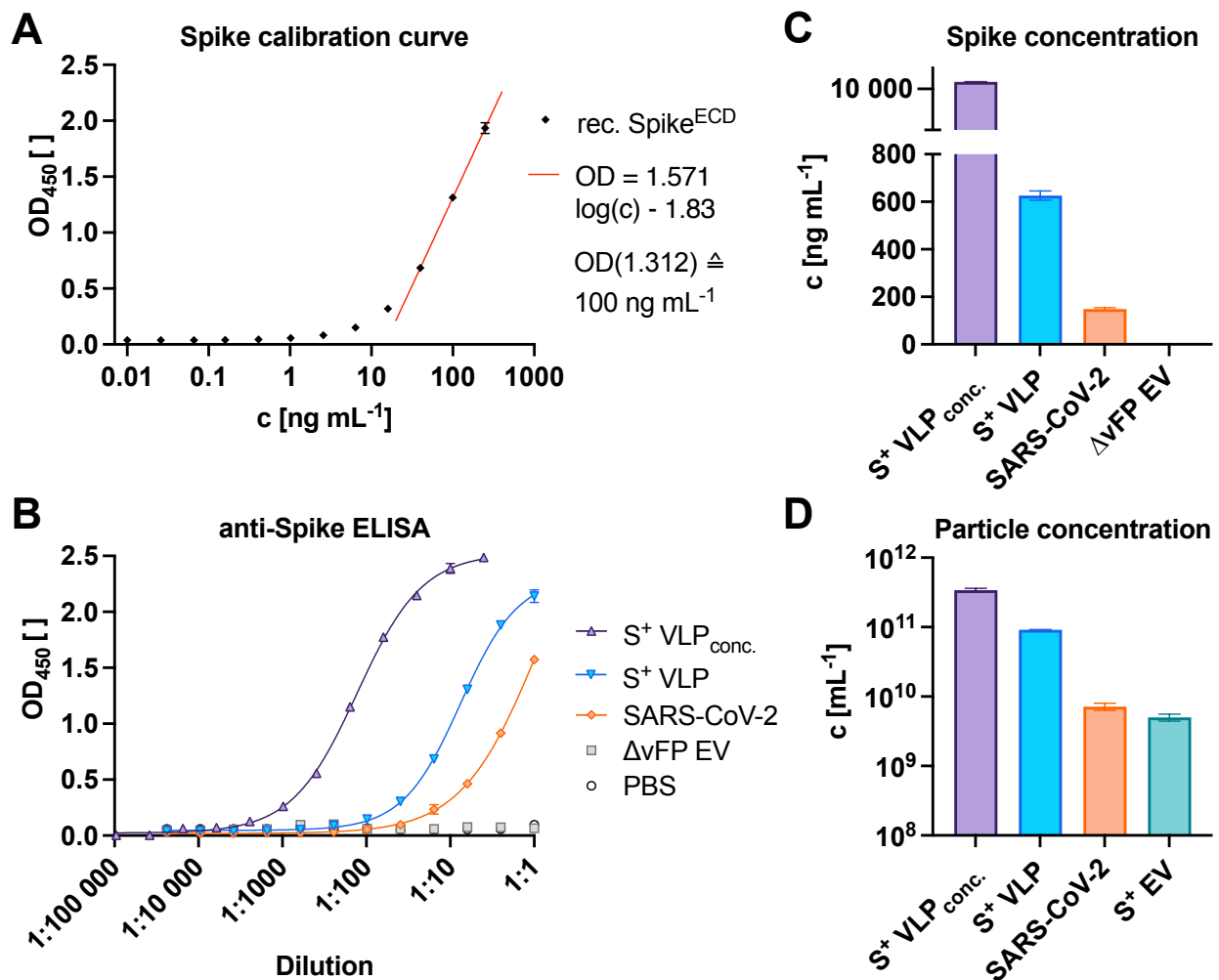


Figure 9. ELISA and particle analysis of S⁺ VLP and SARS-CoV-2 preparations.

(A) To quantify S protein, a sandwich ELISA using the two mAbs 43A11 and 55E10 was used. Calibration of the ELISA was performed using a commercially available, recombinant (rec.), S protein standard, encompassing the extracellular domain (ECD). Mean values with standard deviations are indicated. The calibration curve of three independent replicates allows for the calculation of S protein concentration (c) in samples within the linear range of optical density (OD) values ($0.7 \leq OD \leq 1.7$, $r^2 > 0.99$). The detection limit of this assay was estimated to correspond to 3 ng mL^{-1} rec. S protein.

(B, C) Concentrated (conc.) and unconcentrated S⁺ VLPs from supernatants of transiently transfected HEK293T cells were analyzed for their amount of S^{FL} protein. Based on the linear regression equation in panel A, spike concentrations were calculated from three technical replicates in the linear OD range and compared with inactivated SARS-CoV-2 virus stock with a known ct value (15.3) of its vRNA copies according to RT-qPCR. Controls are solvent (PBS) and EV without a viral fusion protein (Δ vFP EV) harvested from cell culture medium of cells expressing M, N, E and CD63~HiBiT.

(D) Nanoparticle tracking analysis (NTA) of three independent preparations of unconcentrated and conc. S⁺ VLPs (S, M, N, E, CD63~HiBiT) and S⁺ EVs (S, CD63~HiBiT) from cell culture medium of transiently transfected HEK293T cells are shown. For comparison, NTA data from heat-inactivated SARS-CoV-2 virus stock from infected Vero E6 cells are provided. This figure and its legend were adapted from Roessler *et al.* 2022,^[48] under CC BY 4.0.

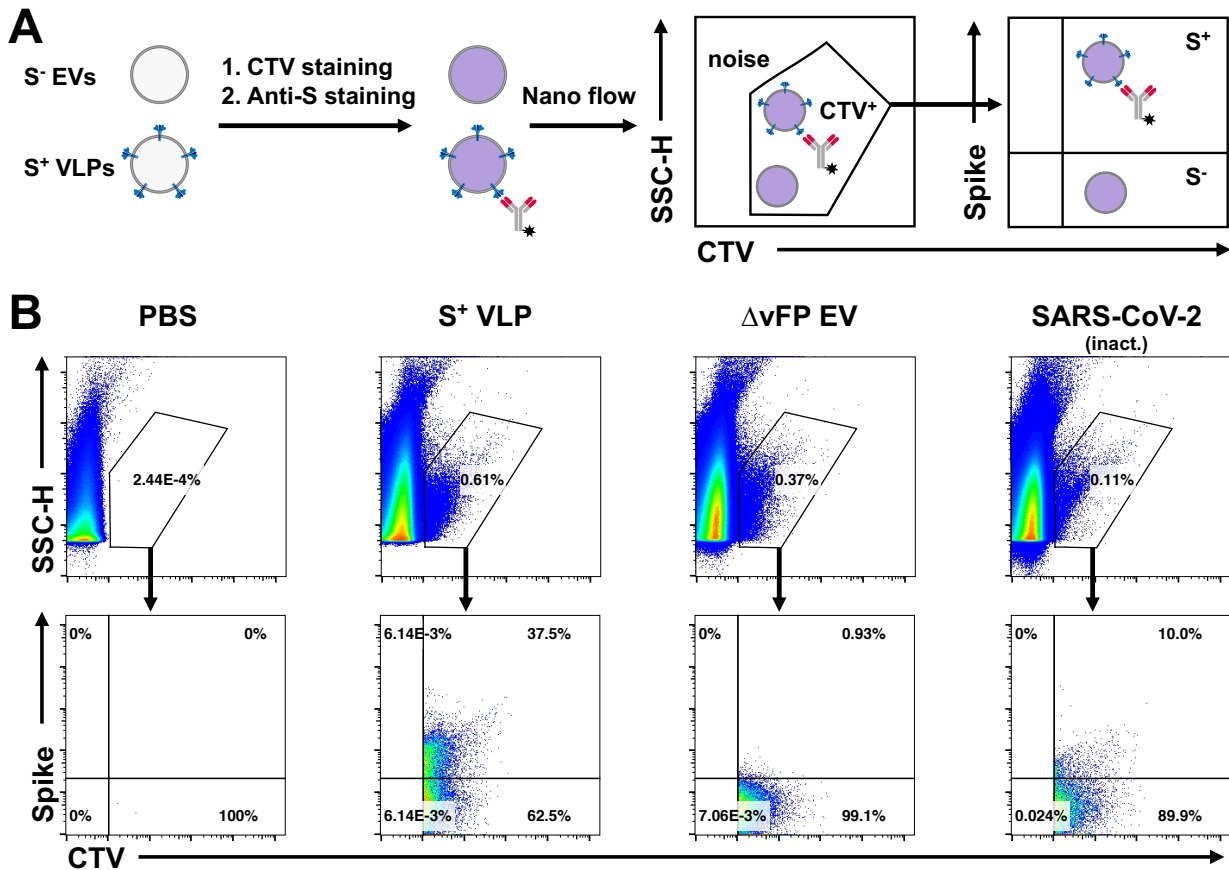


Figure 10. Nano flow technology of S⁺ VLPs and SARS-CoV-2 virions.

(A) Preparations of S⁺ VLPs (S, M, N, E and CD63~HiBiT) and control Δ vFP EVs (M, N, E and CD63~HiBiT) were stained with the membrane permeable dye CellTrace Violet (CTV), which exhibits fluorescence only upon uptake and esterase activation within the lumen of intact membranous vesicles. A heat-inactivated SARS-CoV-2 stock was stained in parallel with CTV for comparison. Subsequently, samples were counter-stained for the presence of surface S protein using fluorescently labeled anti-S mAb 43A11. Samples were diluted and then analyzed using a CytoFLEX LX flow cytometer.

(B) Panels in the top row show recorded events according to their sideward scatter (SSC-H) using a violet excitation laser (y-axis) and CTV staining (x-axis). CTV⁺ events were gated as shown in A to identify sub-cellular, intact particles (S⁺ VLPs, Δ vFP EVs, SARS-CoV-2 virions) and to distinguish them from instrument noise seen in the PBS control. CTV⁺ events were analyzed for their staining with the anti-S antibody (bottom row of panels). 37.5% S⁺ particles were identified in the preparation of S⁺ VLPs, 10% S⁺ particles were identified in SARS-CoV-2 virus stock and fewer than 1% background in control Δ vFP EVs. The low fraction of CTV⁺ events in the virus preparation (0.11%) compared with preparations of S⁺ VLPs (0.61%) and Δ vFP EVs (0.37%) might be the consequence of a reduced esterase activity in virions (and EVs) after heat treatment at 56°C for 15 min to inactivate viral infectivity. This figure and its legend were adapted from Roessler *et al.* 2022,^[48] under CC BY 4.0.

of 134.4 kDa for the truncated recombinant S protein standard, a theoretical number of 82 S molecules (Equation 1), corresponding to 27 trimers, per S⁺ VLP was calculated (Equation 2),^[48] which is well in range for SARS-CoV-2 virions that bear 24 to 40 spikes, as described by others.^[82,84,88]

$$n(S)_{\text{VLP}} = \frac{\frac{m(S)}{M(S)} \frac{N_A}{V}}{\frac{n(S^+ \text{VLP})}{V}} = \frac{\frac{626 \times 10^{-9} \text{ g mL}^{-1}}{134.4 \times 10^3 \text{ g mol}^{-1}} \cdot 6.022 \times 10^{23} \text{ mol}^{-1}}{0.375 \times 9.1 \times 10^{10} \text{ mL}^{-1}} \approx 82 \quad (1)$$

$$n(S_3)_{\text{VLP}} = \frac{n(S)_{\text{VLP}}}{3} = \frac{82}{3} \approx 27 \quad (2)$$

2.4 Virus-free Fusion Assay

2.4.1 Spike EVs with β -Lactamase Readout

The next step towards a virus-free neutralization test was to analyze whether S⁺ VLPs have the potential to fuse with appropriate target cells. Hence, HEK293T, Huh7, Vero and U251MG cells were retrovirally transduced to constitutively overexpress human ACE2, as confirmed by WB. Among those, Huh7 and Vero have been employed for infection with S-pseudotyped retrovirus before.^[64] Recently, U251MG, a SARS-CoV-2 susceptible human cell line,^[90] was shown to efficiently take up EVs, bearing VSV-G, the vFP and glycoprotein of the vesicular stomatitis virus (VSV).^[91] Thus, these cells fulfilled important prerequisites and were likely to be suitable recipient cells. While ultimately S⁺ VLP had to be tested for fusion, S⁺ EV were used at first in a simplified setup. Therefore, EVs were engineered to carry SARS-CoV-2 S protein besides a chimeric reporter enzyme consisting of the human tetraspanin CD63 and at its carboxy terminus β -lactamase (BlaM), CD63~BlaM. These S⁺, CD63~BlaM⁺ EVs were obtained from HEK293T cells as described, concentrated via ultracentrifugation and incubated with recipient cells for 4 h. Upon uptake and fusion, BlaM enzyme is translocated to the cytoplasmic compartment of the recipient cell. Afterwards, cells were loaded with CCF4-AM, a fluorescent dye with β -lactam moiety, which is trapped upon ester hydrolysis as CCF4 within the cell. Only inside BlaM loaded cells, the substrate CCF4 is then cleaved enzymatically, causing a fluorescence shift, which can be quantified via flow cytometry on a single cell level, as first described in the context of HIV-1,^[92] and later also for other viruses.^[91,93-97] As described, hACE2⁺ Vero cells were incubated with a panel of CD63~BlaM⁺, concentrated S⁺ EV, VSV-G⁺ EV, EV lacking a viral fusion protein (Δ vFPEVs) and a medium control without EVs. Upon substrate incubation, cells were analyzed for cleaved CCF4 (Figure 11A). The hACE2⁺ Vero cells displayed cleavage of CCF4, and thus uptake, with S⁺ EVs and VSV-G⁺ EV, but not with Δ vFPEV. Yet, only about 23% of Vero cells turned BlaM-positive with a high dose of S⁺ EVs, while significantly more, 75% of all cells became positive with VSV-G⁺ EV (Figure 11C left chart). Fusion of EVs with recipient cells was furthermore found to be dose dependent and limited by the concentration of added EVs, as shown in a titration experiment (Figure 11C right chart).

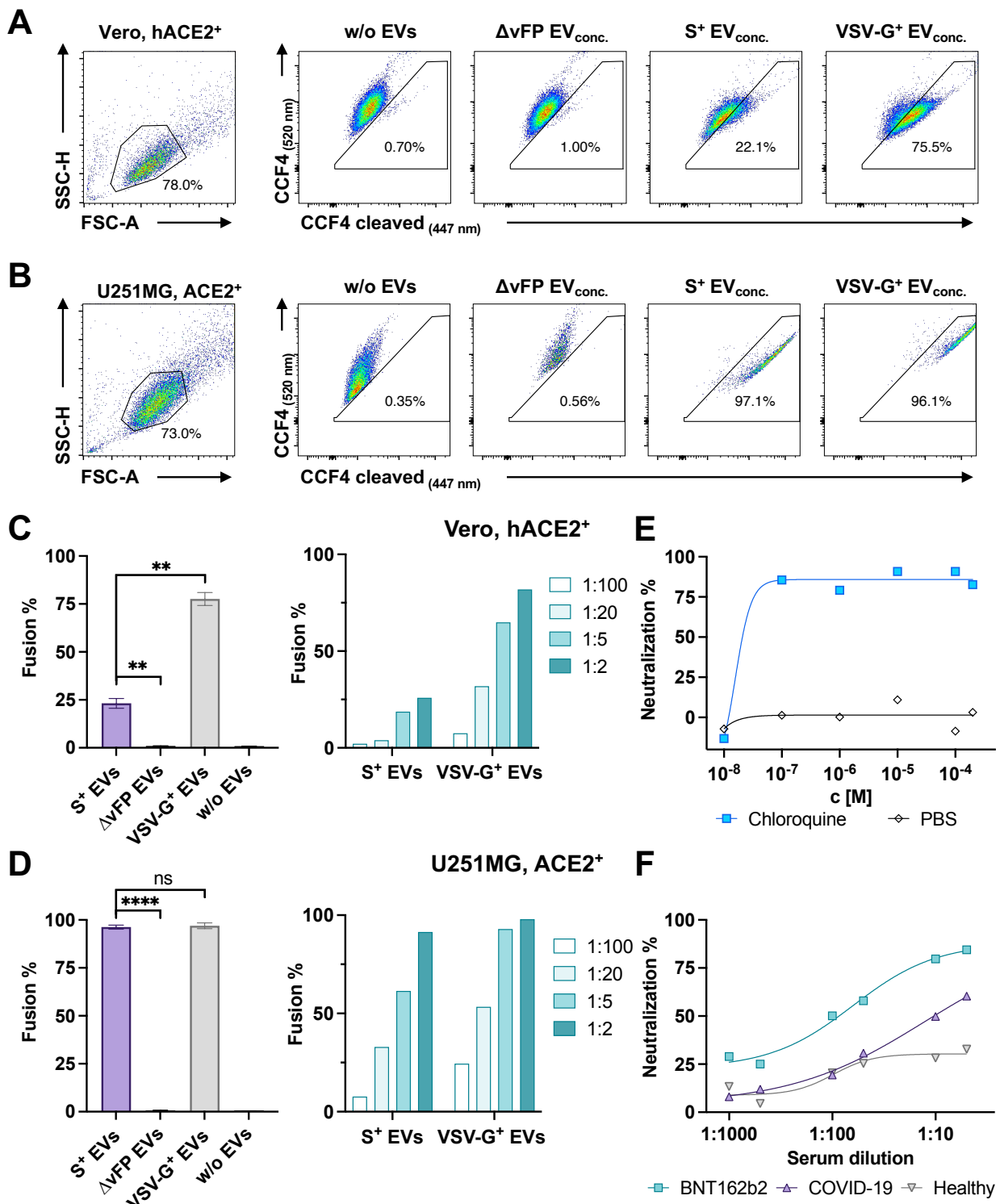


Figure 11. Fusion analysis of S⁺ EVs with single-cell BlaM readout.

Extracellular vesicles (EVs) bearing viral fusion proteins and a chimeric reporter protein, consisting of β -lactamase (BlaM) fused to the carboxy-terminus of human CD63, were incubated with recipient cells and subsequently analyzed by flow cytometry. CD63~BlaM, which is efficiently incorporated into the membrane of EVs, is transferred to the cells' cytoplasm upon fusion, where it cleaves the fluorescent dye CCF4 as substrate, thereby altering the emission spectrum of cells.

(A, B) Flow cytometry plots show the gating and analysis of substrate loaded intact Vero (panel A) and U251MG cells (panel B), engineered to express human ACE2. Cells were either incubated without (w/o) EVs or with concentrated (conc.) CD63~BlaM⁺ EVs bearing: S, VSV-G, or without viral fusion protein (Δ vFP) at all. Fractions of cells which have successfully taken up EVs are indicated in percent.

(C, D) Data from four biological replicates, as in A and B, are summarized and graphically displayed in the left charts. U251MG, ACE2⁺ (panel D) were found to be better targets for S⁺ EVs than hACE2⁺ Vero cells (panel C). Results from t-tests are indicated; ns, not significant ($p > 0.05$); ** $p \leq 0.01$; **** $p \leq 0.0001$. In the right charts, dilutions (1:2 to 1:100) of conc. S⁺ and VSV-G⁺, CD63~BlaM⁺ EVs were incubated with recipient cells, to demonstrate the respective dose-response relationship.

Figure 11. continued from previous page.

(E) Fusion of S⁺ EVs with hACE2⁺ Vero cells was efficiently inhibited by a low concentration (c) of chloroquine, indicative of the endosomal uptake.

(F) Neutralization experiments with three human sera, using ACE2⁺ U251MG cells and S⁺ EVs, are shown. Specimens of an individual vaccinated with BNT162b2, a COVID-19 convalescent patient and a naive and healthy donor are compared. Parts of this figure and its legend were adapted from Roessler *et al.* 2022,^[48] under CC BY 4.0.

With ACE2⁺ U251MG cells, the panel of EV preparations resulted in a similar profile of susceptibility (Figure 11B), yet in contrast to hACE2⁺ Vero cells, 97% of ACE2⁺ U251MG cells became BlaM-positive with S⁺ EVs, while cells incubated with Δ vFP EVs remained again BlaM-negative. Moreover, fusion of S⁺ EV and VSV-G⁺ EV was found to be equally efficient in this setting (Figure 11D left chart). Even though, the respective titration later revealed a saturation effect for VSV-G⁺ EV, which had masked their better fusogenicity (Figure 11D right chart), fusion of S⁺ EV with ACE2⁺ U251MG recipient cells was found to be superior compared to hACE2⁺ Vero cells (Table 1).

Table 1. Comparison of Vero and U251MG cells as recipients for BlaM⁺ EVs.

CD63~BlaM⁺, concentrated S⁺ EVs and VSV-G⁺ EVs were diluted and incubated with hACE2⁺ Vero or ACE2⁺ U251MG cells. Upon turnover of substrate, portion of fusion among cells was quantified via flow cytometry. Values from the right charts of Figure 11C, D are listed.

Dilution [1:]	Fusion with cells in %			
	hACE2 ⁺ Vero		ACE2 ⁺ U251MG	
	S ⁺ EV	VSV-G ⁺ EV	S ⁺ EV	VSV-G ⁺ EV
100	2	8	8	24
20	4	32	33	53
5	19	65	61	93
2	26	82	91	98

To test the fusion of S⁺ EV with hACE2⁺ Vero cells for the endosomal uptake route, cells were pre-treated with chloroquine prior to incubation with S⁺ EVs (Figure 11E). Chloroquine deacidifies endosomes and inactivates the endosomal-pH-dependent cysteine protease CTSL, which primes S for SARS-CoV-2 entry *in vitro*, in certain cell lines.^[13,65,66] As delivery of BlaM was efficiently inhibited by the drug, S⁺ EV fusion was found to be dependent on endosomal processing of S in Vero cells. Next, ACE2⁺ U251MG cells were used in a preliminary neutralization experiment, to test and quantify the reduced uptake of S⁺ EVs by neutralizing serum antibodies. Sera from a COVID-19 vaccinee and a COVID-19 convalescent patient displayed dose-dependent neutralization, while sera from a healthy and naive donor barely showed any effect (Figure 11F). Therefore, it was concluded that all steps of the S-mediated cellular uptake of S⁺ EVs are highly reminiscent of the initial steps of a SARS-CoV-2 infection.

To investigate the tropism of S bearing particles on a single cell level more thoroughly, confocal fluorescence microscopy was conducted with the ACE2⁺ and an ACE2⁻ U251MG cell line. While for the experiments with flow cytometry readout CD63~BlaM⁺, S⁺ EV have been used, here CD63~BlaM⁺, S⁺ VLP were used, which additionally contain M, N

and E. In detail, ACE2^{+/-} U251MG were incubated with S⁺ VLP or medium as negative control and loaded with CCF4 substrate or alternatively permeabilized and stained with a fluorescently labeled anti-S mAb and a DNA dye before imaging (Figure 12). When analyzed for the presence of S, the antibody did not display any background signal on the cells for the sample without S⁺ VLP, yet showed distinct foci in the samples with S⁺ VLP, mostly around the nuclei, but distributed all over the cell. Thus, detected foci were found to be specific for S, but occurred independently of the ACE2 status of the target cell. As the S signal could originate from intracellular S, as well as from S on the outside of the cell, a possible explanation for this phenomenon could be that at least for the ACE2⁻ cells, the S⁺ VLP were stuck on the cell membrane. To analyze the cells for S⁺ VLP entry and fusion via the translocated BlaM, substrate- and cleavage product channels were evaluated separately. While cells in all samples were found to be equally loaded with CCF4 substrate, turnover and cleaved CCF4 were only observed in the combination of ACE2⁺ cells with S⁺ VLP, but

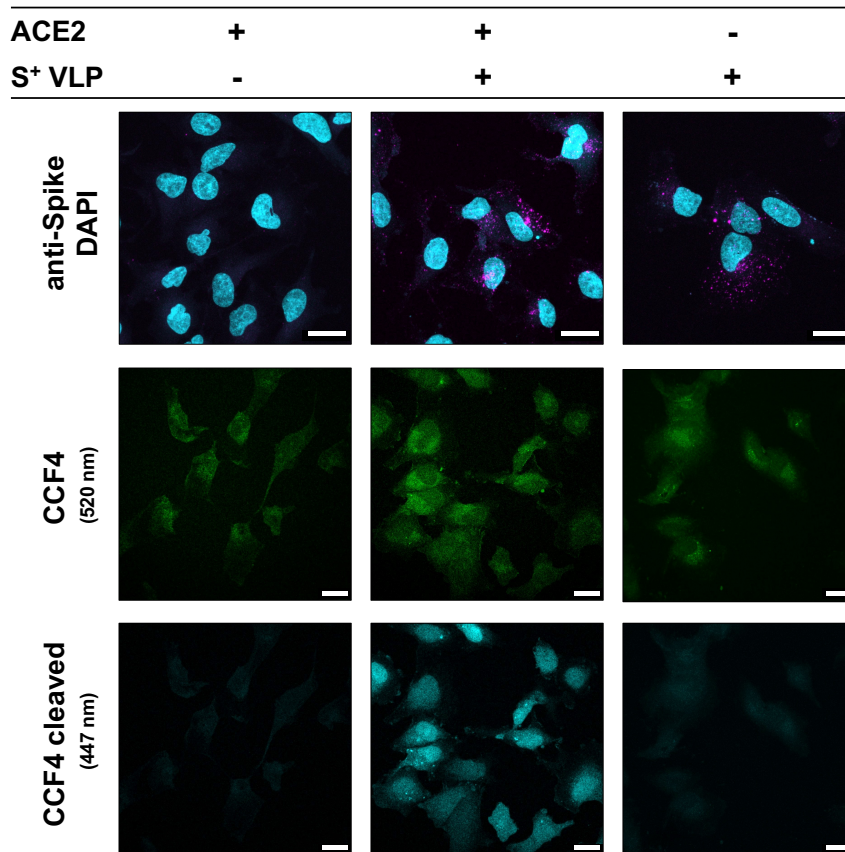


Figure 12. Confocal fluorescence microscopy with S⁺ VLPs.

SARS-CoV-2 VLPs were incubated with U251MG ACE2^{+/-} cells and analyzed by laser scanning confocal microscopy (LSCM) for entry and S signal. Therefore, S⁺ VLPs (S, M, N, E and CD63~BlaM)⁺ were generated, incubated with target cells, grown on slides, and cells subsequently stained with CCF4, a β -lactamase (BlaM) cleavable fluorescent dye. Pairs of identical images, either filtered for substrate emission (middle row) or product emission (bottom row), are shown. Efficient entry, as identified in the form of CCF4 turnover by CD63~BlaM⁺, S⁺ VLPs was only observed on ACE2⁺ cells (middle column), while samples without S⁺ VLPs (left column) or with ACE2⁻ cells (right column) did only yield background signals in the product channel. Alternatively, cells were stained with a fluorescently labeled anti-S mAb, 43A11, and DNA intercalating DAPI. Images of the respective individual channels were merged (top row). There, S specific signal, colored in pink, was observed independently of the ACE2 status of target cells. White scale bars indicate 20 μ m.

not with ACE2⁻ cells or the sample without S⁺ VLP. Thus, exclusively ACE2⁺ cells were found to be susceptible for S⁺ VLP entry.

2.4.2 VLPs with Nanoluciferase Readout

The applicability of the assay with BlaM is limited as its readout relies on flow cytometry or fluorescence microscopy, requires an overnight incubation step for the intracellular accumulation of cleaved CCF4 and depends on concentrated S⁺ EVs preparations. Therefore, this assay was developed further to a bioluminescence based readout by replacing BlaM with nanoluciferase (nLuc). To avoid expected background problems due to protein leakage of intact nLuc, its split variant consisting of an incomplete and inactive nLuc polypeptide (LgBiT) and a self-associating peptide of 11 amino acids (HiBiT) was adapted.^[98-100] Similar to CD63~BlaM, the activator HiBiT was fused to the C-terminus of CD63 (CD63~HiBiT),^[101] to be incorporated into S⁺ particles. As recipient cells, ACE2⁺ U251MG cells were engineered to constitutively express *N*-myristoylated LgBiT (NM~LgBiT) as membrane-associated reporter enzyme. Since both, LgBiT and HiBiT are tightly associated with the cellular and vesicular membrane, respectively and thus cannot be secreted, the system is almost free of leakage. Fully active enzymes can be problematic as reporter proteins because they often result in high background signals. As the split nLuc system requires successful intracellular reconstitution of both nLuc parts to catalyze its substrate,^[98] this assay barely displayed background luminescence. Mechanistically, a CD63~HiBiT⁺ engineered S⁺ particle contacts a recipient cell in an ACE2 receptor-dependent manner, undergoes correct processing of S by proteases and enters the cell by endocytosis followed by endosomal escape. Alternatively, S⁺ particles may directly fuse with the plasma membrane via the post-fusion conformation of S, a process reminiscent of the initial infection with a SARS-CoV-2 virion. Upon fusion, membrane anchored HiBiT is delivered into the cytoplasm of the LgBiT⁺ cell, where the functional enzyme is reconstituted *in situ* to support substrate turnover and emission of light as shown schematically in Figure 13C.^[48] This principle is illustrated in a scientific animation.[†]

This simplified readout allowed to introduce a number of improvements to the fusion assay, as the resulting signal can be detected in a standard luminometer within seconds, without complex prior sample preparation. Even though it only allows for a bulk readout, instead of an analysis on single cell level, it turned out to be much more sensitive, such that even unconcentrated supernatants of S⁺ EV could be used. One additional major breakthrough for suitable S⁺ particle preparations was to investigate the optimal DNA amount of S and CD63~HiBiT encoding plasmids for the transfection of HEK293T cells, in order to generate fusogenic S⁺ EV. Experiments with supernatants from a DNA dose escalation with S plasmid but fixed amount of CD63~HiBiT plasmid, revealed an adverse effect of high amounts of S DNA and a critical optimum of plasmid ratios for fusion with ACE2⁺, NM~LgBiT⁺ U251MG cells (Figure 14A). With the optimized transfection protocol, S⁺ EV and VSV-G⁺ EV were

[†]https://youtu.be/6wckXobT_bM

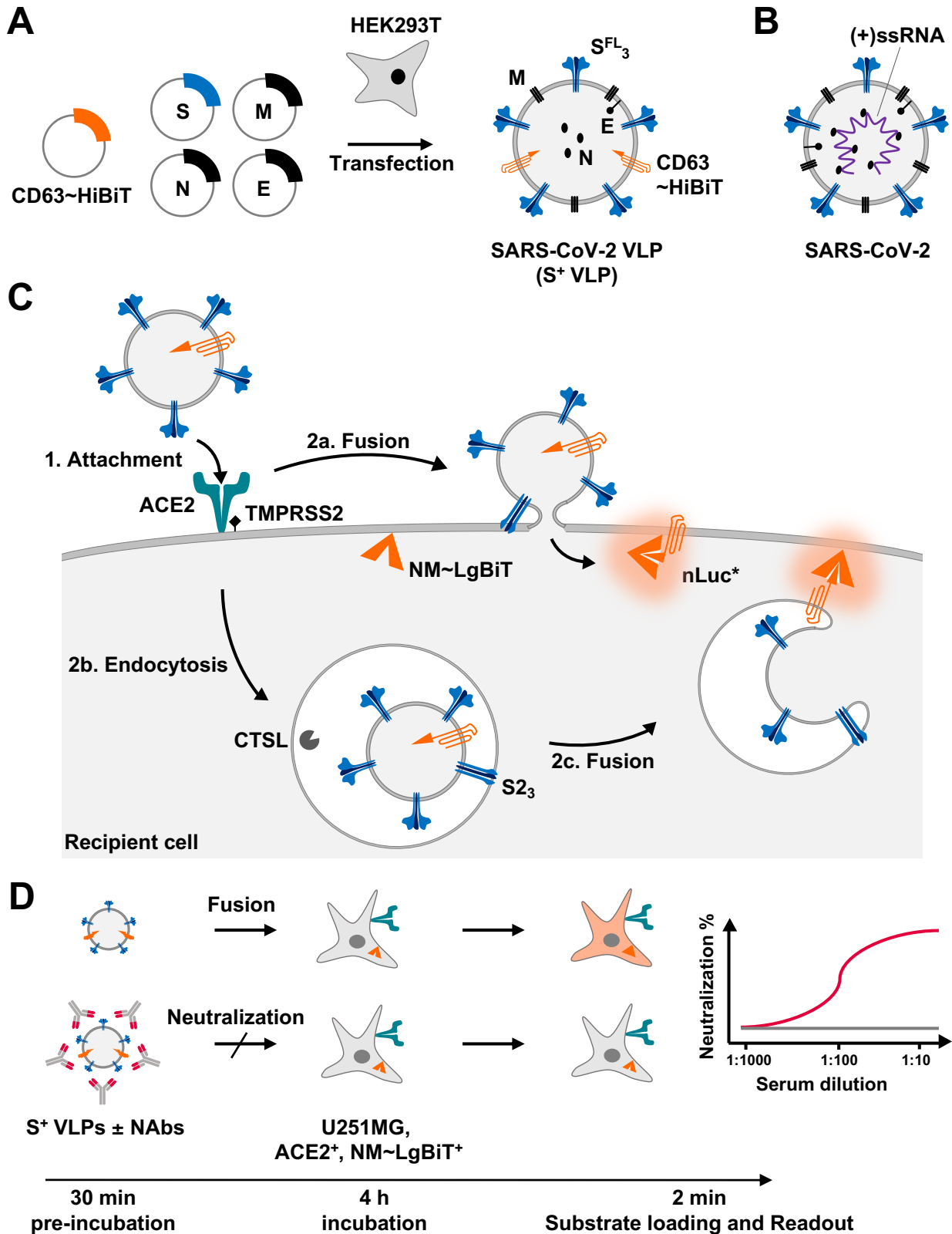


Figure 13. Scheme of S⁺ VLP fusion mechanism and neutralization test, VLPNT.

(A) Engineered VLPs were generated by transient co-transfection of HEK293T cells with an optimized ratio of expression plasmids encoding the four SARS-CoV-2 structural proteins S, M, N, E and a chimeric membrane anchored activator peptide (CD63~HiBiT). The resulting particles were termed S⁺ VLP and obtained from conditioned cell culture medium three days after DNA transfection.

(B) Schematic view of a SARS-CoV-2 virion with the four structural proteins S, M, N and E and the viral genome of positive sense, single-stranded RNA, (+)ssRNA complexed with N.

Figure 13. continued from previous page.

(C) Basic steps of S⁺ VLP entry and reconstitution of nanoluciferase (nLuc). Similar to infection with SARS-CoV-2, spike, the trimeric viral fusion protein in the envelope of S⁺ VLPs mediates attachment (step 1) to the host cell receptor ACE2, triggering either proteolytic processing by TMPRSS2 and direct fusion at the plasma membrane (step 2a) or endocytosis (step 2b), cleavage by CTSL and subsequent fusion with the endosomal membrane (step 2c). Fusion of the S⁺ VLP envelope with cellular membranes via both pathways expose the HiBiT activator peptide to make contact with *N*-myristoylated LgBiT (NM~LgBiT), which is stably expressed in the cytoplasm of the ACE2⁺ target cell. Upon *in situ* reconstitution of the functional reporter (nLuc*), addition of substrate will induce bioluminescence, which can be quantified in a standard luminometer in 96-well cluster plates.

(D) To test samples for the content of SARS-CoV-2 neutralizing antibodies (NAbs) in the VLP neutralization test (VLPNT), S⁺ VLP are pre-incubated with a serial dilution of the specimens for 30 min. Suitable medical samples are sera of COVID-19 patients and vaccinated or naive individuals, but also recombinant NAbs can be evaluated with ease. SARS-CoV-2 NAbs will interfere with all steps of S⁺ VLP attachment to ACE2, receptor-mediated uptake, endosomal fusion of the VLP envelope with the endosome and escape to the cytoplasm. Target cells are U251MG cells engineered to express both ACE2 and NM~LgBiT. Upon encounter with S⁺ VLP-borne CD63~HiBiT, NM~LgBiT is reconstituted into a fully functional nLuc reporter enzyme, which can be quantitated. SARS-CoV-2 NAbs reduce or even block the delivery of CD63~HiBiT activator entirely, which can be quantified in a standard clinical laboratory with aid of a luminometer and within 4.5 h. A freely accessible scientific animation narrates the principle of the VLPNT (https://youtu.be/6wckXobT_bM). This figure and its legend were adapted from Roessler *et al.* 2022,^[48] under CC BY 4.0.

generated, titrated by dilution and incubated with increasing amounts of seeded recipient cells. As expected, higher doses of S⁺ or VSV-G⁺ EVs during the incubation resulted in more emitted light. In parallel, the optimal cell number yielding the best signal to noise ratio was investigated (Figure 14B). In concordance with flow cytometric data for CD63~BlaM⁺ EVs (Figure 11D right chart), VSV-G⁺ EV similarly displayed higher overall fusogenicity than S⁺ EV (Figure 14B). A brief study of stability found S⁺ EV to be surprisingly stable towards thermal inactivation, as treatment at 60°C for 30 min did not impair their fusion capacity (Figure 14C). A loss of fusogenicity was only observed upon incubation at 80°C, suggesting that thermal inactivation of SARS-CoV-2 virus stocks at medium temperatures is rather mediated by e.g. degeneration of the genomic RNA-nucleoprotein complex, than by denaturation of the vFP spike. Next, the readout of the fusion assay was improved by use of a full-white 96-well microtiter plate with measurement from above (Figure 14D, Type 2), instead of a clear-bottom plate with measurement from below (Type 1). Furthermore S⁺ EV particles were replaced with SARS-CoV-2 VLPs, i.e., S⁺ VLPs encompassing all four structural proteins of the virus, as co-expression of M, N and E together with S and CD63~HiBiT (Figure 13A) led to higher particle numbers (Figure 9D) and enhanced fusogenicity of VLPs (Figure 14E). Similarly as in Figure 14A, the optimal stoichiometry of plasmids was also investigated for S⁺ VLP in a readout-based approach. The resulting S⁺ VLPs were shown to resemble SARS-CoV-2 in many aspects as documented by cryo-EM, WB, ELISA, NTA, nano flow technology and confocal fluorescence microscopy, as shown from Figure 7 on to Figure 10 and Figure 12. Luminescence signal in this system was found to undergo rapid decay over time upon addition of substrate (Figure 14F), thus immediate readout was applied for all further experiments.

Analogous to the BlaM reporter system, it was assessed whether S⁺ VLPs fuse exclusively with susceptible ACE2⁺ cells. Therefore, S⁺ VLPs (S, M, N, E, CD63~HiBiT)⁺,

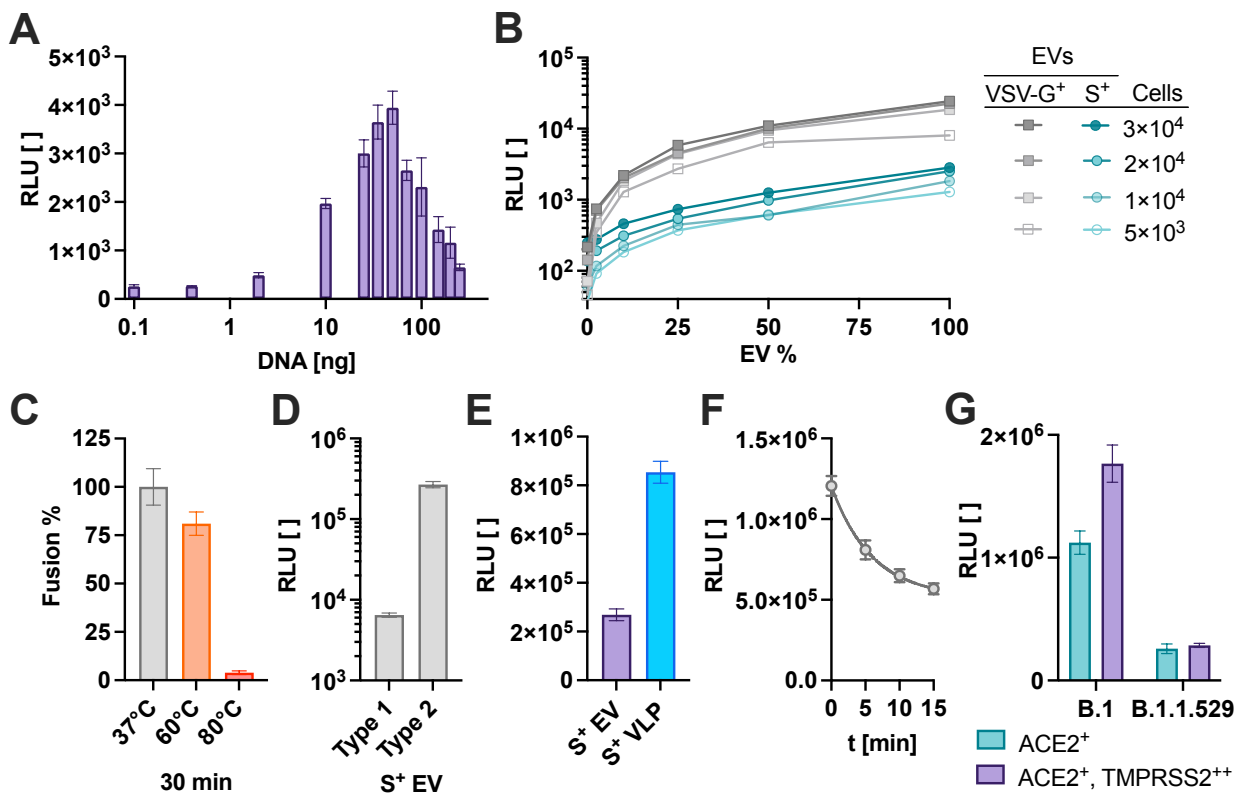


Figure 14. Characterization of the VLP and spike EV fusion assay.

(A) HEK293T cells were transiently transfected with a fixed DNA amount of expression plasmids, encoding CD63~HiBiT and a titration of 100 pg to 0.25 μ g plasmid DNA encoding S. CD63~HiBiT⁺, S⁺ EVs were harvested 72 h post-transfection from conditioned medium of producer cells and incubated with ACE2⁺, NM~LgBiT⁺ U251MG recipient cells. The resulting luminescence was quantified in relative light units (RLU) and reveals an optimum for S encoding plasmid DNA.

(B) Increasing numbers of ACE2⁺, NM~LgBiT⁺ U251MG cells were seeded per 96-well, cultivated overnight, prior to incubation with increasing concentrations of CD63~HiBiT⁺, S⁺ or VSV-G⁺ EV supernatants.

(C) CD63~HiBiT⁺, S⁺ EVs were heat inactivated at three different conditions for 30 min prior to incubation with ACE2⁺, NM~LgBiT⁺ U251MG cells, to test particle stability and functionality. Resulting luminescence was normalized to the 37°C signal.

(D) Two different 96-well plates and measurement techniques were compared in a standard luminometer for their resulting luminescence signal with CD63~HiBiT⁺, S⁺ EVs and ACE2⁺, NM~LgBiT⁺ U251MG cells: Type 1, clear-bottom microtiter plate with measurement from below; Type 2, full-white microtiter plate with measurement from above.

(E) HEK293T cells were transiently transfected with expression plasmids encoding CD63~HiBiT and either S only, giving S⁺ EVs or with additional plasmids encoding S, M, N and E, yielding S⁺ VLPs. Resulting supernatants were incubated with ACE2⁺, NM~LgBiT⁺ U251MG cells and compared for luminescence. Use of S⁺ VLP instead of S⁺ EV resulted in stronger signals and better signal to noise ratio.

(F) CD63~HiBiT⁺, S⁺ VLPs were incubated with ACE2⁺, NM~LgBiT⁺ U251MG cells and luminescence signal decay was quantified 0 to 15 min upon substrate addition.

(G) S(B.1)⁺ and S(B.1.1.529 BA.1)⁺, CD63~HiBiT⁺ VLPs were incubated with TMPRSS2 overexpressing (++) ACE2⁺, NM~LgBiT⁺ U251MG cells and the respective parental cell line. Resulting luminescence was quantified.

VSV-G⁺ EVs (VSV-G, CD63~HiBiT)⁺ and Δ vFP EVs (M, N, E, CD63~HiBiT)⁺ were generated, incubated with ACE2⁺ or ACE2⁻, NM~LgBiT⁺ U251MG cells for 4 h and fusion was quantified for the different target cell lines. As expected, S⁺ VLPs exclusively fused with ACE2⁺ cells but not with ACE2⁻ cells (Figure 15A). Furthermore, fusion relied strictly on the presence of a vFP such as S since Δ vFP EVs were barely taken up. In contrast, VSV-G⁺ EVs fused with ACE2⁺ and ACE2⁻ cells at similar levels due to VSV's broad tropism. To elucidate the entry pathway of S(B.1)⁺ VLPs, cells were pre-treated either with chloroquine or with the serin protease inhibitor camostat-mesylate (Figure 15B), which inhibits TMPRSS2,^[102] and blocks entry of SARS-CoV-2 in certain cell-lines *in vitro*.^[13,65] In contrast to results with Vero cells (Figure 11E), chloroquine did not reduce S⁺ VLP entry into U251MG cells, but camostat-mesylate efficiently inhibited up to 84% of S⁺ VLP entry with an IC₅₀ of 0.09 μ M. Entry of S⁺ VLP in U251MG cells was therefore found to be independent of CTSL and thus the endosomal uptake route and instead to primarily proceed via TMPRSS2 cleavage and direct fusion at the plasma membrane (Figure 13C). Which other protease or what entry pathway drives the remaining 16% of fusion, remains up to speculation, but the matrix metalloprotease (MMP), ADAM17 has recently been suggested to facilitate SARS-CoV-2 entry.^[103]

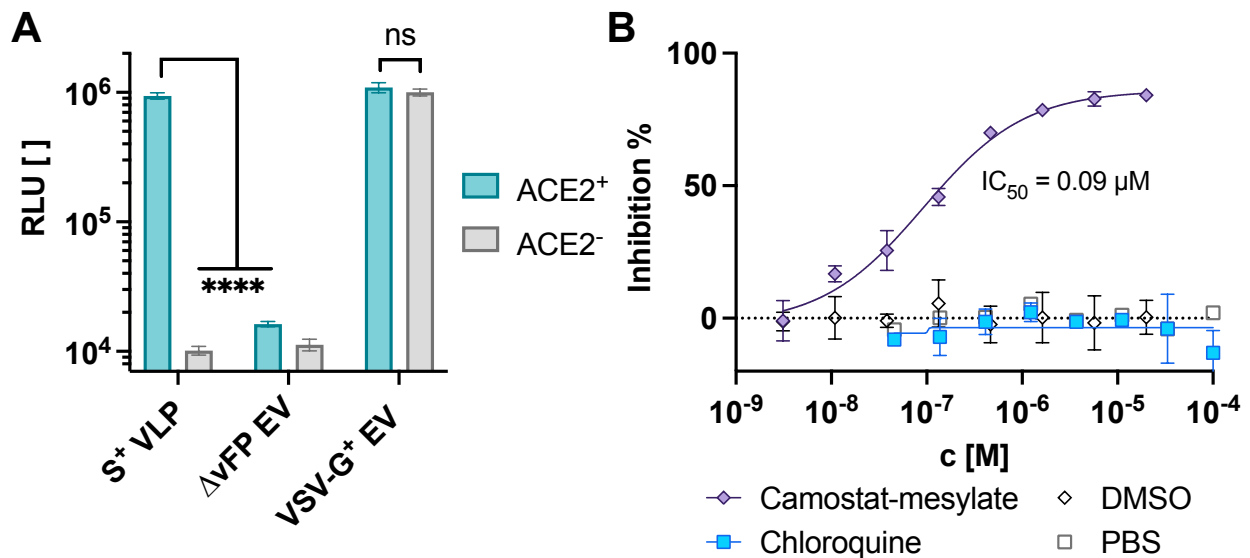


Figure 15. Tropism and specificity of S⁺ VLPs.

(A) Two cell line derivatives of U251MG cells, which express NM~LgBiT with or without human ACE2 receptor (ACE2⁺ or ACE2⁻) were incubated with S⁺ VLPs carrying CD63~HiBiT, with CD63~HiBiT⁺ EVs without a viral fusion protein (Δ vFP EVs) or with CD63~HiBiT⁺ EVs bearing VSV-G. Luciferase activity upon reconstitution of split-nanoluciferase was measured in relative light units (RLU) and validated the exclusive tropism of S⁺ VLPs for ACE2⁺ target cells and the necessity of a viral fusion protein e.g. spike. Data are based on at least four independent experiments. p-values of three independent t-tests are indicated; ns, not significant ($p > 0.05$); **** $p \leq 0.0001$.

(B) Inhibitor studies with chloroquine, an inhibitor of endosomal acidification and of CTSL, and camostat-mesylate, a TMPRSS2 inhibitor, are shown using S⁺ VLPs and ACE2⁺ U251MG cells. DMSO and PBS served as negative controls for camostat-mesylate and chloroquine, respectively. Mean values of three biological replicates are displayed with error bars indicating standard deviations. This figure and its legend were adapted from Roessler *et al.* 2022,^[48] under CC BY 4.0.

As the fusion assay with U251MG cells was shown to largely depend on TMPRSS2, additional overexpression of the protease was thought to enhance S⁺ VLP uptake further. Thus,

ACE2⁺, NM~LgBiT⁺ U251MG were retrovirally transduced with a respective vector and incubated with S(B.1)⁺ or S(B.1.1.529 BA.1)⁺, CD63~HiBiT⁺ VLP. While overexpression of TMPRSS2 did enhance fusion with the B.1 variant, fusion with B.1.1.529 remained unaltered (Figure 14G), suggesting that the latter VOC makes less use of the respective pathway and instead uses alternative ones. Because TMPRSS2 overexpression did not improve the assay for the most recent VOC tested, all further experiments were carried out with the parental cell line, using the endogenous expression level. Other than that, an overall reduced fusion of S(B.1.1.529 BA.1)⁺ VLP with ACE2⁺ U251MG cells was found, compared to S(B.1)⁺ VLP (Figure 14G). Even though this might seem contradictory to early reports of enhanced transmission and the rapid spread of the Omicron variant,^[104] the infectivity of the variant was reported to be reduced, as its fusion efficiency was in fact compromised.^[105] Hence, the increased transmissibility of the Omicron variant was rather an effect of improved S stability,^[105] widespread immune evasion and broad antibody escape.^[36,106]

In sum, results from the fusion assay characterization state that S⁺ VLP fuse with target cells spike-mediated and ACE2-dependent and thus with great specificity. Therefore, this system was concluded to meet important requirements of a VLP-based neutralization test.

2.5 VLP Neutralization Test

NAbs can mediate protection from SARS-CoV-2 infection as they block virion entry into host cells via various modes of action. Most S specific NAbs prevent the attachment of S to ACE2 by binding to the RBM of S1,^[107,108] or stall S in its closed, i.e. RBD ‘down’, pre-fusion conformation.^[109] Yet, some also neutralize without disrupting the interaction with ACE2.^[110] Alternative mechanisms comprise the inhibition of proteolytic processing of S, or the interference with heptad repeats and glycosylated surfaces in S2, which are required to promote fusion of the viral envelope with the endosomal membrane as shown for SARS-CoV or MERS-CoV.^[33,111] NAbs that disrupt the function of S also interfere with or even block S⁺ VLPs and thus reduce the delivery of CD63~HiBiT to susceptible target cells. Consequently, reduction of luminescence from reconstituted nLuc correlates with SARS-CoV-2 neutralization (Figure 13D).^[48]

2.5.1 Serum Analysis

For a VLP neutralization test (VLPNT), a defined amount of S⁺ VLPs was pre-incubated with serial dilutions (starting from 1:10 to 1:1801) of sera from acute or convalescent COVID-19 patients, COVID-19 vaccinees or healthy, naive donors. This mix was then incubated with ACE2⁺, NM~LgBiT⁺ U251MG cells and the resulting dose-dependent neutralization was quantified as shown in Figure 16A. The mean luminescence level of S⁺ VLPs with PBS instead of serum, was set to 0% neutralization, while background luminescence obtained with Δ vFP EVs was defined as 100% neutralization. A 50% neutralization titer was determined

by extrapolating sigmoidal curve values that correspond to 50% absolute signal reduction upon background correction. This value was termed $VLPN_{50}$. It is considered equivalent to VNT_{50} and $PRNT_{50}$ of cVNTs and PRNTs, respectively.^[48] Sera of naive donors resulted in little to no signal reduction, i.e., weak neutralization even at high serum concentrations. Of 12 sera from healthy, naive donors obtained from mid 2019 and earlier, most did not reach 50% neutralization and few showed $VLPN_{50}$ titers of 1:16 or lower (Figure 16B). Sera of 13 COVID-19 vaccinees after prime-boost immunization from 2021 showed high neutralization potential consistently up to 100% inhibition of S^+ VLP fusion and $VLPN_{50}$ titers of 1:27 to 1:352 (Figure 16B).^[48] Data on individual titers and types of vaccines which the donors received can be found in Supplementary Figure S1B and Supplementary Table S2. Based on the maximal titer of naive sera in the VLPNT, an additional margin was added and a preliminary minimal cutoff of $1: \geq 25$ defined to classify samples with neutralizing activities. Since individual laboratories use various versions of SARS-CoV-2 VNTs, there is considerable demand for a global harmonization and standardization of NAb titers.^[112] Thus, the WHO supplies research facilities with a plasma standard, pooled from 11 British reconvalescent COVID-19 patients.[‡] This standard (NIBSC 20/136), which has a defined neutralization activity of 1000 international units per mL ($IU\ mL^{-1}$), was applied. $VLPN_{50}$ values of multiple individual experiments with the WHO standard were obtained (Figure 16B) and used to convert the serum $VLPN_{50}$ titers to harmonized titers expressed as $IU\ mL^{-1}$ as shown in Supplementary Figure S1C. In six independent VLPNT experiments (including separate S^+ VLP batches) with the WHO standard, a coefficient of variation (CV) for \log_{10} transformed titers of $CV = 0.04$ and $CV = 0.23$ for untransformed titers was calculated, for the within-laboratory repeatability and the resulting imprecision of quantification, respectively.^[48] Clearly, additional experiments and standardizations have to be conducted to generate data for an assessment according to the Clinical Laboratory Standards Institute (CLSI) guidelines.^[113] Based on these results it was concluded that the VLPNT qualifies for the measurement of neutralizing activities in additional clinical samples.^[48]

2.5.2 Correlation of VLPNT and cVNT

For the validation of the VLPNT, $VLPN_{50}$ titers of a defined set of sera were compared with results from a cVNT using infectious SARS-CoV-2, the ‘gold standard’ in the field.^[46] To this end, 80 well documented serum samples from 49 patients with confirmed SARS-CoV-2 infection were tested under double-blinded, randomized conditions in the VLPNT. Relevant details about their clinical status and neutralizing serum titers data are presented in Supplementary Table S2. When analyzed, $VLPN_{50}$ serum titers of the 80 COVID-19 sera varied from 1:15 to $1: >2000$ and therefore scattered wider than serum titers from vaccinees, even though the medians were similar (Figure 16B). Data on the individual titers and the patients’ clinical symptoms can be found in Supplementary Figure S1A. Due to the previously defined cutoff of $1: \geq 25$ for the $VLPN_{50}$, 75 out of 80 COVID-19 samples were classified as neutral-

[‡]Mattiuzzo *et al.*, 2020, WHO/BS/2020.2403

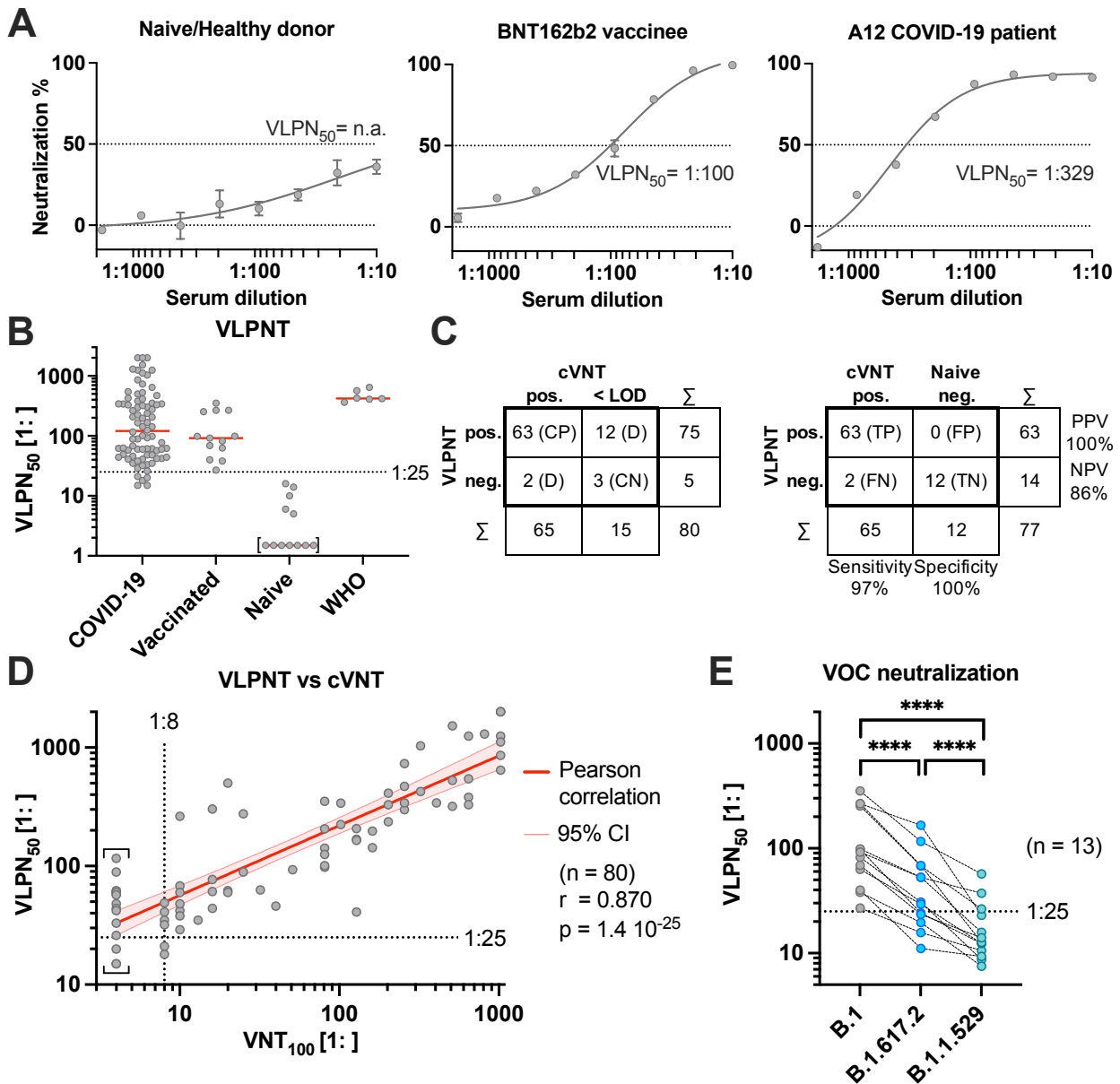


Figure 16. VLP neutralization test validation.

(A) Sera of three individuals, a naive healthy donor, a BNT162b2 vaccinee and the COVID-19 patient A12 were analyzed in the VLP neutralization test (VLPNT) with S(B.1)⁺ VLPs. Graphs are exemplary and include mean neutralization results from three independent biological replicates. Serum dilution which resulted in 50% signal reduction, equivalent to neutralization, was extrapolated and termed VLPN₅₀ titer.

(B) VLPN₅₀ titers of sera from 80 COVID-19 patients, 13 COVID-19 vaccinees, 12 healthy naive donors and 6 independent replicates of the WHO convalescent COVID-19 reference serum (NIBSC 20/136), tested in the VLPNT with S(B.1)⁺ VLPs, are shown. Median values are indicated in red. Titers above the dotted line ($1: \geq 25$) indicate samples which scored positive for S specific neutralizing antibodies according to the criteria applied. Titers in square brackets indicate sera with VLPN₅₀ below the limit of detection (LOD).

(C) In the left panel, results of 80 COVID-19 samples tested in the VLPNT and a cVNT are compared. Concordant positive (CP), concordant negative (CN), and discrepant (D) results are indicated. In the right panel, sensitivity, specificity, positive predictive value (PPV) and negative predictive value (NPV) of the VLPNT were calculated based on the 65 COVID-19 serum samples with neutralizing capacity, according to the cVNT and 12 serum controls of healthy naive donors collected prior to mid 2019. Test results are indicated as: pos., positive; neg., negative; < LOD, below limit of detection; TP, true positive; FN, false negative; FP, false positive; TN, true negative.

(D) Correlation of VLPN₅₀ titers from the VLPNT versus VNT₁₀₀ titers obtained in a conventional virus neutralization test (cVNT) using infectious SARS-CoV-2. Pearson correlation data (coefficient r , confidence interval CI, sample size n and p -value) of 80 sera from confirmed COVID-19 patients are shown and the linear relationship is indicated. Data below the dotted horizontal line denote sera which scored negative in the VLPNT. Results left of the dotted vertical line denote sera which scored below the limit of detection ($1: < 8$) in the cVNT; these VNT₁₀₀ values were defined as 1:4 and indicated in square brackets.

Figure 16. continued from previous page.

(E) Adaptation of the VLPNT to two SARS-CoV-2 variant of concerns (VOCs). VLPs were generated bearing either B.1 (Wuhan-2019, D614G), B.1.617.2 (Delta-VOC) or B.1.1.529 BA.1 (Omicron-VOC) S protein, besides M, N, E, and CD63~HiBiT and used in the VLPNT. NABs in sera of 13 COVID-19 vaccinees (after prime-boost vaccination) were cross-neutralizing, but less potent in neutralizing B.1.617.2 compared with B.1. The majority of serum samples however, failed to neutralize the B.1.1.529 variant effectively. Data derived from 13 samples were analyzed using a matched one-way ANOVA, with Tukey’s multi comparison test and a single pooled variance. Results are indicated: **** $p \leq 0.0001$. Parts of this figure and its legend were adapted from Roessler *et al.* 2022,^[48] under CC BY 4.0.

izing. The 80 COVID-19 samples were also tested in a cVNT with replication competent SARS-CoV-2 virus,^[114] in an accredited laboratory for medical laboratory diagnostics.[§] The titers were determined based on 100% reduction of CPE (VNT_{100}) and their values ranged from 1:8 to 1:>1024 (Figure 16D). In the cVNT, 65 out of 80 samples were found to have neutralizing activity with VNT_{100} 1: \geq 8, while the 15 remaining sera performed below the limit of detection (LOD) and were set to 1:4 per definition.^[48]

To compare the VLPNT with the cVNT directly, $VLPN_{50}$ titers of all 80 COVID-19 samples were correlated with the respective VNT_{100} titers (Figure 16D). The Pearson coefficient of \log_{10} transformed data ($n = 80$) revealed a highly significant positive correlation ($r = 0.870$ and $p = 1.4 \times 10^{-25}$). These results indicate that the VLPNT is not only a qualitative test for the *in vitro* diagnostics of NABs but also reliably quantitates them, faithfully reflecting titers obtained in a cVNT with infectious SARS-CoV-2. A comparison of the 80 COVID-19 samples in both tests found 63 sera to be concordant positive (CP), 3 were concordant negative (CN), whereas 14 sera were found to be discrepant (D) (Figure 16C, left table). This discrepancy likely resulted from experimental differences between the two tests.^[44] The multi-cycle cVNT relies on 100% reduction of CPE (VNT_{100}) while the VLPNT is single-cycle and scores at 50% reduction of S^+ VLP fusion ($VLPN_{50}$) suggesting that the latter test is more sensitive and identifies serum samples with weakly neutralizing activities. Given this uncertainty, the calculation of sensitivity and specificity of the novel VLPNT was based on clearly attributable positive (neutralizing) and negative (non-neutralizing) specimens, using the 65 COVID-19 samples which scored above the LOD in the cVNT along with 12 sera from healthy, naive donors from mid 2019 and earlier (Figure 16C, right table). Of the 65 positive samples, the VLPNT classified 63 samples true positive (TP), while all 12 negative sera were considered true negative (TN). Therefore, the sensitivity of the VLPNT was calculated to be 97%, while its specificity was 100% (Equation 3 and 4). Based on the analyzed data set ($n = 77$), the positive predictive value (PPV) of the test was 100% and the negative predictive value (NPV) 86% (Equation 5 and 6), suggesting that the SARS-CoV-2 VLPNT has the potential to become a reliable diagnostic tool.^[48]

$$Sensitivity = \frac{TP}{TP + FN} \quad (3)$$

$$PPV = \frac{TP}{TP + FP} \quad (5)$$

$$Specificity = \frac{TN}{FP + TN} \quad (4)$$

$$NPV = \frac{TN}{FN + TN} \quad (6)$$

[§]DIN EN ISO 15189

2.5.3 Test Adaptation to Variants of Concern

Additionally, the VLPNT was adapted to test and compare three VOCs of SARS-CoV-2, with spike proteins from strains B.1 (Wuhan-2019, D614G), B.1.617.2 (Delta) and B.1.1.529 BA.1 (Omicron) to generate respective S⁺ VLPs. Their comparison necessitated an ‘inter-variant’ normalization of S⁺ VLP, which was achieved by dilution of stocks, to equal RLU. To reassess an effective normalization, the pan-variant NmAb 35B12 was employed (Figure 17). The resulting VLPN₅₀ of 0.9 to 1.1 nM for all three variants allowed to calculate a CV = 0.11 in-between variants. Then, all 13 sera of COVID-19 vaccinees (Figure 16B) were re-tested in the VLPNT with S(B.1.617.2)⁺ and S(B.1.1.529)⁺ VLPs, their VLPN₅₀ titers determined and compared to titers obtained with the B.1 variant (Figure 16E). Pearson coefficient of log₁₀ transformed data (n = 13) was calculated and showed strong positive correlation for B.1 vs. B.1.617.2 (r = 0.911; p = 1.5 × 10⁻⁵) and a reduced correlation for B.1 vs. B.1.1.529 (r = 0.700; p = 0.0077).^[48] Apparently, NAbS induced by different COVID-19 vaccines based on Wuhan-2019 spike cross-neutralized VOC B.1.617.2, but failed to cross-neutralize VOC B.1.1.529 efficiently. Further, neutralization titers significantly differed in-between variants as shown by a matched one-way ANOVA of log₁₀ transformed data (p < 0.0001, n = 13) (Figure 16E).^[48] While the mean titer for B.1 was found to be 1:135, the mean titers for B.1.617.2 (1:52) or B.1.1.529 (1:19) were significantly reduced by factor 0.39 or 0.14, respectively (Supplementary Figure S1D). Notably, of 13 prime-boost vaccinated individuals with B.1 titers above cutoff level (1: ≥25), only three showed some neutralizing activity against Omicron BA.1 indicative of immune escape and reflecting its independent serotype. A reduced capacity of convalescent or vaccinee sera to cross-neutralize B.1.617.2 has been demonstrated previously in a pVNT,^[115] and also in a cVNT.^[116] For B.1.1.529, substantially reduced titers in vaccinated individuals have also been reported using cVNTs.^[35,117] Thus, the findings appear to be consistent with published work. For the WHO serum standard (NIBSC 20/136), a similar progressive reduction of neutralization titers was observed for the three variants (Figure 17). Consequently, the designated titer of the WHO reference serum should be defined specifically for the B.1 strain but redefined for other VOCs. The successful adaptation of the VLPNT to VOCs indicates that the novel test is flexible and versatile to address and answer questions on cross-neutralizing antibodies between existing and future SARS-CoV-2 variants.^[48]

2.5.4 Neutralizing Monoclonal Antibodies

Besides the human sera, a set of anti-S mAbs was analyzed in the VLPNT. Among the four in-house generated COVEV3 anti-S mAbs, 5B9, 35B12 and 42E2 were found to be potently neutralizing S(B.1)⁺ VLP with VLPN₅₀ between 1.1 and 1.9 nM, while 5D1 was found to be non-neutralizing (Figure 17). Additionally, two potently neutralizing recombinant mAbs, REGN10987, imdevimab and REGN10933, casirivimab, with emergency use authorization for the treatment of COVID-19 by the FDA were tested.^[39,56,57] Their VLPN₅₀ were found to be 1.8 and 7.3 nM, respectively, while a human IgG isotype control mAb did not show

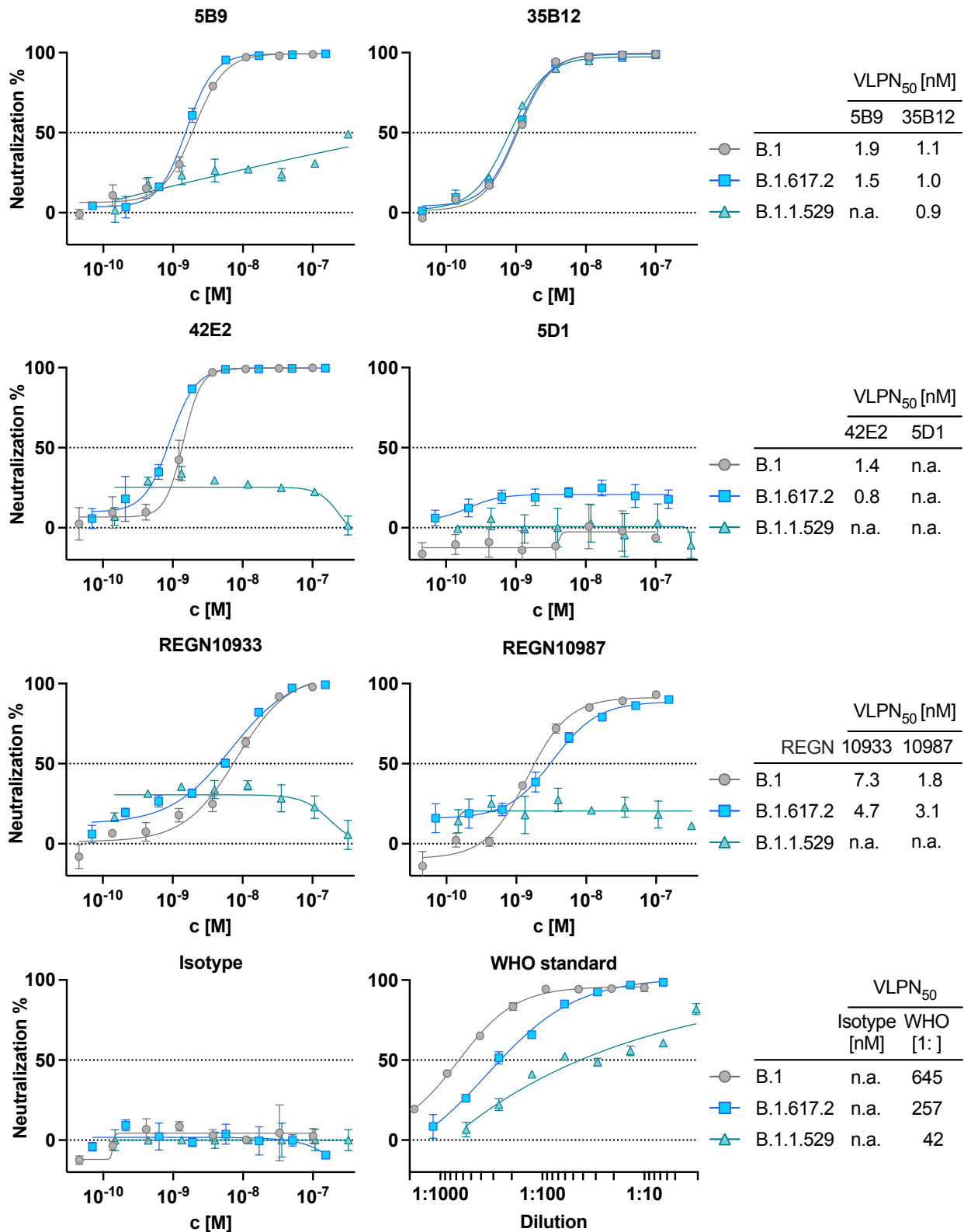


Figure 17. Neutralization capacity of monoclonal antibodies.

Four COVEV anti-S mAbs, two recombinant human mAbs, REGN10987 and REGN10933, a human IgG isotype control and the WHO reference serum (NIBSC 20/136) were analyzed in the VLPNT for their SARS-CoV-2 neutralization capacity against B.1 (S:Wuhan-2019, D614G), B.1.617.2 (Delta-VOC) and B.1.1.529 BA.1 (Omicron-VOC) S⁺ VLPs. Mean neutralization values of three biological replicates are displayed with error bars indicating standard deviations. VLPN₅₀ values were calculated and are listed or indicated as not applicable (n.a.). S⁺ VLP stocks used for VLPNTs were diluted, for inter-batch and inter-VOC normalization, based on adjusted relative light units. S⁺ VLP stocks were then analyzed using the SARS-CoV-2 pan-variant neutralizing monoclonal antibody (NmAb) 35B12. Congruent neutralization curves, further supported by similar VLPN₅₀ values, demonstrate the efficient normalization of VLP preparations. While the NmAbs 5B9, 42E2, REGN10933 and REGN10987 displayed potent neutralization in the assay at low molar concentration (c) for B.1 and B.1.617.2, they failed to efficiently neutralize B.1.1.529. ...

Figure 17. continued from previous page.

... The anti-S mAb 5D1, as well as a human IgG isotype negative control mAb did not show any neutralizing activity. The WHO reference serum for international standardization, showed a successive reduction of neutralization titers following the evolution of SARS-CoV-2 VOCs: B.1 > B.1.617.2 > B.1.1.529. Parts of this figure and its legend were adapted from Roessler *et al.* 2022,^[48] under CC BY 4.0.

any neutralization (Figure 17). Interestingly, the 5B9, 42E2, REGN10987 and REGN10933 antibodies retained their capacity to neutralize B.1.617.2 but failed to neutralize B.1.1.529 effectively. Only 35B12, the NmAb also used for the normalization of S⁺ VLP stocks, retained not only its binding affinity for S(B.1.1.529) (Figure 4A), but also its neutralization capacity (Figure 17) and was therefore found to be a pan-variant neutralizing mAb for the VOCs tested.

2.6 Cell-free Fusion Assay

Even though the VLPNT proved to be a reliable and accurate novel VNT, which gets along without infectious virus, it requires viable cells as recipients for the S⁺ VLP. Living cells complicate *in vitro* diagnostic products (IVDs), as they have to be cultivated appropriately, often increase test variance and worsen reproducibility. Therefore, a further development of the test was drafted, which is independent of cells and uses EVs as recipients. The main premises for such a test were that a VLP could act as a donor and fuse with an EV acceptor and that NAbs can neutralize this fusion (Figure 18). To investigate this, ACE2⁺ EVs had to be generated and equipped with the readout enzyme, which was comprised by the recipient cells beforehand. For an optimal incorporation into EVs, another chimeric reporter was constructed, consisting of CD63 and at its carboxy terminus the LgBiT polypeptide of split-nLuc (CD63~LgBiT). Next, an ACE2⁺ U251MG cell line, which constitutively expresses CD63~LgBiT was generated by retroviral transduction with a respective vector. ACE2⁺, CD63~LgBiT⁺ EVs, naturally released by these cells were then harvested and tested for fusion with S⁺ VLP comprising S, M, N, E and CD63~HiBiT. The resulting strong bioluminescence signal suggested that co-incubation of both particle classes led to receptor attachment, fusion of vesicular membranes and *in situ* reconstitution of functional nLuc and thus VLP-EV fusion. The use of ACE2⁺ EVs as decoy for SARS-CoV-2 virions has recently been suggested in order to block interaction with cellular ACE2,^[118] and preliminary reports also found evidence for fusion of an ACE2⁺ EV with a S-pseudotyped virus particle,^[119] yet the findings presented here might mark a novel concept for VNTs.

As for the cell based assay, it was assessed whether S⁺ VLPs fuse exclusively with susceptible ACE2⁺ EVs via the viral entry factor S. Therefore, S⁺ VLPs (S, M, N, E, CD63~HiBiT)⁺, VSV-G⁺ EVs (VSV-G, CD63~HiBiT)⁺ and Δ vFP EVs (M, N, E, CD63~HiBiT)⁺ were generated, incubated with ACE2⁺ or ACE2⁻, CD63~LgBiT⁺ EVs for 4 h and fusion quantified for the different target EVs. As expected, S⁺ VLPs fused exclusively with ACE2⁺ EVs but not with ACE2⁻ EVs (Figure 19A). Furthermore, fusion relied strictly on the presence of S since Δ vFP EVs did only result in background luminescence values. Surprisingly and in

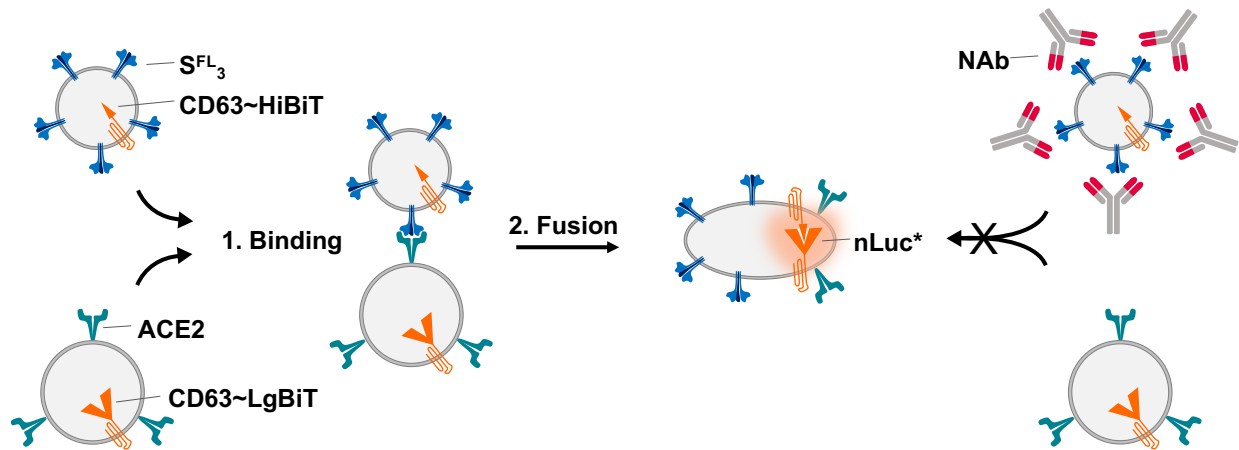


Figure 18. Scheme of cell-free fusion of a S^+ VLP with an $ACE2^+$ EV.

Besides entry into $ACE2^+$ cells, S^+ VLP are capable to fuse with $ACE2^+$ EV, in a fully cell-free manner. Incubation of $CD63\sim HiBiT^+$, S^+ VLPs with $CD63\sim LgBiT^+$, $ACE2^+$ EVs, led to *in situ* reconstitution of functional reporter enzyme (nanoluciferase, nLuc*) and bioluminescence. SARS-CoV-2 VLP fusion with an EV is likely mediated via receptor binding (step 1) and direct fusion of vesicular membranes (step 2), yet can effectively be inhibited by a neutralizing antibody (NAb), blocking the viral fusion protein, spike.

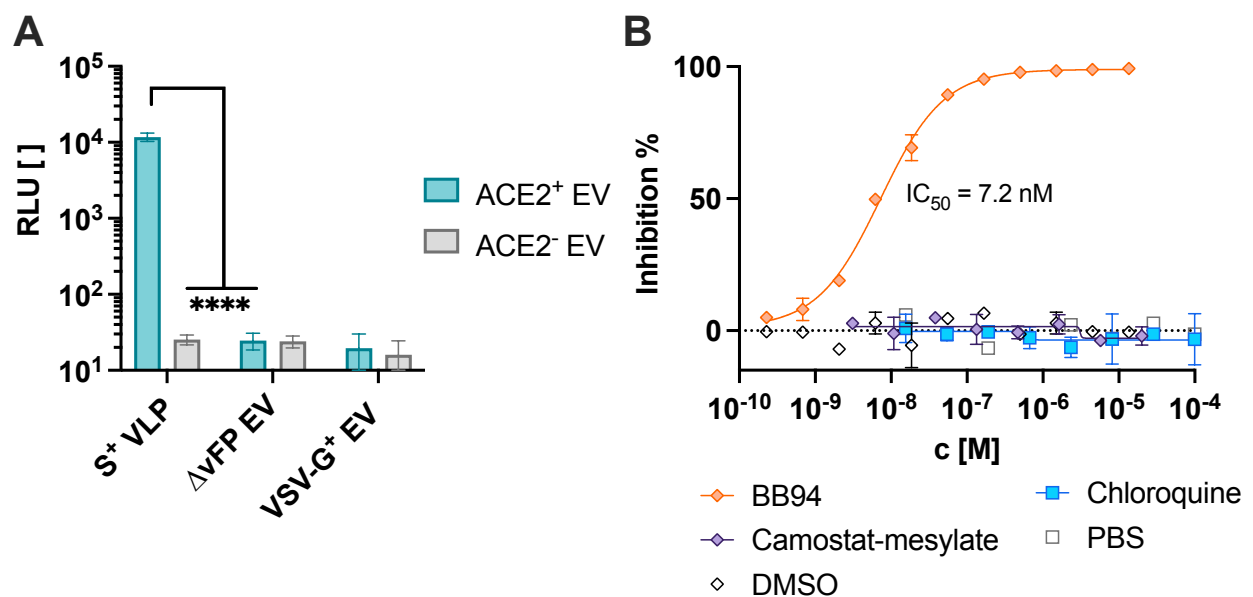


Figure 19. Tropism and specificity of cell-free S^+ VLP and $ACE2^+$ EV fusion.

(A) EVs of two U251MG cell lines, expressing $CD63\sim LgBiT$ with or without human $ACE2$ receptor ($ACE2^+$ or $ACE2^-$) were incubated with $CD63\sim HiBiT$ bearing S^+ VLPs, EVs without a viral fusion protein (ΔvFP EVs) or EVs bearing VSV-G. Luciferase activity upon VLP-EV fusion and reconstitution of split-nanoluciferase was measured in relative light units (RLU) and validated the exclusive tropism of S^+ VLPs for $ACE2^+$ target EVs and the necessity of a viral fusion protein e.g., spike. Data are based on at least four independent experiments. p-values of two independent t-tests are indicated; **** $p \leq 0.0001$.

(B) Cell-free fusion of S^+ VLP and $ACE2^+$ EV was further characterized in an inhibitor study with BB94, batimastat, a broad-spectrum matrix metalloprotease (MMP) inhibitor, camostat-mesylate, a TMPRSS2 inhibitor and chloroquine, an inhibitor of endosomal acidification and of CTSL. DMSO and PBS served as negative controls for BB94, camostat-mesylate and chloroquine, respectively. Mean values of three biological replicates per concentration (c) are displayed with error bars indicating standard deviations.

contrast to results with U251MG cells, VSV-G⁺ EVs did fuse neither with ACE2⁺, nor with ACE2⁻ U251MG EVs. VSV-G, a class III vFP does not require proteolytic priming for fusion but a drop in pH.^[120,121] Yet, also a pH pulse with HCl_{aq.} to pH = 5.0 during the incubation period did not rescue fusion of VSV-G⁺ EV with U251MG EVs. Despite VSV's broad tropism, U251MG EVs seem to lack an appropriate receptor or other co-factors necessary for fusion. Therefore, VSV-G⁺ EV could not be used as positive control in these experiments. Fusion of S⁺ VLP with ACE2⁺ EV was yet demonstrated by a functional readout to be ACE2-specific and S-mediated.

To characterize fusion of S(B.1)⁺ VLPs with ACE2⁺ EVs further, donor and acceptor particle preparations were pre-treated separately either with chloroquine, camostat-mesylyate or with BB94, batimastat, a broad MMP inhibitor,^[122] before incubation with each other (Figure 19B). As chloroquine and camostat-mesylyate did not affect VLP-EV fusion, TM-PRSS2 and CTSL seem to be irrelevant for this process, unlike for fusion with cells, where TM-PRSS2 mediates a large portion (Figure 15B). VLP-EV fusion seems to be catalyzed via yet another protease, as BB94 efficiently inhibited fusion up to 100% with an IC₅₀ of 7.2 nM. Which protease catalyzes S⁺ VLP fusion with ACE2⁺ EVs, and whether it is the same that also accounts for the residual fusion activity with U251MG cells besides TM-PRSS2, remains to be determined. One possible candidate could again be ADAM17.^[103] As a result, fusion of both particles likely takes place via direct membrane fusion, but essentially requires processing by a protease and is not a phenomenon of arbitrary fusogenic particles.

Next, fusion kinetics of the cellular and the cell-free fusion assay were analyzed by incubation of S⁺ VLP with acceptor cells or EVs for various periods of time. After a short lag phase (0 to 5 min), which likely corresponds to an initial association of donor S⁺ VLP to acceptor cells or EVs, luminescence signal above baseline was detected from 15 min onwards and accumulated linearly for both assays (Figure 20A). In both types of fusion assays, B.1.1.529 showed less fusion or slower kinetics than B.1 S⁺ VLP. However, this difference was less pronounced for fusion with EVs instead of cells, which could be a consequence of the difference in protease usage. Also, the limiting component of the cell-free assay was determined by experiments with fixed amounts of S⁺ VLP and a titration of concentrated and unconcentrated ACE2⁺ EV and vice versa. In these experiments, acceptor EVs were found to be the limiting component when working with supernatants. Up to 20 vol% concentrated acceptor EVs those were limiting, before the effect was inverted (Figure 20B, left chart). As acceptor EVs were anyway limiting in the system, use of concentrated S⁺ VLP instead of unconcentrated preparations did alter luminescence less distinct (Figure 20B, middle chart). However, with more than 20 vol% S⁺ VLP of any preparation an adverse effect was observed, suggesting that those contain a soluble interfering substance, which acts inhibitory but cannot be concentrated via ultracentrifugation. When concentrated S⁺ VLP and ACE2⁺ EV preparations were incubated at 50 vol% each to overcome an early shortfall of one component, resulting signal increased 30-fold (Figure 20B, right chart).

To substantiate the thesis of a cell-free VLP-EV fusion, donor and acceptor particles were isolated, characterized and analyzed for fusogenicity. In detail, CD63~HiBiT⁺, S⁺ VLP and

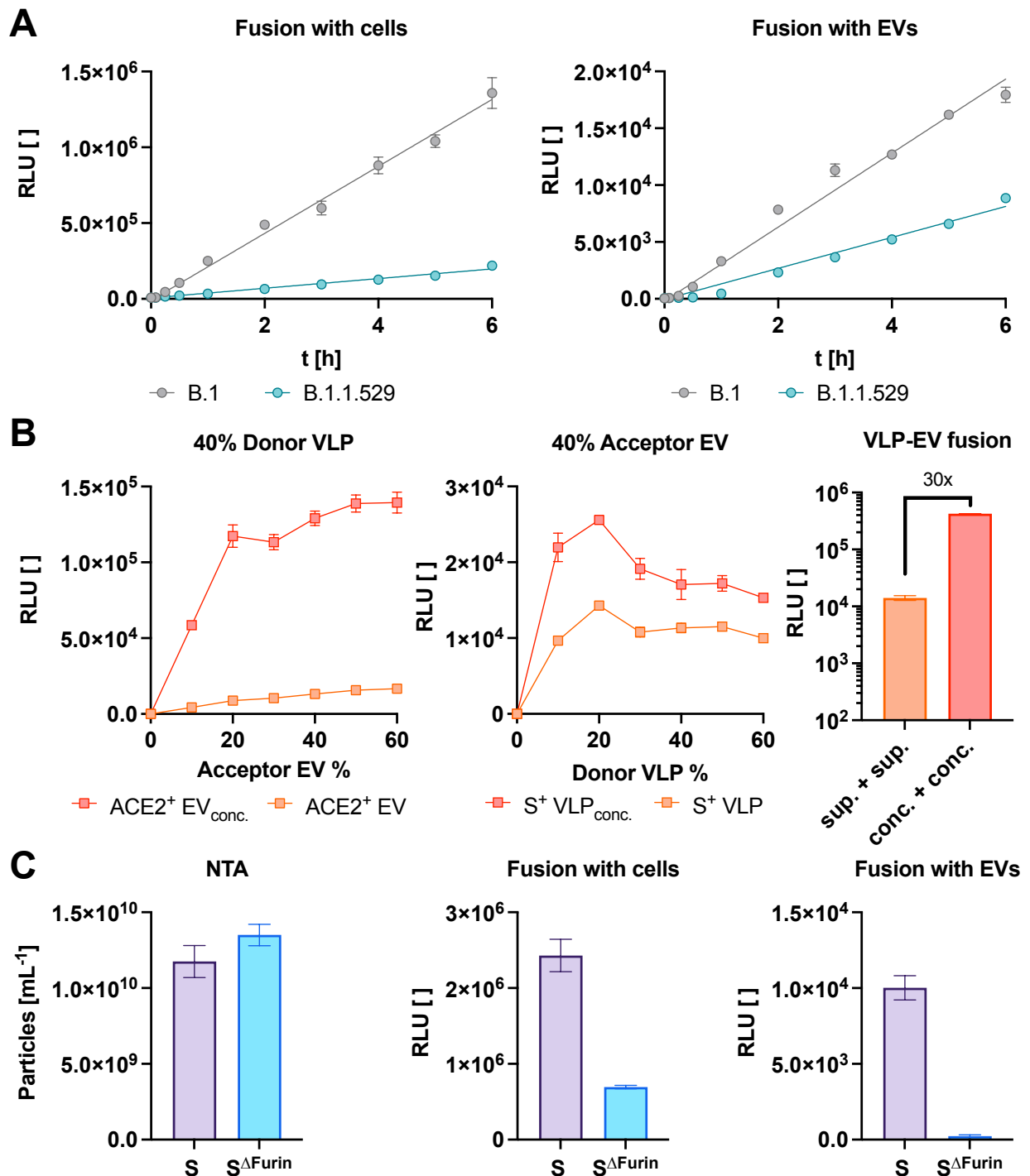


Figure 20. Characterization of the cell-free fusion assay.

(A) Kinetic and time course of B.1 and B.1.1.529 BA.1 S⁺ VLP fusion with ACE2⁺ U251MG cells and ACE2⁺ EVs was resolved by incubation for defined periods of time (t), subsequent addition of substrate and immediate luminescence readout.

(B) Donor and acceptor particles were titrated by incubating a fixed amount (40 vol%) of S⁺ VLP supernatant (sup.) with increasing vol% of concentrated (conc.) and sup. ACE2⁺ EV. Likewise, S⁺ VLP were titrated vice versa for a fixed amount of ACE2⁺ EV. Additionally, equal volumes of S⁺ VLP and ACE2⁺ EV, sup. or conc. preparations were incubated as indicated and relative light units (RLU) measured.

(C) For further mechanistic insight, VLPs bearing a S1/S2 cleavage deficient S protein were generated by expression of a spike mutant with deleted furin site (Δ Furin). S ^{Δ Furin} and control S⁺ VLP were then analyzed by nanoparticle tracking analysis (NTA) for total particle concentration and incubated with ACE2⁺ U251MG cells or ACE2⁺ EV, respectively.

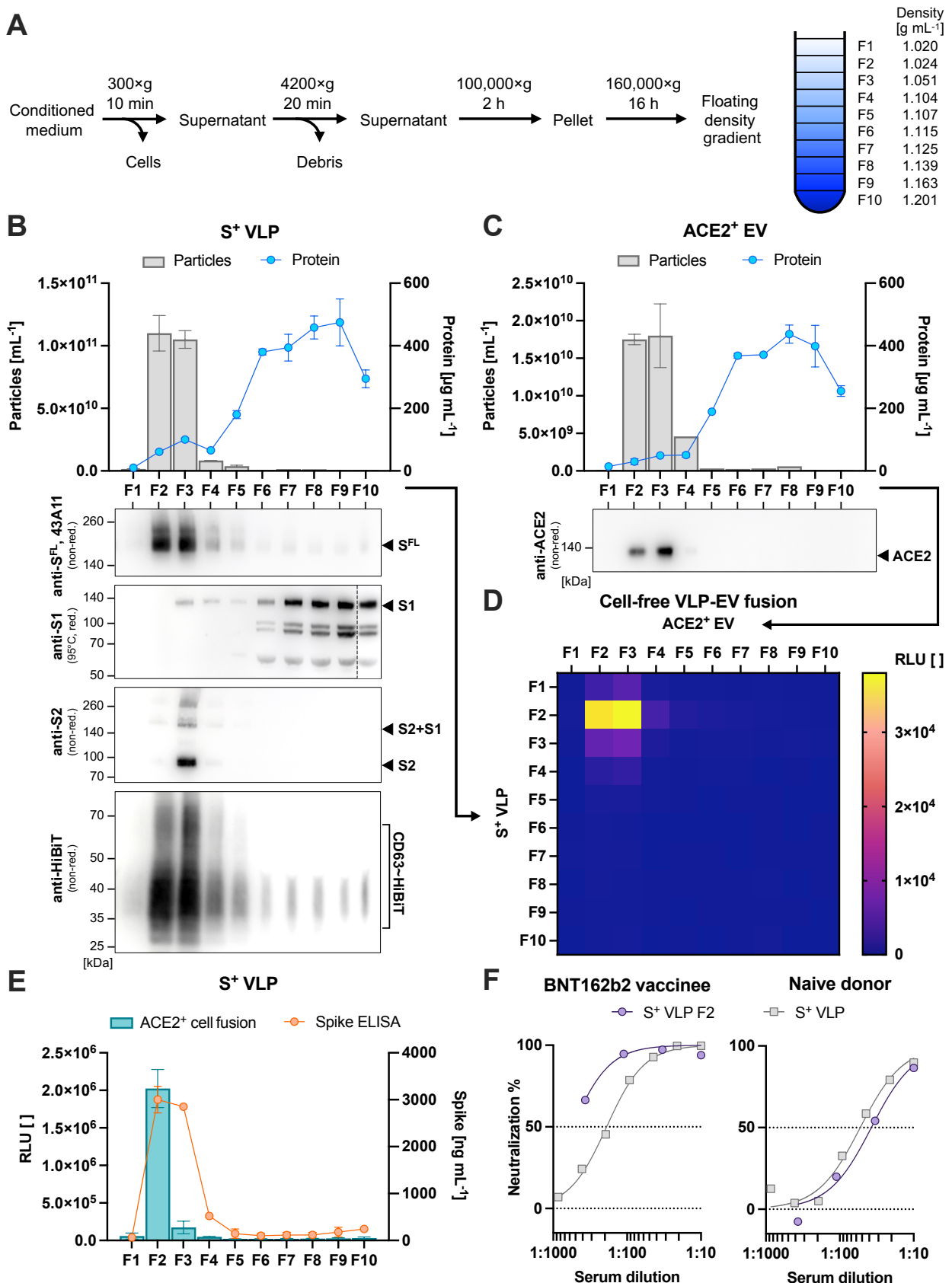


Figure 21. Fractionation of donor and acceptor particles and cell-free fusion assay.

(A) Preparations of S⁺ VLP (CD63~HiBiT⁺) and ACE2⁺ EV (CD63~LgBiT⁺) were purified by sequential centrifugation, ultracentrifugation and fractionation in a density gradient according to their specific weight relative to the medium. Densities of the collected fractions F1-F10 were determined by gravimetric analysis. (B, C) S⁺ VLP and ACE2⁺ EV fractions were examined by NTA and BCA assay for total particle- and total protein concentration accordingly. While the majority of free protein was found in the lower fractions, F2-3 contained most of the particles, i.e. vesicles. Additionally, fractions were analyzed by reducing (red.) and non-reducing (non-red.) WB, using anti-S antibodies specific for full-length (FL) spike, S^{FL} or subunits S1 and S2, as well as antibodies specific for HiBiT or ACE2.

Figure 21. continued from previous page.

(D) Combinations of one S⁺ VLP and one ACE2⁺ EV fraction each were mixed, incubated and analyzed for luminescence. Resulting relative light units (RLU) are visualized in a heat map. Reconstitution of split-nLuc reporter and therefore productive VLP-EV fusion was found to be mainly limited to the particle bearing fractions F2 of S⁺ VLP and F2-3 of ACE2⁺ EV.

(E) F1-10 of S⁺ VLP were further analyzed in the S^{FL} specific sandwich ELISA and the cell-based fusion assay with ACE2⁺, NM~LgBiT⁺ U251MG recipient cells. In concordance with results obtained from the cell-free assay in panel D, fusogenic activity of S⁺ VLP was largely mediated by F2 particles, while S⁺ VLP species in F3 were rather non-functional.

(F) While S⁺ VLP preparations appear to be contaminated with free, soluble, S1 subunit and S⁺ VLP from F3 are rather non-fusogenic, S⁺ VLP from F2 were used as inoculum in a cell-free VLP neutralization test (cfVLPNT), besides raw S⁺ VLP preparations. Serial dilutions of sera from a COVID-19 vaccinee and a healthy, naive donor were pre-incubated with S⁺ VLP and ACE2⁺ EV, before donor and acceptor particles were incubated and analyzed for neutralization. Use of purified F2 S⁺ VLP in a cfVLPNT increased specific neutralization capacity in a neutralizing sample, while slightly decreasing the non-specific neutralization from a naive specimen, thus being potentially beneficial for the sensitivity of the cfVLPNT.

CD63~LgBiT⁺, ACE2⁺ EV were generated from HEK293T and U251MG cells respectively, as described and harvested from conditioned culture media by sequential centrifugation. Upon pre-concentration by ultracentrifugation, pelleted particles were resuspended and purified by rise and floatation in a density gradient according to their specific weight. Subsequent fractionation from top to bottom resulted in ten fractions F1-F10 of various density (Figure 21A), which were analyzed by NTA, BCA assay and WB (Figure 21B, C). For both sample types, physical particles were almost exclusively found in F2 and F3, fractions that correspond to vesicular structures with a lipid membrane and therefore a reduced specific weight. As demonstrated for the unpurified preparations (Figure 9D) and by functional data (Figure 20B, left chart), S⁺ VLP fractions contained substantially more particles than ACE2⁺ EV preparations. While most of the total protein was found from F5 onwards in the dense fractions of the gradient and thus is free and soluble protein, curves also showed a minor peak for the particle containing fractions F2 and F3. Specific protein analysis by WB with the anti-S mAb 43A11 and an anti-HiBiT antibody found S^{FL} and highly glycosylated CD63~HiBiT mainly in F2 and F3 of S⁺ VLP (Figure 21B). Analysis of ACE2⁺ EV with an anti-ACE2 antibody similarly found ACE2 solely in the same fractions (Figure 21C). Thus, S^{FL} and ACE2 were proven to be embedded in vesicular structures, VLP and EV, exclusively. Next, combinations of single S⁺ VLP and ACE2⁺ EV fractions were incubated 1:1 and analyzed for fusion and luminescence (Figure 21D), as previously described for the cell-free fusion assay. As expected, luminescence and therefore fusion of particles was only observed with F2 and F3 of ACE2⁺ EV. Yet surprisingly, solely F2 of S⁺ VLP resulted in a strong signal. F3, which contained identical numbers of particles and was indistinguishable from F2 in the 43A11 and anti-HiBiT WB, did not contain fusogenic S⁺ VLP. Additionally, F1-F10 of S⁺ VLP were analyzed with the quantitative anti-S^{FL} ELISA, which also found identical amounts of S^{FL} protein (Figure 21E) and therefore no difference in F2 and F3. To reassess the finding that only F2 of S⁺ VLP seem to mediate fusion in the cell-free assay, F1-F10 were re-analyzed in the cell-based fusion assay with NM~LgBiT⁺, ACE2⁺ U251MG (Figure 21E). Similarly, also the cellular assay revealed that exclusively F2 of S⁺ VLP were fusogenic, while F3 displayed only minor signals. Thus, F2 and F3 of S⁺ VLP were shown to

be identical with respect to S^{FL} and CD63~HiBiT protein and particle numbers but differ substantially with respect to fusogenicity. S^+ VLP preparations therefore seem to consist of two different subtypes, which appear in fraction F2 and F3. During the applied method of purification, samples are separated according to their specific weight, causing vesicles of lower molecular weight to rise higher than heavier ones. Therefore, F2 S^+ VLP were assumed to be lighter or smaller than the particles contained in F3. In order to investigate the difference in S^+ VLP subtypes, fractions were additionally analyzed by anti-S1 and anti-S2 WB (Figure 21B). While F2 was found to be completely free of cleaved S1 subunit, S2- and VLP-associated S1 was found in F3. Notably, most of the S1 protein and smaller bands of degraded products e.g. RBD, were detected in the fractions from F6 onwards and thus in fractions of high total protein content. Hence, S^+ VLP preparations seem to be largely contaminated with free, soluble S1 subunit. Another difference between F2 and F3 was that cleaved S2 and complexes of associated S2+S1 were mostly found in F3. Taken together, F2 and F3 contain equal amounts of particles and S^{FL} but only F2 S^+ VLP are fusogenic. F3 S^+ VLP on the other hand bear proteolytically cleaved S2 and S1 but appear heavier. These findings seem contradictory, as partial loss of S1 subunits upon priming should result in lighter particles and is thought to enhance fusion.^[10] Even if cleaved S1 would have an inhibiting effect, e.g. by blocking interactions with ACE2, this does not explain the difference in weight.

Experiments with purified S^+ VLP and ACE2⁺ EV ultimately confirmed fusion of donor and acceptor vesicles but raised questions about difference in F2 and F3 S^+ VLP subtypes. Furthermore, analysis revealed a contamination with soluble S1 protein, which is prone to compromise any neutralization of S^+ VLP, as NAbs are likely intercepted by free S1 or RBD instead of S on S^+ VLP. To learn more about the VLP-EV fusion and to make a pragmatic attempt to eliminate free S1 during the VLP egress, a S(B.1) mutant was constructed, $S^{\Delta Furin}$, which contains three amino acid substitutions of arginine to delete the protease site Arg682-Arg683-Ala684-Arg685 (RRAR) of spike.^[7] By replacing the recognition motif of furin and furin-like proteases, cleavage at the S1/S2 site was impeded. Next, preparations of CD63~HiBiT⁺, S^+ VLP were generated with plasmids for S(B.1) or $S^{\Delta Furin}$, compared for particle concentration by NTA and analyzed for fusion with NM~LgBiT⁺, ACE2⁺ U251MG cells or U251MG derived CD63~LgBiT⁺, ACE2⁺ EV (Figure 20C). While fusion with cells was impaired down to 29% residual fusion, cell-free fusion with EVs was blocked entirely. According to the cellular fusion assay, the RRAR motif and thus proteolytic cleavage at this site is beneficial for S fusogenicity, as $S^{\Delta Furin}$ VLPs showed reduced entry, which is in concordance with published literature on the role of furin for SARS-CoV-2 transmissibility.^[10,123] In previous experiments with chloroquine and camostat-mesylate, cell-free fusion of S^+ VLP with ACE2⁺ EV was found to be CTSL and TMPRSS2 independent, but to undergo cleavage via a protease, which can be inhibited by BB94 (Figure 19B). The experiment with $S^{\Delta Furin}$ additionally demonstrated that VLP-EV fusion exclusively occurs with S^+ VLP that are processed at the furin site of S (Figure 20C). For this cell-free process, two possible scenarios would be plausible that either follow a two-step model or require just a single step.

If priming at the RRAR site occurred already during the S⁺ VLP egress, an additional second cleavage step, e.g. at the S2' site during the fusion with a recipient EV would require another cofactor, which could then be inhibited by BB94. Alternatively, S⁺ VLP are not primed during their egress but rather processed at the S1/S2 site only upon fusion with an ACE2⁺ EV, which can then be inhibited by BB94. As use of S^{ΔFurin} impairs fusion, which would mainly be mediated by F2 S⁺ VLP that contain S^{FL} but no cleaved S1 or S2 and therefore are not primed, the second model is more likely. Thus, S⁺ VLP that fuse with ACE2⁺ EV are not primed during their egress but processed by a cofactor on the recipient EV. In conclusion, VLP-EV fusion was found to be distinct from fusion with cells in terms of protease usage but other than that is also S-mediated and ACE2 receptor specific.

2.7 Cell-free VLP Neutralization Test

Just as the VLPNT uses S⁺ VLP fusion with cells to quantify NAbs, a similar cell-free VLP neutralization test (cfVLPNT) was developed, which is based on S⁺ VLP fusion with ACE2⁺ EV. As described, NAb block S on VLPs and therefore also delivery of CD63~HiBiT to CD63~LgBiT⁺, ACE2⁺ EVs (Figure 18). For such a test, fixed amounts of S⁺ VLP and ACE2⁺ EV were each pre-incubated separately with a serial dilution of sample and then mixed. After 4 h, substrate was added and luminescence was quantified in a standard luminometer. Similar to the VLPNT, the mean luminescence level of S⁺ VLPs and ACE2⁺ EV with PBS instead of diluted samples, was set to 0%, while background luminescence obtained with ΔvFP EV and ACE2⁺ EV was defined as 100% neutralization. The 50% neutralization titer VLPN₅₀ was determined alike.

2.7.1 Neutralizing Monoclonal Antibodies

To demonstrate specific neutralization of S⁺ VLP in the cfVLPNT, the four in-house generated COVEV3 anti-S mAbs were tested, of which 5B9, 35B12 and 42E2 were known to be neutralizing. These three NmAbs were shown to potently neutralize S(B.1)⁺ VLP also in the cell-free test, with VLPN₅₀ between 0.8 and 1.6 nM, while 5D1 was found to be non-neutralizing, as expected (Figure 22A). Results with purified mAb samples in the cfVLPNT were therefore qualitatively in concordance with results from the VLPNT.

2.7.2 Serum Analysis

To investigate the performance of the cfVLPNT, sera from a fraction of the COVID-19 patient cohort, from exemplary COVID-19 vaccinees and all healthy, naive donors were analyzed (Figure 22B). Sera of naive donors resulted in unexpectedly strong neutralization at higher concentrations. Of 12 sera from healthy and immunologically naive donors obtained from mid 2019 and earlier, 11 reached 50% neutralization and more, with some showing

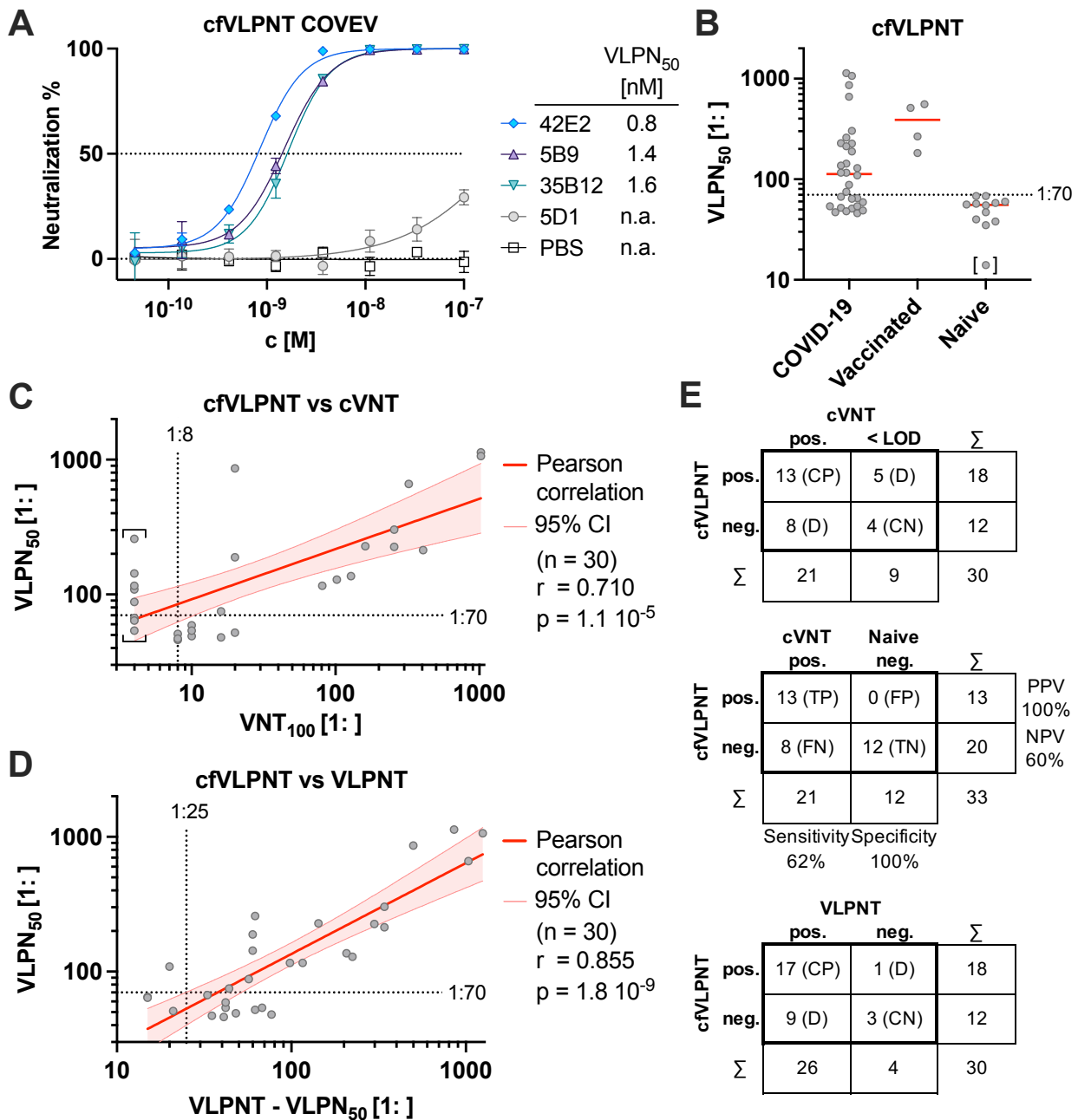


Figure 22. Cell-free VLP neutralization test validation.

(A) Four anti-S specific mAbs and the negative control PBS were analyzed in the cell-free VLP neutralization test (cfVLPNT), which is based on fusion of S⁺ VLP with ACE2⁺ EV, for their SARS-CoV-2 B.1 neutralization capacity. Mean values of three biological replicates are displayed, error bars indicate standard deviations. 50% neutralization values, VLPN₅₀, are listed or indicated as not applicable (n.a.).

(B) Titers of sera from 30 COVID-19 patients, 4 COVID-19 vaccinees and 12 healthy naive donors, tested in the cfVLPNT with S(B.1)⁺ VLPs, are shown. Median values are indicated in red. Titers above the dotted line (1: ≥ 70) indicate samples which scored positive for spike specific neutralizing antibodies according to the criteria applied. Titers in square brackets indicate sera with VLPN₅₀ below the limit of detection (LOD).

(C) Correlation of VLPN₅₀ titers from the cfVLPNT versus VNT₁₀₀ titers obtained in a conventional virus neutralization test (cVNT) using infectious SARS-CoV-2. Pearson correlation data (coefficient r , confidence interval CI, sample size n and p -value) of 30 sera from COVID-19 patients are shown and the linear relationship is indicated. Data below the dotted horizontal line denote sera which scored negative in the cfVLPNT. Results left of the dotted vertical line denote sera which scored below the limit of detection (1: < 8) in the cVNT; these VNT₁₀₀ values were defined as 1:4 and indicated in square brackets.

(D) Correlation of VLPN₅₀ titers from the cell-free (y-axis) and the cellular (x-axis) VLPNT. Pearson correlation data of 30 sera from COVID-19 patients are shown, as in panel C, with linear relationship indicated. Data below the dotted horizontal line denote sera which scored negative in the cfVLPNT. Results left of the dotted vertical line denote sera which scored negative (1: < 25) in the VLPNT.

Figure 22. continued from previous page.

(E) In the upper table, results of 30 COVID-19 samples tested in the cfVLPNT and a cVNT are compared. Concordant positive (CP), concordant negative (CN), and discrepant (D) results are indicated. In the middle table, sensitivity, specificity, positive predictive value (PPV) and negative predictive value (NPV) of the cfVLPNT were calculated based on the 21 COVID-19 serum samples with neutralizing capacity, according to the cVNT and 12 serum controls of healthy naive donors collected prior to mid 2019. In the bottom table, results of 30 COVID-19 samples tested in the cfVLPNT and the VLPNT are compared. Test results are indicated as: pos., positive; neg., negative; < LOD, below limit of detection; TP, true positive; FN, false negative; FP, false positive; TN, true negative.

VLPN₅₀ titers as high as 1:68. Based on the maximal titers of naive sera in the cfVLPNT, an additional small margin was added and a preliminary minimal cutoff of 1: ≥ 70 defined, to classify samples as neutralizing in this test format and yet ensure specificity for SARS-CoV-2 *in vitro* neutralizing antibodies. The 4 sera of COVID-19 vaccinees after prime-boost immunization from 2021 showed high neutralization potential consistently up to 100% inhibition of S⁺ VLP fusion and VLPN₅₀ titers of 1:182 to 1:556. Therefore, specimens from these vaccinees were all classified to contain NAbs. Strikingly, results with 30 sera from acute or convalescent COVID-19 patients were inconsistent with VLPN₅₀ titers ranging from 1:46 to 1:1134. As a consequence of the defined cutoff, only 18 out of 30 COVID-19 specimens were classified as neutralizing in the cfVLPNT. Additional data and all the individual titers are listed in Supplementary Table S2. Obviously, with the cfVLPNT in its applied methodology, weakly and moderately neutralizing serum samples were hardly separable from non-neutralizing ones. Apparently, sera from healthy and naive donors seem to cause a strong unspecific neutralization, either by antibodies binding other antigens than S or by non-specific matrix effects from other blood components. This critically impacts the performance of the cfVLPNT, as only serum specimen with high neutralization capacity can be identified, while still ensuring the specificity of the test.

In an attempt to overcome this issue, serum samples were treated prior to the cfVLPNT at 56°C for 30 min and afterwards centrifuged to inactivate complement system components and eliminate debris. Yet, this also did not alter unspecific neutralization of naive specimens. Similarly, also use of concentrated ACE2⁺ EV to overcome the shortfall of acceptor particles compared to donor S⁺ VLPs, resulted in higher RLU baselines but could not overcome the problem. With the insight about the contamination of S⁺ VLP preparations with free S1, preceding results of the VLPNT and cfVLPNT probably underestimated the concentration of NAbs in serum and recombinant samples, compared to a hypothetical test with a S⁺ VLP stock free of unbound S1. All other types of cVNT and pVNT most likely also suffer from this issue, as they similarly utilize raw virus stocks as inocula and therefore also contain free S1 and defective virus particles that seemingly lower the neutralization capacity of a sample. For the VLPNT and other VNTs, this is probably rather a matter of the titers' numerical values, than a serious problem. In the cfVLPNT however, weak discrimination between neutralizing and non-neutralizing samples has to be tackled. To test the effect of purified inocula free of unbound S1, F2- and raw S⁺ VLP were used in a cellular VLPNT and a cfVLPNT with serum from a vaccinee and a naive donor (Supplementary Figure S3 and Figure 21F). While non-specific neutralization was barely affected in both tests, use of

F2- over raw S⁺ VLP resulted in increased specific neutralization capacity of the neutralizing sample. Especially for the cfVLPNT, this could therefore be a possible solution to increase the hitherto limited potential to discriminate between a neutralizing and a non-neutralizing serum sample. Yet, the generation of such F2 S⁺ VLP preparations in larger quantities is effortful and time consuming, which is why this workaround was only demonstrated in principle but not applied in general for the cfVLPNT. A more practical approach to eliminate the contamination by using S^{ΔFurin}, which cannot be cleaved to S1, is considered impossible as such S⁺ VLP do not support cell-free fusion with U251MG derived ACE2⁺ EV.

2.7.3 Correlation of cfVLPNT to cVNT and VLPNT

For the validation of the cfVLPNT, results of the 30 COVID-19 sera tested were compared with their results in the cVNT with infectious SARS-CoV-2.^[114] As described, titers in the cVNT ranged from 1:8 to 1: >1024 also for this subset of the cohort and 21 out of 30 samples were found to be neutralizing with VNT₁₀₀ of 1: ≥8, while the 9 remaining sera performed below the LOD and were denoted as 1:4. To compare the cfVLPNT with the cVNT directly, VLPN₅₀ titers of the 30 COVID-19 samples were correlated with the respective VNT₁₀₀ titers (Figure 22C). The Pearson coefficient of log₁₀ transformed data (n = 30) revealed a significant positive correlation (r = 0.710 and p = 1.1 × 10⁻⁵). This indicates that the cfVLPNT in principle allows to quantitate the SARS-CoV-2 *in vitro* neutralization capacity. An analysis of the 30 COVID-19 samples in both tests found 13 sera to be CP, 4 were CN, whereas 13 sera were found to be discrepant (Figure 22E, upper table). The discrepant results were likely caused by experimental differences between the two tests,^[44] as the cVNT is a multi-cycle assay that requires 100% reduction of CPE (VNT₁₀₀), while the cfVLPNT is a single-cycle assay just as the VLPNT and scores at 50% reduction of S⁺ VLP fusion (VLPN₅₀). Also mechanistic differences could cause inconsistency, as the cfVLPNT is based on a single, rather delicate fusion mechanism between S⁺ VLP and ACE2⁺ EV, instead of multiple uptake routes into cells. As described, the calculation of sensitivity and specificity of the novel cfVLPNT was again based on clearly attributable positive (neutralizing) and negative (non-neutralizing) specimens, using the 21 COVID-19 samples which had scored above the LOD in the cVNT along with 12 sera from healthy, naive donors (Figure 22E, middle table). Of the 21 positive samples, the cfVLPNT classified 13 samples as TP, while all 12 negative sera were considered TN with the applied cutoff. Therefore, the sensitivity of the VLPNT was calculated to be 62%, while its specificity was 100%. Based on the analyzed data set (n = 33), the PPV of the test was 100% and the NPV 60% (Equations 3 to 6 on page 39). As the high cutoff lowers the sensitivity, the current version of the cfVLPNT requires optimization.

Additionally, the cfVLPNT results of the tested COVID-19 sera were compared with their results in the cellular VLPNT with U251MG cells. As described, titers in the VLPNT ranged from 1:15 to 1:1250 for this subset of the cohort and 26 out of 30 samples were found to have neutralizing activity with VLPN₅₀ 1: ≥25, while the 4 remaining sera had

been classified as negative. To compare the cfVLPNT with the VLPNT directly, VLPN₅₀ titers of the 30 COVID-19 samples from one test were correlated with the respective VLPN₅₀ titers of the other (Figure 22D). The Pearson coefficient of log₁₀ transformed data (n = 30) revealed a significant and strong positive correlation (r = 0.855 and p = 1.8 × 10⁻⁹). The direct comparison of the 30 COVID-19 samples in both tests found 17 sera to be CP, 3 were CN, whereas 10 sera were found to be discrepant (Figure 22E, bottom table). Especially the high cutoff of 1: ≥70 in the cfVLPNT caused a lot of the COVID-19 samples to be classified as negative, although they do contain NAbs according to the other tests. Overall, results from the cfVLPNT correlated better with those from the VLPNT, than those of the cVNT.

3 Discussion

3.1 Monoclonal Spike Antibodies

During the first months of the COVID-19 pandemic, clinics were not only overwhelmed by the sheer number of patients but also faced an acute lack of treatment options and antivirals. Simultaneously, it was uncertain whether a universally effective vaccine would ever become available. Therefore, also therapeutic monoclonal antibodies were urgently needed, even though they often only display moderate efficacy in the context of viral infections. For these applications and especially respiratory diseases, a common problem of mAbs is their limited circulation and tissue infiltration, as e.g., IgG is inefficiently translocated into the lung epithelium, a major site of viral replication in case of SARS-CoV-2.^[39] Additionally, treatments often require large quantities of mAbs, which is problematic as their production is costly and industrial scale up limited. Therefore, from early on mAbs were likely to be only part of treatment regimens in addition to safe and effective vaccines. Nevertheless, therapeutic mAbs were thought to benefit individuals without strong immune responses to vaccination, such as elderly or immunocompromised patients, as they could also be used for prophylaxis.^[39] Passive immunizations but also therapy, especially require NmAbs, antibodies that have the potential to neutralize viral infections. Thus, multiple candidates that partly also showed promising activity in animal models were immediately published.^[124,125] Antibodies were often used in combination, as so called cocktails, to reduce the risk of becoming obsolete by escape mutants in the antigen.^[57,126] Later, use of therapeutic mAbs was shown to reduce hospitalization and mortality, and thereof to be especially promising in individuals that were seronegative upon infection.^[26]

As also the novel VNT required anti-S antibodies as molecular tools and reference, mAbs and NmAbs had to be generated. Due to their favorable properties to present complex antigens in their native state,^[51,55] EVs were engineered to carry S protein and used for immunizations of rats (Figure 3). EVs in general but also SARS-CoV S bearing EVs have already qualified as potential vaccine candidates.^[52,127] From three immunizations, several antibodies were generated by hybridoma technique. The efficiency of specific clones obtained, varied between the single immunizations, but was probably an effect of quality and quantity of the administered antigen batch, not the use of Freund's incomplete adjuvant. As especially NmAbs were of interest, a selection of candidates from the third immunization was pre-screened for *in vitro* SARS-CoV-2 neutralization with the novel VLPNT to determine the most promising ones. In total, six S specific antibodies were pursued further and characterized in detail (Table 2). The affinity of the individual antibodies to native S protein was

determined and compared to two recombinant human mAbs REGN10987, imdevimab and REGN10933, casirivimab, with emergency use authorization for the treatment of COVID-19 (Figure 4A).^[39,56,57] For S(B.1), K_D values of the novel mAbs were found to be of similar scale as the two therapeutic ones and published values.^[58,59] Therefore, especially 43A11, 5B9, 35B12 and 42E2 were concluded to be S specific, high-affinity antibodies. When analyzed with S(B.1.1.529 BA.1), all affinities were severely impaired, except for 35B12, which approximately retained its binding. Among these mAbs, 35B12 is therefore the only one, that was unaffected by the most recent variant tested.

Additionally, the epitopes of the COVEV mAbs were roughly localized to the individual domains of S by WB experiments (Figure 4B). All six antibodies were found to bind conformational epitopes, which is indicative of the exceptional properties of mAbs obtained by immunizations with engineered EVs compared to immunizations with e.g., plain peptides that often yield antibodies against linear epitopes. Two of the novel antibodies, 43A11 and 55E10 were furthermore found to bind unconventional epitopes, as they exclusively recognize bands of ~ 210 kDa (Figure 4B). As the individual subunits appear at 120 kDa and 90 kDa for S1 and S2 respectively (Figure 8C), both mAbs recognize a complex of both subunits. Yet, uncleaved full-length spike S^{FL} , as well as cleaved but non-dissociated S1+S2 could both contribute to this complex. Experiments with fractionated S^+ VLP gave access to two populations, F2 and F3, which displayed equal patterns in WB for the 210 kDa band when analyzed with 43A11, but disparate ones when analyzed with an anti-S2 mAb that also recognizes the single subunit S2 (Figure 21B). Possible explanation for this disparity could be that both fractions contain equal amounts of S^{FL} , but only F3 additionally contains associated S1+S2 complex of cleaved subunits detected with the anti-S2 antibody. As a consequence, 43A11 would necessarily recognize intact, uncleaved spike protein and bind an epitope close to the S1/S2 cleavage site (Figure 2A). Even though this hypothesis was found to be a plausible explanation which is not in conflict with the results presented, confirmation by a structural elucidation technique such as e.g., x-ray crystallography, cryo-EM or cross-linking mass spectrometry, is missing.^[60] For the remaining four mAbs, simpler epitope regions were identified by WB (Figure 4B). The three antibodies 5B9, 35B12 and 42E2, which were specifically selected because of their strong neutralization capacity, were found to recognize epitopes within the S1 subunit. This was not surprising given the fact that most SARS-CoV-2 NAbs are elicited against the RBD of S,^[107,108] or partly also against the NTD.^[128,129] Therefore, the absolute majority of neutralizing epitopes are located in S1. In concordance with this, all novel NAbs obtained from the conducted immunizations, were specific for S1. The epitope of the remaining antibody 5D1 could not be specified further, as not only S1+S2, but also bands for both individual subunits were detected. It seems like the antibody recognizes epitopes that occur not only in S2, but also in S1. Thus, further experiments would be necessary to clarify the exact epitope.

For 55E10, 43A11 and 35B12, also the amino acid sequences and CDRs were determined. Computational annotation of the sequences unambiguously allocated the obtained amino acid sequences to V_H , V_L , C_L and C_H chains of IgG. Alignment of their amino acid sequences

revealed no augmented homology in their CDRs and therefore distinct paratopes. These sequences (Supplementary Table S1) were then used to recombinantly express human IgG chimeric antibodies of those rat mAbs and test them for S binding and specificity (Figure 4D). Secreted, chimeric antibodies were again found to selectively bind SARS-CoV-2 S protein, confirming the integrity of the amino acid sequence. In order to develop a sandwich ELISA for the detection of S, the mAbs 43A11 and 55E10 were additionally tested for identical epitopes. In a competition experiment, 55E10 was found to be incapable of displacing 43A11 from occupied S molecules and vice versa (Figure 4C). Therefore, both antibodies were found to bind orthogonal epitopes. As this prerequisite was fulfilled, a protocol for a sensitive sandwich ELISA was optimized to detect S in biological samples such as S⁺ EV or S⁺ VLP preparations at minor concentrations. Calibration with recombinant S protein revealed a LOD of low nanomolar range and testing of S-negative samples did not result in elevated non-specific signal (Figure 9). Thus, the S protein assay was found to be highly sensitive and specific.

Table 2. Characteristics of the novel monoclonal anti-spike antibodies.

From immunizations with animals, six novel mAbs have been generated, that bind the S protein of SARS-CoV-2. Among other techniques, antibodies were analyzed with the novel VNTs for their *in vitro* neutralization capacity. Besides the ancestral strain, also two VOCs were tested.

			COVEV1		COVEV3			
			55E10	43A11	5D1	5B9	35B12	42E2
Subclass			IgG2b	IgG2b	IgG2b	IgG2b	IgG2a	IgG2b
Affinity	K _D (B.1)	[nM]	4.2	1.0	5.0	2.5	2.5	1.4
	K _D (B.1.1.529)	[nM]			5.9	5.8	1.0	~10
Neutralization	VLPN ₅₀ ^a (B.1)	[nM]				1.9	1.1	1.4
	VLPN ₅₀ ^b (B.1)	[nM]				1.4	1.6	0.8
	VLPN ₅₀ ^a (B.1.617.2)	[nM]				1.5	1.0	0.8
	VLPN ₅₀ ^a (B.1.1.529)	[nM]					0.9	
Sequence			✓	✓			✓	
Epitope			S ^{FL}	S ^{FL}	S2/S ^{FL}	S1/S ^{FL}	S1	S1

^aDetermined by VLPNT

^bDetermined by cfVLPNT

In a collaboration with the TUM university hospital, this assay was then used to assess whether circulating S protein can be found in the blood of COVID-19 patients. In those samples, the partners at MRI successfully detected S⁺ EVs or S⁺ exosomes by nanoscale flow cytometry, using fluorescently labeled 43A11 mAb. A conventional approach to detect S protein should thus confirm their finding. S protein on vesicular structures found in blood could give important insight into the biogenesis and tropism of SARS-CoV-2 and also affect neutralization in the circulatory system.^[62] Before this question could be addressed, the ELISA had to be optimized for human plasma samples, which posed a problem in certain control samples. Some samples of healthy donors exhibited strong signals in the assay, which were found to be non-specific. Rat Fc binding autologous antibodies were therefore

suspected to crosslink capture and detection antibody and to result in an arbitrary signal. In concordance with this hypothesis, pre-incubation of plasma samples with a rat IgG isotype as decoy effectively quenched this unspecific signal but retained specific S signals (Figure 5B). Yet, this phenomenon has already been reported by Degn *et al.*, who found anti-rat κ light chain antibodies with a prevalence of 40% among blood donors.^[130] Next, a set of plasma samples from COVID-19 patients with acute SARS-CoV-2 infection and from healthy donors was tested in the anti-Spike ELISA and WB but found no signals for S protein (Figure 5C, D). Thus, the tested samples did not contain detectable amounts of S protein, according to the applied methods. It is worth mentioning though that the collaborators at MRI detected S⁺ EVs in the blood of COVID-19 patients using nanoscale flow cytometry, which is thought to be a more sensitive method.

As described, the 43A11 anti-S mAb was shown to be an essential molecular tool throughout this work, not only because of its use in flow cytometry, WB and ELISA, but also for sophisticated applications such as the nano flow technology (Figure 10). There, fluorophore coupled 43A11 was used to detect S⁺ VLP and SARS-CoV-2 virions on single particle level. Additionally, the antibody conjugate was used to localize S inside or on top of S⁺ VLP loaded cells via confocal fluorescence microscopy (Figure 12). This suggests that the antibody could be a valuable tool for further imaging applications, such as e.g. in histology for the staining of SARS-CoV-2 infected cells. Furthermore, the antibody could be used to investigate potential differences in the biogenesis of S⁺ VLP and the viral replication machinery of SARS-CoV-2. Subcellular localization of S with a resolution on the level of single compartments could give important insight into the egress mechanisms of S⁺ VLP from transfected cells and virions from infected cells.

The key characteristic of a therapeutic mAb, used for treatment of a viral infectious disease, is its capacity to neutralize infection of cells. A NmAb with the necessary specificity and affinity to bind to a virus and block its entry can therefore mitigate the pathology associated with a productive infection.^[131] In order to be a successful candidate, a NmAb has to display potent *in vitro* neutralization in a suitable VNT, as well as a certain resilience to mutations in the antigen of escape variants.^[39] After fulfilling certain safety criteria in pre-clinical models, such as absence of antibody dependent enhancement (ADE), a candidate can enter clinical studies to evaluate tolerance and later its effectiveness to minimize virulence *in vivo*.^[131] Neutralization per se is mediated by antibodies that prevent entry of virions into host cells and thus protect from initial infection. In the case of SARS-CoV-2, NAbs were found to be specific for the viral glycoprotein spike but mediate neutralization via diverse modes of action. Most NAbs block the attachment of S to the cellular receptor ACE2 by binding to the RBM of S1,^[107,108] or stall S in its closed, i.e. RBD ‘down’, pre-fusion conformation (Figure 2).^[109] To investigate the *in vitro* neutralization of the novel COVEV mAbs, they were tested in the novel VLPNT. Of the six antibodies, three (5B9, 35B12 and 42E2) were found to be potently neutralizing S of the B.1 strain (Figure 17), with VLPN₅₀ values in the low nanomolar range (Table 2). 35B12 and 42E2 showed even lower VLPN₅₀ values than two fully human therapeutic mAbs REGN10987 and REGN10933, with known

activity.^[57,132] All of these NmAbs also effectively neutralized the SARS-CoV-2 Delta VOC B.1.617.2, whereas only one of them, 35B12, retained the capacity to also neutralize the Omicron variant B.1.1.529 BA.1. This complete loss of neutralization is attributable to the many mutations in the S gene of Omicron, that account for immune evasion and broad antibody escape.^[36,106] Thus, the absolute majority of clinically applied therapeutic antibodies, including REGN10987 and REGN10933, is severely impaired by the emergence of the novel VOC and consequences for clinical studies and therapy have yet to be evaluated.^[106,133,134] Because of its characteristics regarding the B.1, the B.1.617.2 and the B.1.1.529 BA.1 variants, 35B12 was concluded to be a pan-variant neutralizing antibody.

3.2 VLP Neutralization Test

NAb levels in human serum samples are considered a predictive and easily accessible correlate of protection from viral infectious diseases, including COVID-19.^[40–42] In clinical virology, detection and quantitation of NAbS in biological samples is generally performed using cVNTs that mainly depend on CPE and the formation of plaques in monolayers of infected cells. This type of assay depends on replication competent virus and consequently requires the regulatory and safety measures of a BSL-3 containment in the case of SARS-CoV-2. Moreover, these tests take several days for the CPE to progress and are visually evaluated by trained personnel. Therefore, PRNTs are labor intensive, cumbersome and difficult to normalize and standardize between laboratories.^[44] To overcome these problems, the focus reduction neutralization test (FRNT), also known as microneutralization assay (MNA) can be conducted, which relies on the identification of infected cells as foci by immunostaining.^[45,135,136] Yet, this test requires numerous steps to completion and also takes several days.

Surrogate assays have thus been developed, which are often based on pseudotyped retro- or lentiviruses and *de novo* expression of a reporter enzyme or fluorescent protein, encoded by the viral vector (Figure 6). These pVNTs are manageable in BSL-2 laboratories but still require up to two to three days for a final assessment.^[44,64,137] These artificial replication deficient vectors can be problematic as the glycoproteins, which mediate attachment, uptake and fusion with cellular membranes, might perform differently in the context of the original virus.^[44,138] For instance, S-pseudotyped retro- or lentiviruses mostly bud from the plasma membrane where S is incorporated into the envelope with uncertain stoichiometry,^[67,138] while the envelopes of coronaviruses carry a discrete number of S trimers per particle, which assemble in the ERGIC together with M, N and E in a given, optimal stoichiometry.^[71] The unfavorable time-to-readout problem of pVNTs was reconsidered by Miyakawa *et al.*, who substituted the HIV-borne reporter gene with a chimeric reporter protein consisting of the HIV capsid protein with a carboxy-terminal HiBiT domain,^[99] following the principle proposed by Cavrois *et al.* in 2002.^[92] Similar to the approach of the VLPNT (Figure 13), recipient Vero cells expressed LgBiT constitutively to monitor the fusion of the S-pseudotyped HIV particles, which shortened the time-to-readout to 3 to 4 hours.^[99] However, this ap-

proach does not improve the partly moderate correlations of pVNTs and cVNTs observed in clinical samples with r values ranging from 0.31 to 0.89 for SARS-CoV and SARS-CoV-2.^[41,45,46,139,140] Inconsistencies between the two types of tests have also been reported with MERS-CoV and are often neglected to justify the use of pVNTs.^[141,142] Differences in morphogenesis, composition and mode of entry probably account for the disparities between S-pseudotyped vectors and SARS-CoV-2 virions.

Another type of test is the sVNT, which can be performed within short time in a standard laboratory at BSL-1. However, this assay does not specifically quantitate NAb, but antibodies that interfere with the RBD-ACE2 receptor interaction. As the majority of NAb are not necessarily elicited against the RBD, and not every NAb can displace the interaction with ACE2 but blocks by other mechanisms,^[142] they display rather weak correlation to cVNTs.^[45–47] Therefore, they are of limited applicability, only.

Table 3. Comparison of various types of virus neutralization tests (VNTs).

To evaluate the SARS-CoV-2 *in vitro* neutralization by serum- or recombinant antibodies, alternatives to cVNTs have been developed, which each possess various advantages and disadvantages. The following table is a side by side comparison of exemplary methods from the superordinate test categories, as well as the two novel VNTs based on SARS-CoV-2 VLPs.

	sVNT	pVNT	cVNT	VLPNT	cfVLPNT
Analyte	anti-RBD Ab	NAb	NAb	NAb	NAb
BSL	1	2	3	1	1
Time	2-3 h	2 d	5 d	4.5 h	4.5 h
Inoculum	rec. RBD	pseudotyped e.g. HIV	SARS-CoV-2	VLP	VLP
Basis	binding	infection	infection	fusion	fusion
Target	rec. ACE2	cells	cells	cells	ACE2 ⁺ EV
Readout	HRP	<i>de novo</i> GFP	CPE	BlaM, nLuc	nLuc
Reference	[143]	[48]	[114]	[48]	

Ideally, methods for the quantitation of NAb as summarized in Table 3, should resemble the biological system of infection very closely and yet be safe. For SARS-CoV,^[69] and later also SARS-CoV-2, VLPs were shown to mediate transport and delivery of reporter transcripts that encompass *cis*-acting packaging signal sequences.^[138] Uptake of VLPs, release of RNA and subsequent translation, kind of mimic an infection by SARS-CoV-2, yet without the replication machinery. This was a major achievement as VLPs resemble the shell of virions, but the readout described by Hsieh *et al.* still depends on *de novo* expression of GFP, encoded by the reporter transcript. Simultaneously, the aim of this project was to develop a novel VNT for SARS-CoV-2, which is quick, safe and yet depicts the process of a native infection.

The current limitations of quantitating NAb are overcome by the VLPNT, as it is based on harmless, non-infectious, engineered VLPs, which are authentic morphological and functional mimics of SARS-CoV-2 virions. At first, conditions for the generation of S⁺ VLP

were investigated and revealed an optimum for the transfected amount of S encoding plasmid (Figure 14A), as observed by others.^[138] Next, the particles were characterized using WB (Figure 8), ELISA (Figure 9), negative stain- and cryo-EM (Figure 7), NTA (Figure 9D) and nano flow technology (Figure 10). Thus, S⁺ VLPs were shown to authentically resemble the shell of SARS-CoV-2 virions and to contain S^{FL} trimers at a comparable molecular number per particle.^[82,84,88]

Secondly, the S⁺ VLPs were characterized functionally, to evaluate their capability to enter cells. Therefore, they were engineered to carry a chimeric, membrane anchored and lumenally oriented enzyme (BlaM) or activator peptide (HiBiT). Additionally, hACE2⁺ Vero cells and an ACE2⁺ U251MG cell line that carries inactive, membrane-associated split nLuc enzyme (LgBiT) were generated. Carryover of BlaM or reconstitution of nLuc (Figure 13C) thus indicates successful fusion. Experiments with CD63~BlaM⁺, S⁺ EV and S⁺ VLP qualitatively showed that fusion depends on the presence of a vFP, e.g. spike (Figure 11A-D) and that only ACE2⁺ cells are susceptible (Figure 12). Of note, self-assembling S⁺ VLP not only resemble SARS-CoV-2 virions more accurately than S⁺ EV but were secreted more abundantly (Figure 9D) and showed greater fusogenicity (Figure 14E). Quantitative experiments confirmed that CD63~HiBiT⁺, S⁺ VLPs only fuse with ACE2⁺ cells and that uptake strictly depends on S (Figure 15A). These findings indicate that S⁺ VLPs not only resemble SARS-CoV-2 virions structurally and molecularly, but also share their specific fusogenic characteristic and tropism. Yet, a limitation of Vero cells was that mostly CTSL mediated spike processing (Figure 11E), while natural infection of human lung cells *in vivo* with SARS-CoV and SARS-CoV-2 is largely facilitated by TMPRSS2.^[13,144-147] Since fusion with U251MG cells was shown to largely depend on TMPRSS2 (Figure 15B), they were used for further experiments. Additional overexpression of TMPRSS2 did enhance fusion with S⁺ VLP of the B.1 variant, but not with B.1.1.529 BA.1 (Figure 14G), suggesting that Omicron makes less use of this pathway and uses alternative proteases instead. This is concordant with recently published results that also showed no enhanced infectivity but a shift of tropism away from TMPRSS2 with Omicron.^[137,148,149] Compared to B.1, an overall reduction of S⁺ VLP fusogenicity was observed for Omicron, which might seem contradictory to the rapid spread of the variant.^[104] Yet, its infectivity was reported to be reduced and the increased transmissibility of the variant allocated to improved S stability,^[105] widespread immune evasion and broad antibody escape.^[36,106] As the VLPNT with B.1.1.529 BA.1 did not benefit from overexpression of TMPRSS2, the U251MG cell line with endogenous expression level was used for the test.

With the thoroughly characterized S⁺ VLPs and reporter system, the proof-of-principle of a rapid and safe VLPNT was demonstrated (Figure 13D). The assay was put to the test with sera from COVID-19 patients and vaccinees (Figure 16B), as well as recombinant NmAbs (Figure 17) and controlled with non-neutralizing mAbs and sera from healthy and immunologically naive donors. Based on the tested cohort, a minimal titer was defined to classify a serum sample with SARS-CoV-2 specific NAbs. Below this level matrix effects from naive sera interfered that could not be distinguished from artefacts. For the COVID-

19 samples, titers were correlated with double-blinded results from a cVNT, resulting in convincing quantitative concordance (Figure 16D). Thereby, results from the VLPNT were verified and good sensitivity and specificity parameters found. Quantitating NABs is epidemiologically and clinically relevant since a decrease below a certain threshold impacts the individual protection from infection and increases the personal risk to develop COVID-19. Khoury *et al.* found that 20% of the mean NAb level detected in convalescent sera provided 50% protection from symptomatic disease.^[42] Such findings could be used as basis to recommend booster shots if a minimal NAb titer is undercut.

In the S gene in particular, the SARS-CoV-2 genome has undergone several mutations since the onset of the pandemic. With the VLPNT, it can be tested, whether emerging strains such as the Omicron VOC present immune escape and resist neutralization by sera from vaccinees, convalescents or people with BTI of a previous variant. As S⁺ VLP that contain newly identified S mutants can be rapidly produced, the VLPNT can be adapted quickly. Exemplary sera from vaccinees were re-analyzed using S⁺ VLPs of B.1.617.2 or B.1.1.529 BA.1 spike and partial cross-neutralization found (Figure 16E). Yet, a significant and severe reduction of neutralization titers was observed for both variants, which is in concordance with published findings.^[115–117,150] Among the NmAbs tested, none of them showed major impairment with the Delta variant, yet 4 out of 5 entirely lost their neutralization efficacy when tested with Omicron (Table 2). The broad antibody escape of Omicron in particular is indicative of a widespread immune evasion and can explain the high number of BTIs.^[36,106]

Furthermore, the gradual decline of NABs in the body poses a problem to the immunity of the population. Within 6 months after the last natural or artificial immunization, titers in the blood of convalescents, vaccinated and individuals with BTI were shown to decrease.^[106,151–153] In a small case report of three vaccinees, this process could also be reconstituted with the VLPNT (Supplementary Figure S2). While the seronegative specimens were also non-neutralizing, clear seroconversion and effective neutralization were observed only upon second vaccination. Serum drawn 6 months after, was found to neutralize below threshold for all three individuals accordingly. A third exposure to the antigen, by vaccination in the form of an additional third shot (booster dose) or also a BTI, was reported to increase NAb titers again and was indeed observed for the three vaccinees.^[106,117,152] Repeated affinity maturation by somatic hypermutation gives access to memory B cells and antibodies with even greater affinities.^[129,153] Thus, booster shots were found to retrieve vaccine efficacy, partly even for the novel variants.^[34,154] In principle, the VLPNT should also be capable of identifying opposite effects such as ADE, which is known for various viruses and has also been reported in the context of SARS-CoV-2 infection.^[155]

As stated above, the VLPNT is a rapid novel test, which has the potential to surpass other VNTs and still exhibits the authenticity and validity of a cVNT but without infectious virus (Table 3). However, a limitation of this assay is its dependency on living cells. Ideally, an IVD would not require a cell culture laboratory, handling and maintenance of cell lines and should only have long-lived components at basic storage conditions. Furthermore, the VLPNT was solely demonstrated with a single human cell line, U251MG and

the most common non-human primate line in the field, Vero cells. Even though both cell lines are not only susceptible for SARS-CoV-2 infection, but also permissive for its replication, they are exemplary and by no means the only legitimate cell types for VNTs.^[90] As there are partly substantial differences between cell lines concerning *in vitro* infection with SARS-CoV-2, other human e.g., lung derived types might be preferential over the neuronal U251MG cells. Yet, it is questionable whether an ideal cellular model that is universal for all VOCs can be defined at all, as also human lung epithelial Calu3 or human intestinal epithelial Caco2 cells perform differently with individual variants.^[148] Another limitation of this study could be the serum sample set of COVID-19 patients. A bias in age and sex are allegedly the disparities towards older (median age 62) and male (67%) individuals. However, as exclusively hospitalized patients were recruited to the cohort, this simply reflects the epidemiological situation of an overproportionate disease severity and mortality among males and in the advanced age groups.^[156] Hence, individuals with severe (31%) or critical (31%) disease progression are highly overrepresented by the cohort, compared to the situation among the whole population (Table 13).^[4] For natural infections, disease severity was shown to be positively correlated with neutralizing and binding antibody titers.^[40] Thus, specimens from the cohort could display a bias in NAb titers and might not be suitable for general interpretations on the humoral immune response to COVID-19 (Supplementary Figure S1A). Yet, as demonstrated by a cVNT, this set of specimens covers the full range of highly, as well as weakly neutralizing samples (Figure 16D). Therefore, it can be considered as an ideal data set for the purpose of validating a novel quantitative VNT.

3.3 Cell-free VLP Neutralization Test

With the aim of developing a simplified assay, the possibility of substituting living cells by ACE2⁺ EV as acceptors for the S⁺ VLP was investigated. As this implies fusion of two vesicles, repulsive forces between the membranes must be overcome. Commonly, hydrophobic effects, elastic restraints and electrostatic repulsion between negatively charged phospholipids prevent spontaneous fusion of vesicles with cells. Thus, specialized proteins are needed, which undergo a series of irreversible conformational changes that facilitate membrane approximation and ultimately enable fusion. Viruses have evolved three classes of fusion proteins for this purpose that partly require proteolytic processing or a drop in pH for activation.^[121] To test whether EVs could serve as recipients for S⁺ VLP, the VLPNT described above was adapted to CD63~LgBiT for an optimal incorporation of the reporter protein into EVs. Successfully, co-incubation of CD63~HiBiT⁺, S⁺ VLP and CD63~LgBiT⁺, ACE2⁺ EV resulted in strong luminescence, indicating efficient VLP-EV fusion (Figure 18). The potential of ACE2⁺ EV to block the binding of spike RBD and to function as decoys has recently been published by El-Shennawy *et al.*^[118] While they also demonstrated that ACE2⁺ EV can protect transgenic mice from infection with SARS-CoV-2, they did not investigate whether the finding is caused by attachment or fusion of ACE2⁺ EV and virions. Direct membrane fusion of vesicles has been demonstrated with isolated and immobilized plasma membrane EVs on a

surface but only with S pseudotyped HIV particles.^[119] According to a thorough search of the relevant literature, the data presented in this work is the first report of a cell-free VLP-EV fusion entirely mediated by the vFP, the corresponding receptor and necessary cofactors.

Initially, fusion of S⁺ VLP with vesicles was characterized and found to strictly depend on ACE2 on EVs and S on VLPs (Figure 19A). Therefore, S⁺ VLP exhibit the identical tropism towards acceptor EVs, as compared to recipient cells. Surprisingly, VSV-G⁺ EV used as positive control in the cell-based assay were found to be completely incapable of fusing with U251MG derived EVs. As VSV-G is a class III fusion protein that requires a drop in pH for activation,^[121] an acidic pulse was examined but could not rescue fusion. Thus, the receptor of the VSV or relevant cofactors seem to be absent on these EVs. As expected, VLP-EV fusion was independent of CTSL processing. But in contrast to fusion with cells, fusion of S⁺ VLP with ACE2⁺ EV was found to be entirely independent of TMPRSS2 (Figure 19B). When tested with a broad MMP inhibitor BB94, batimastat, fusion was completely inhibited at nanomolar concentrations. Therefore, VLP-EV fusion is a delicate process, presumably mediated by a single protease on the surface of the recipient EV. It is tempting to speculate that this protease is ADAM17, that has recently been proposed for SARS-CoV-2 entry at the plasma membrane.^[103] Experiments with S^{ΔFurin}, a S1/S2 cleavage defective mutant with deleted RRAR motif, showed that S⁺ VLP fusion with cells benefits from priming at the S1/S2 site, presumably by furin (Figure 20C). Yet when S^{ΔFurin} VLP were tested with ACE2⁺ EV, cell-free fusion was entirely impaired. Thus, S processing at the S1/S2 site is a mandatory prerequisite for fusion with EVs. Consequently, two distinct models can be drafted for the proteolytic processes involved: i. One possibility would be that the VLPs are primed at S1/S2 during their biogenesis, before they are later processed at S2' by a protease on the ACE2⁺ EVs. ii. Alternatively, VLPs could also egress without priming and rather be cleaved at both sites just upon contact with the ACE2⁺ EVs. As S⁺ VLP preparations were shown to be largely cleaved (Figure 8A) and HEK293T producer cells are known to efficiently process S on VLPs by furin,^[10] the first model (i.) is more likely to describe the proteolytic process accurately in concordance with the current literature.^[9]

Fractionation of S⁺ VLP and ACE2⁺ EV preparations in density gradients found that fusion only occurs with intact vesicles (Figure 21). Furthermore, the presence of two S⁺ VLP subtypes was revealed, which differ in molecular weight, S1 and S2 composition and explicitly in fusogenicity, but not in S^{FL} content. While F2 S⁺ VLP fused with ACE2⁺ EV and ACE2⁺ cells, F3 S⁺ VLP did so much less efficiently. Thus, the lighter or smaller particles in F2, which presumably were not primed at the S1/S2 site, constitute the only subtype capable of fusion with EVs and cells. This is contradictory to the hypothesis (i.) discussed above, that only furin primed S⁺ VLP can fuse with ACE2⁺ EV and more in support of the second model (ii.), as priming during egress seemed to be adverse, as seen with F3 S⁺ VLP. Paradoxically, primed particles from F3 should account for the lighter particles, due to partial loss of S1 subunit and should not be found at higher density in the gradient than the unprimed ones of F2. A difference in size between the subtypes could also account for the separation but would not necessarily cause a difference in fusogenicity. The exact cause of these observations

and effects could not be unveiled and remains to speculation. Thus, further experiments with fractionated S⁺ VLP and S mutants are necessary. Additionally, analysis revealed a contamination of the raw S⁺ VLP preparations with soluble S1 protein, as large amounts were found in the gradient fractions that do not contain particles. Free S1 was shown to compromise the VLPNT and the cfVLPNT, as NAbs are intercepted and therefore can no longer neutralize S⁺ VLP (Supplementary Figure S3). Yet, cVNTs and pVNTs are similarly compromised, as they use raw virus stocks as inocula, and therefore also contain free S1 and defective virus particles. While the VLPNT and other VNTs tolerate this issue, this caused problems in the cfVLPNT, so that weakly neutralizing and non-neutralizing serum samples could hardly be discriminated. Use of F2 S⁺ VLP, which are free of soluble S1, increased specific neutralization and could therefore improve the cfVLPNT performance.

Nevertheless, the proof-of-principle of a cfVLPNT could be successfully demonstrated with NmAbs and non-neutralizing controls (Figure 22A). Importantly, the VLPN₅₀ values obtained only differed marginally from their results in the VLPNT (Table 2). Yet, first results obtained with human serum samples were less clear, as an analysis of a subset from the cohort of COVID-19 patients, vaccinees and healthy and immunologically naive donors revealed (Figure 22B). Because the naive sera displayed strong neutralization, a high cutoff value had to be defined, in order to still ensure high test specificity. Probably due to interfering matrix effects by the serum, weaker neutralization was indistinguishable from artefacts. Heat inactivation of the complement system or use of concentrated ACE2⁺ EV were unsuccessful in eliminating this background. Still, for the COVID-19 samples, the cfVLPNT performance correlated well with results from the cVNT and the VLPNT (Figure 22C, D). Because of its high threshold value that ensures the necessary specificity, an evaluation of the cfVLPNT revealed only a poor sensitivity (Figure 22E). Taken together, the cfVLPNT in its current form is only suitable to detect serum samples with high titers and needs further improvement to be used as an IVD.

Both, the VLPNT and the cfVLPNT follow simple and quick protocols that just require standard laboratory equipment, luminescence substrate, qualified S⁺ VLP preparations and dedicated cells or EVs (Supplementary Figure S4). For the cfVLPNT, even plating of cells on the day before can be omitted. The VLPNT can also be evaluated primitively with a camera of a mobile phone instead of a luminometer and is thus suitable for poorly equipped laboratories (Supplementary Figure S5). In addition, both assays significantly reduce safety issues and the amount of work and time, when compared to a cVNT or a pVNT (Table 3). Additionally, the authenticity of the S⁺ VLP based tests is superior to tests with pseudotyped particles and faithfully reflects the original virus.

4 Conclusion

In summary, the development of two novel VNTs that are based on SARS-CoV-2 VLPs is described, as well as the generation and characterization of several monoclonal, high affinity, S specific antibodies that effectively neutralize SARS-CoV-2 *in vitro*.

The novel VLPNT is a rapid, virus-free and safe assay to quantitate SARS-CoV-2 NAbs. It uses authentic S⁺ VLP, which were structurally and biochemically well characterized, faithfully replicate the initial steps of SARS-CoV-2 infection and can be quantitatively traced upon cell entry. When put to the test with a set of COVID-19 patient sera, NAb titers determined with the VLPNT were shown to correlate very well with results from a benchmark cVNT with fully infectious SARS-CoV-2. Furthermore, the VLPNT is adaptable to emerging VOCs, as demonstrated for the B.1.617.2 Delta- and B.1.1.529 BA.1 Omicron variants. As this technology fulfills important criteria for automation and up-scaling, it could be developed into a high-throughput screening approach for potential NmAbs or anti-viral-entry drugs in laboratories of low BSL. Most importantly, the VLPNT could simplify the testing of samples in clinical studies during vaccine development, the immune status surveillance among, e.g., healthcare workers or people at risk and the evaluation of immunity to emerging VOCs. In principle, this assay could be suitable as a platform technology for other enveloped viruses such as Dengue virus, West Nile Virus, EBV, respiratory syncytial virus (RSV) and human cytomegalovirus (CMV). If adaptable to enveloped emerging viruses other than SARS-CoV-2, this assay could play an important role in future disease preparedness.

Additionally, the proof-of-concept for a cell-free version of this test is demonstrated, which is based on the fusion of S⁺ VLP with ACE2⁺ EV. The findings presented here are among the first reports of fusion between a viral and a non-viral vesicle but to fully understand the underlying mechanisms, e.g. the protease usage, demands further elucidation. Preliminary results from the cVLPNT successfully demonstrated the quantitation of NAbs and their correlation with the cVNT but leave room for improvement of essential test parameters. Although this second novel test could profit from its independence from living cells, it first requires further optimization to perform serodiagnosis of comparable quality with the VLPNT.

5 Experimental Procedures

5.1 Materials

The following tables list relevant materials which have been essential for this work and all conducted experiments. Table 4 summarizes compounds and drugs that have been used for inhibitor studies of the VLPNT and cfVLPNT, as well as selected chemicals, which were commercially obtained by the supplier, indicated in the methods section. Table 5 and Table 6 list all DNA plasmids used for transient protein expression and stable transduction with retroviral vectors for this project. Identifiers (IDs), ORFs, backbone vectors, constructs and reference sources are indicated, with amino acid modifications in single letter code. Cell lines and plasmids are deposited at the department of gene vectors (AGV), Helmholtz Zentrum München. Table 7 gives an overview on all antibodies used for this work, with supplier ID or clone ID, antigen specificity, host species, subtype, producer, usage and conjugates, if applicable. Antibodies and conjugates were either obtained from the monoclonal antibody core facility of the Helmholtz Zentrum München (HMGU) or purchased from the respective supplier as indicated. Table 8 states all eukaryotic cell lines used in this work with their respective cell line identifier (CID), phenotype, species and ID of genomically integrated plasmids. Table 9 shows sequences of primers' used for rat antibody sequencing. DNA primer were ordered and commercially synthesized (Metabion). Table 10 states special centrifuges and rotors for ultracentrifugation, essential for this work. In Table 11, relevant software products can be found, with their respective usage.

Table 4. Drugs and compounds.

Substance	CAS RN	Mode of action
Chloroquine	50-63-5	Deacidifying lysosomotropic agent ^[66]
Camostat-mesylate	59721-29-8	TMPRSS2 inhibitor ^[102]
BB94 (Batimastat)	130370-60-4	MMP inhibitor ^[122]
Probenecid	57-66-9	Organic anion transporter (OAT)-1 and -3 inhibitor ^[92]
Protaminesulfate	9009-65-8	Transduction enhancing polycation ^[157]

Table 5. Expression plasmids.

ORF	ID	Vector	Construct and amino acid mutations	Species	GenBank/NCBI ref.
S	p7386	pcDNA3.1(+)	S(Wuhan-Hu-1) ^[3] :1-1273, 1274G, 1275P	SARS-CoV-2	YP_009724390.1
S	p7400	pcDNA3.1(+)	S(Wuhan-Hu-1) ^[3] :1-1256, ΔEER-tag	SARS-CoV-2	
S(B.1) ^[17]	p7417	pcDNA3.1(+)	S(Wuhan-Hu-1) ^[3] :1-1273, D614G	SARS-CoV-2	
S(B.1) ^[17]	p7413	pcDNA3.1(+)	S(Wuhan-Hu-1) ^[3] :1-1256, D614G, ΔEER-tag	SARS-CoV-2	
S(B.1.617.2)	p7487	pcDNA3.1(+)	S(Wuhan-Hu-1) ^[3] :1-1256, T19R, Δ157-158, L452R, T478K, D614G, P68R, D950N, ΔEER-tag	SARS-CoV-2	UFEM53021.1
S(B.1.1.529 BA.1)	p7501	pcDNA3.1(+)	S(Wuhan-Hu-1) ^[3] :1-1256, A67V, Δ69-70, T95I, G142D, Δ143-145, Δ211, L213I, ins214EPE, G339D, S371L, S373P, S375F, K417N, N440K, G446S, S477N, T478K, E484A, Q493K, G496S, Q498R, N501Y, Y505H, T547K, D614G, H655Y, N679K, P681H, N764K, D796Y, N856K, Q954H, N969K, L981F, ΔEER-tag	SARS-CoV-2	UJT03851.1
S(B.1) ^{ΔFurin}	p7519	pcDNA3.1(+)	S(Wuhan-Hu-1) ^[3] :1-1256, D614G, R682G, R683G, R685G, ΔEER-tag	SARS-CoV-2	
M	p7395	PCMV-C19	M(Wuhan-Hu-1) ^[3] :1-222	SARS-CoV-2	YP_009724393.1
N	p7391	pcDNA3.1(+)	N(Wuhan-Hu-1) ^[3] :1-419	SARS-CoV-2	YP_009724397.2
E	p7396	pcDNA3.1(+)	E(Wuhan-Hu-1) ^[3] :1-75	SARS-CoV-2	YP_009724392.1
VSV-G	p5451	pMD2.G	VSV-G:1-511	VSV	NP_041715.1
Mock	p5025	PCMV			
CD63~Blam	p7200	pcDNA3.1(+)	hCD63:1-238, GSGGGGS, class A β-lactamase (Blam):1-262	<i>Homo sapiens</i>	NP_001244318.1
CD63~HiBiT	p7447	pcDNA3.1(+)	hCD63:1-238, GSGGGSSGSSG, HiBiT:VSGWRLFKKIS	<i>Homo sapiens</i>	NP_001244318.1
h43A11 HC		pcDNA3.1(-)	1-20, 21-144:V _H 43A11, 145-474:hC _{H1} , hC _{H2} , hC _{H3}	<i>Homo sapiens</i>	Supplementary Table S1
h43A11 LC		pcDNA3.1(-)	1-22, 23-130:V _L 43A11, 131-237:hC _L	<i>Homo sapiens</i>	Supplementary Table S1
h55E10 HC		pcDNA3.1(-)	1-20, 21-141:V _H 55E10, 142-471:hC _{H1} , hC _{H2} , hC _{H3}	<i>Homo sapiens</i>	Supplementary Table S1
h55E10 LC		pcDNA3.1(-)	1-22, 23-131:V _L 55E10, 132-238:hC _L	<i>Homo sapiens</i>	Supplementary Table S1

Table 6. Viral vectors for transductions.

ORF	ID	Vector	Construct and amino acid mutations	Species	GenBank/NCBI ref.
ACE2	p7406	MP71	hACE2:1-805, K631R	<i>Homo sapiens</i>	BAB40370.1
ACE2	p7440	MP71	hACE2ACE2:1-805, 806-1024:T2A-PuromycinR	<i>Homo sapiens</i>	NP_001358344.1
TMPRSS2	p7504	MP71	hTMPRSS2:1-529	<i>Homo sapiens</i>	NM_001135099.1
NM~LgBiT	p7454	MP71	NM:MGARAS, GGGG, LgBiT:1-158	<i>Oplophorus gracilirostris</i>	QWVT72353.1
CD63~LgBiT	p7458	MP71	hCD63:1-238, GSGGGGS, LgBiT:1-158	<i>Homo sapiens</i>	NP_001244318.1
gag/pol	p4037	pcDNA3	Group-specific antigen (gag) polyprotein:1-569, matrix protein p15, RNA-binding phosphoprotein p12, capsid protein p30, nucleocapsid protein p10; polymerase (pol) polyprotein:1-1090, protease, reverse transcriptase/ribonuclease H, integrase	<i>Oplophorus gracilirostris</i>	QWVT72353.1
env	p4038	pALF	Envelope and fusion protein (env) polyprotein	<i>Moloney murine leukemia virus</i>	AAA46514.1
eGFP	p6895	MP71	5' long terminal repeat (LTR) packaging signal, eGFP, 3'LTR	<i>Aequorea victoria</i>	ADQ43426.1
	p6896	MP71	5'LTR packaging signal, 3'LTR		

Table 7. Primary and secondary antibodies.

ID	Antigen	Clonality	Host	Subtype	Supplier	Use	Conjugate
Primary antibodies							
AC18F	hACE2	mAb	Mouse	IgG1	AdipoGen	WB	
FAB933A	hACE2	pcAb	Goat	IgG	R&D systems	FC	APC
GLTX632604	SARS-CoV-2 S2	mAb	Mouse	IgG1	GeneTex	WB, FC	
PA5-81795	SARS-CoV-2 S1	pcAb	Rabbit	IgG	Thermo Fisher	WB	
43A11	SARS-CoV-2 S ^{FL}	mAb	Rat	IgG2b	HMGU	WB, FC, ELISA	HRP, AlexaFluor488 & 647
55E10	SARS-CoV-2 S ^{FL}	mAb	Rat	IgG2b	HMGU	WB, FC, ELISA	AlexaFluor647
5D1	SARS-CoV-2 S2/S ^{FL}	mAb	Rat	IgG2b	HMGU	WB	
5B9	SARS-CoV-2 S1	mAb	Rat	IgG2b	HMGU	WB, VLPNT	
35B12	SARS-CoV-2 S1	mAb	Rat	IgG2a	HMGU	WB, VLPNT	
42E2	SARS-CoV-2 S1	mAb	Rat	IgG2b	HMGU	WB, VLPNT	
REGN10987	SARS-CoV-2 S1	mAb	Human	IgG1	HMGU	VLPNT	
REGN10933	SARS-CoV-2 S1	mAb	Human	IgG1	HMGU	VLPNT	
4H3	FLAG	mAb	Rat	IgG2b	HMGU	ELISA	
30E5	HiBiT	mAb	Mouse	IgG	Promega	WB	
N7100	LgBiT	mAb	Mouse	IgG	Promega	FC	
24F9	hCDD63	mAb	Rat	IgG	HMGU	WB, FC	HRP
Secondary antibodies							
7076S	Mouse IgG	mAb	Horse	IgG	Cell Signaling	WB	HRP
7074S	Rabbit IgG	mAb	Goat	IgG	Cell Signaling	WB	HRP
709-035-149	Human IgG	pcAb	Donkey	IgG	Jackson	WB	HRP
1112-035-062	Rat IgG	pcAb	Goat	IgG	Jackson	WB	HRP
415-605-166	Mouse IgG	pcAb	Rat	IgG	Jackson	FC	AlexaFluor647
212-605-082	Rat IgG	pcAb	Mouse	IgG	Jackson	FC	AlexaFluor647

Table 8. Cell lines.

Cell type	CID	Phenotype	Plasmid ID	Species
HEK293	3093			<i>Homo sapiens</i>
	4618	SARS-CoV-2 S(B.1) ⁺	p7413	<i>Homo sapiens</i>
HEK293T	3915	HEK293, SV40 TA _g		<i>Homo sapiens</i>
	4594	hACE2 ⁺		<i>Homo sapiens</i>
U251MG	4629	hACE2 ⁻		<i>Homo sapiens</i>
	4663	hACE2 ⁺	p7440	<i>Homo sapiens</i>
	4685	hACE2 ⁻ , NM~LgBiT ⁺	p7454	<i>Homo sapiens</i>
	4684	hACE2 ⁺ , NM~LgBiT ⁺	p7406, p7454	<i>Homo sapiens</i>
	4697	hACE2 ⁺ , NM~LgBiT ⁺	p7406, p7454	<i>Homo sapiens</i>
	4694	hACE2 ⁻ , CD63~LgBiT ⁺	p7458	<i>Homo sapiens</i>
	4693	hACE2 ⁺ , CD63~LgBiT ⁺	p7406, p7458	<i>Homo sapiens</i>
4727	hACE2 ⁺ , CD63~LgBiT ⁺	p7440, p7458	<i>Homo sapiens</i>	
Vero	690			<i>Cercopithecus aethiops</i>
	4608	hACE2 ⁺	p7406	<i>Cercopithecus aethiops</i>
Huh7	4619			<i>Homo sapiens</i>

Table 9. Primer for rat antibody sequencing.

Primer	Specificity	Sequence 5'-3'
cDNA	C _H 1 IgG2a	ACAAGGATTGCATTCCCTTGG
	C _H 1 IgG2b	GCATTTGTGTCCAATGCCGCC
	C _L κ	CTCATTCCCTGTTGAAGCTCTTGACGAC
Anchor	Poly-dC-tail	CUACUACUACUAGGCCACGCGTCTGACTAGTACGGGIIGGGIIGGGIIG
Nested	C _H 1 IgG2a/b	CTACTAGCATGCTCGAGCTCAATTTTCTTGTCCACCTTGGTGC
	C _L κ	CTACTAGCATGCTCGAGCTCATTCCCTGTTGAAGCTCTTGACGACGGG

(I: deoxyinosine)

Table 10. Ultracentrifugation equipment.

Centrifuge	Rotor	rpm [min ⁻¹]	× g at r _{av}	Producer
Optima L-70	SW28Ti	24 000	100 000	Beckman Coulter
	SW32Ti	24 000	100 000	Beckman Coulter
	SW60Ti	39 000	160 000	Beckman Coulter
Sorvall MTX150	S55-AT2	43 000	100 000	Thermo Fisher Scientific

Table 11. Software aids.

Name	Version	Usage	Producer
Bio-1D	CFR21	WB documentation	Vilber
ChimeraX	0.92	Molecular modeling	UC
Diva	8.0.1	Flow cytometry (FC) measurement	Becton Dickinson
Excel	16.54	Data analysis	Microsoft
FlowJo	10.8.0	FC analysis	Becton Dickinson
ImageJ (Fiji)	2.1.0/1.53c	Image processing	NIH
L ^A T _E X	1.40.24	Text editing (MacTex)	TeXnical group
MacVector	18.1.4	Nucleotide and protein analysis	MacVector
MARS	V4.01 R4	Lumino- & photometer plate reader	BMG Labtech
PowerPoint	16.54	Illustrations	Microsoft
Prism	9.3.1	Data analysis and visualization	GraphPad Software

5.2 Methods

Substantial parts of the experimental procedures described in this study have previously been published and can therefore also be found partially identically in the material & methods section of the respective manuscript.^[48]

5.2.1 Plasmid Production in Prokaryots

Chemically competent bacteria, *Escherichia coli* (*E. coli*), strain DH5 α (Invitrogen), were transformed by heat-shock at 42°C with plasmid deoxyribonucleic acid (DNA) and let recover at 37°C, before plating on LB agar plates with the respective antibiotic (100 $\mu\text{g mL}^{-1}$ ampicillin, Carl Roth; 30 $\mu\text{g mL}^{-1}$ chloramphenicol, Carl Roth; 30 $\mu\text{g mL}^{-1}$ kanamycin, Carl Roth) and over night (o/n) incubation at 37°C. Single colonies were picked to inoculate sterile LB medium, supplemented with the respective antibiotic and cultivated at 37°C o/n. Cultures were harvested by centrifugation, cryo-stocks prepared in glycerol and flash frozen in liquid N₂ before storage at -80°C. Plasmid DNA was prepared from *E. coli* pellets using Endofree Plasmid Maxi Kit (12362, Qiagen) according to the manufacturer's instructions. Concentration and purity of DNA preparations was assessed using a Nanodrop ND-1000 spectrophotometer (Peqlab Biotechnologie) and the respective absorbance profile at 260 nm and 280 nm.

5.2.2 Eukaryotic Cell Lines and Cell Culture*

HEK293 (CID3093); HEK293T (CID3915); HEK293, S⁺ (CID4618); U251MG, hACE2^{+/-} (CID4663, CID4629), U251MG, hACE2^{+/-}, NM~LgBiT⁺ (CID4697, CID4685), as well as U251MG, hACE2^{+/-}, CD63~LgBiT⁺ (CID4727, CID4694) cells were maintained in DMEM

*As published by Roessler *et al.* 2022.^[48]

(Gibco, Thermo Fisher Scientific), supplemented with 8% FBS (AC-SM-0143, Anprotec), penicillin (Pen) and streptomycin (Strep) (Gibco, Thermo Fisher Scientific). Vero (CID690) and Vero, hACE2⁺ (CID4608) cells were maintained in RPMI 1640 (Gibco, Thermo Fisher Scientific), supplemented with 8% FBS (AC-SM-0143, Anprotec) and Pen/Strep (Gibco, Thermo Fisher Scientific). Adherent cell lines (Table 8) were cultivated at 37°C in a water-saturated atmosphere with 5% CO₂. Cell viability was monitored by trypan blue exclusion and cultures with more than 95% viable cells were used in all experiments. Cell lines constitutively expressing hACE2, TMPRSS2, NM~LgBiT, CD63~LgBiT or S were generated by retroviral transduction or transient transfection of parental cells with expression plasmids followed by selection with the respective antibiotic or single cell seeding and flow cytometric cell sorting.^[48] For cryopreservation of eukaryotic cells, cultures were washed once with PBS, trypsinized or detached with TrypLE (Gibco, Thermo Fisher Scientific), washed again with PBS and pelleted by centrifugation, resuspended in pre-cooled freezing medium (Bambanker, Nippon Genetics Europe), before frozen at -80°C. For long term storage, cells were transferred and stored in the gas phase of liquid N₂. Frozen cells were quickly thawed by resuspending and washing in 37°C pre-warmed cell culture medium and centrifugation, before seeding on cell culture plates.

5.2.3 Flow Cytometry

For flow cytometry, 2×10^5 cells were washed once with buffer (PBS, 3 vol% FBS), centrifuged for 6 min at $300 \times g$, resuspended in 50 μ L buffer, supplemented 1:100 with a respective primary mAb (Table 7) or supplemented 1:2 with respective hybridoma supernatant and incubated at 7°C for 20 min. For primary antibodies without fluorescence label, cells were washed once with 1 mL buffer as described and resuspended in 50 μ L buffer, supplemented 1:500-20 000 with a respective fluorescently labeled secondary antibody. After repeated washing with 1 mL buffer, 450 μ L buffer were added and cells analyzed in a flow cytometer. For analytical flow cytometry, cells were analyzed in a LSR Fortessa (Becton Dickinson), preparative sorting was performed in a FACSAria III (Becton Dickinson).

5.2.4 Anti-Spike Antibody Generation*

To obtain spike antigen in its authentic conformation for the immunization of rats, a constitutive spike expressing HEK293 cell line (CID4618) expressing SARS-CoV-2 S(B.1) was established. To boost expression levels further, cells were transiently transfected with an S expression plasmid (p7413) prior to the isolation of S⁺ EVs from conditioned medium three days after transfection. EVs were purified and concentrated by ultrafiltration, density gradient ultracentrifugation and subsequently characterized as previously described.^[48] For the generation of anti-spike antibodies (immunizations: COVEV1, COVEV2 and COVEV3),

*As published by Roessler *et al.* 2022.^[48]

S⁺ EVs were used to immunize rats in a prime-boost-boost scheme with up to 1.7×10^{11} particles per injection according to NTA, either with or without addition of Freund's incomplete adjuvant, before splenic B cells were isolated to establish hybridoma cell clones. Specific clones were subsequently identified by screening of hybridoma supernatants for binding to the constitutive spike expressing HEK293 cell line (CID4618) via flow cytometry using a high throughput sampler on a LSR Fortessa instrument (Becton Dickinson). The resulting anti-spike antibodies were then characterized thoroughly to validate their affinities and specificities for spike.^[48]

5.2.5 Antibody Production*

COVEV (43A11, 55E10, 5D1, 5B9, 35B12 and 42E2) and other antibodies (FLAG 4H3, EXOM 24F9) were purified from hybridoma supernatants, while REGN10987 and REGN10933 antibodies were purified from CHO cells transiently transfected with expression plasmids encoding the heavy and light chains. Briefly, cell culture supernatant was loaded on a protein GammaBind Plus Sepharose (17088602, Cytiva) or HiTrap MabSelect SuRe (29049104, Cytiva) column, washed with PBS and antibodies were eluted at pH 2.7 or 3.5, respectively in citric acid buffer. Fractions were pooled, neutralized with 1 M Tris (pH 8.0) and separated on a Superdex200 prep grade (17104301, Cytiva) in PBS for monomers or buffer exchanged to PBS via ultrafiltration, respectively. Directly coupled AlexaFluor488 labelled antibodies were generated using commercial kits (A10235, Thermo Fisher Scientific).^[48]

5.2.6 Antibody Sequencing

Amino acid sequences of COVEV antibodies were determined by sequencing from hybridoma mRNA. Therefore, RNA was isolated from pellets of hybridoma cells (Monarch total RNA miniprep kit, TS2010S, New England Biolabs), reverse transcribed to cDNA and amplified by rapid amplification of cDNA ends (RACE)-PCR (18374058, Thermo Fisher Scientific).^[158] In detail, 2.5 µg isolated RNA and 40 pmol chain specific primer (Table 9) were mixed in 15 µL diethyl pyrocarbonate (DEPC)-treated H₂O, incubated for 10 min at 70°C and placed on ice for 1 min, before adding 2.5 µL 10× PCR-buffer, 2.5 µL 25 mM MgCl₂, 1 µL 10 mM dNTP mix and 2.5 µL 0.1 mM dithiothreitol (DTT). After homogenization, samples were incubated at 42°C for 1 min and mixed with 1 µL SuperScript II reverse transcriptase (18064014, Thermo Fisher Scientific), before incubating at 42°C for 50 min, followed by 70°C for 15 min, to stop the reaction. After brief centrifugation, 1 µL RNase mix was added and samples were incubated at 37°C for 30 min. Next, cDNA was purified (S.N.A.P kit, K199925, Thermo Fisher Scientific), by mixing with 120 µL 6 M NaI, loading on a spin column, repeated washing via centrifugation with buffer and cold 70 vol% EtOH, followed by elution with 50 µL H₂O at 65°C. A fraction of the product, 10 µL, were then subjected to terminal deoxynucleotidyl transferase (TdT) 3'-tailing, by adding 6.5 µL DEPC-treated H₂O, 5 µL 5× buffer,

*As published by Roessler *et al.* 2022.^[48]

2.5 μL 2 mM dCTP, incubating at 94°C for 2.5 min, on ice for 1 min, brief centrifugation and adding 1 μL TdT. Upon, 10 min at 37°C, TdT was heat inactivated at 65°C for 10 min and the reaction placed on ice. 3'-poly-dC-tailed cDNA, was then replicated by mixing 26 μL H₂O, 10 μL 5 \times buffer, 3 μL 25 mM MgCl₂, 1 μL 10 mM dNTP, 5 μL dC-tailed cDNA, 2 μL 10 μM forward anchor primer, 2 μL 10 μM nested RACE reverse primer for C_H1 or C_L (Table 9), 1 μL GoTaq polymerase and subsequent PCR, in a thermocycler (T gradient, Biometra), following the protocol, described in Table 12. Successful amplification was evaluated by electrophoresis (150 V, 30 min) on an analytical 1% (w/v) agarose (Life Technologies) gel in TAE buffer (Tris base, acetate, EDTA, Carl Roth). The remaining PCR product was purified by a spin column kit (11992242, NucleoSpin PCR clean-up kit, Macherey-Nagel), pre-mixed with the respective nested RACE reverse primer for C_H1 or C_L and send for Sanger-sequencing (Eurofins Genomics). Resulting DNA sequences were analyzed and annotated at www.abysis.org.

Table 12. RACE PCR protocol.

Cycles	Temperature	Time	Step
35 \times	94°C	90 s	Initial denaturation
	94°C	30 s	Template denaturation
	55°C	30 s	Primer annealing
	72°C	60 s	DNA extension
	72°C	6 min	Final extension
	4°C	∞	Final extension

5.2.7 Transient Transfection

For transient protein expression, 4×10^5 HEK293T in 2 mL DMEM (8% FBS, Pen/Strep supplemented) were seeded per well in a 6-well plate (140675, Thermo Fisher Scientific) and incubated overnight at 37°C. The next day, medium was exchanged for 1 mL fresh medium and a total of 1 to 2 μg of plasmids in Table 5 were dissolved in 200 μL OptiMEM (Gibco, Thermo Fisher Scientific), mixed with 4.5 μL , 1 mg mL⁻¹ polyethylenimine hydrochloride (PEI_{max}, 24765-1, Polysciences) pH 7.0 in H₂O, per 1 μg DNA and incubated for 15 min at room temperature (RT). Alternatively, 2.5 μL TransIT-293 (MIR-2700, Mirus) per 1 μg DNA were used instead of PEI_{max}. Subsequently, the transfection mix was carefully added on top of cells and the cells incubated at 37°C.

5.2.8 Retroviral Transduction

For constitutive protein expression and cell line generation, cells were transduced with replication deficient retroviral vectors. Retrovirus stocks were generated by co-transfecting expression plasmids (p4037, p4038) coding for the murine leukemia virus (MLV) polyproteins group-specific antigen (gag), polymerase (pol) and envelope and fusion protein (env), as

well as a myeloproliferative sarcoma virus (MPSV) based retroviral vector (MP71),^[159] encoding the respective protein of interest (Table 6) into HEK293T cells using TransIT-293 (MIR-2700, Mirus) according to the manufacturers protocol. After 48 h, the supernatant was harvested and centrifuged at 7°C for 10 min at 300 × g, 20 min at 4200 × g and flash frozen in liquid N₂ for storage at -80°C. For the transduction, 1 × 10⁵ cells were seeded in 1 mL DMEM (8% FBS, Pen/Strep supplemented) per well in a 12-well plate (150628, Thermo Fisher Scientific) and incubated at 37°C, 5% CO₂ overnight. Cells were then incubated with a mix of 500 µL respective retroviral supernatant and 500 µL fresh medium (DMEM, 8% FBS, Pen/Strep), supplemented with 8 µg mL⁻¹ protamine sulfate (110123, Sigma-Aldrich, 4 µg mL⁻¹ final concentration), before centrifuged for 90 min at 800 × g, 32°C. After 48 h at 37°C, protein expression was evaluated via FC and cells were selected via an encoded resistance gene if needed.

5.2.9 Pseudotyped Virus Neutralization Test*

S-pseudotyped retrovirus stocks were generated by co-transfecting expression plasmids coding for S, gag/pol (from MLV) and a MPSV based retroviral vector encoding GFP (p7413, p4037, p6895) into HEK293T cells using TransIT-293 (MIR-2700, Mirus) according to the manufacturers protocol. After 48 h, the supernatant was harvested and centrifuged at 7°C for 10 min at 300 × g, 20 min at 4200 × g and flash frozen in liquid N₂ for storage at -80°C. For pVNTs, 5 × 10³ Vero, hACE2⁺ cells (CID4608) were seeded in 100 µL DMEM (8% FBS, Pen/Strep supplemented) per well in a 96-well plate (353072, Falcon) and incubated at 37°C, 5% CO₂ overnight. Cells were then pre-incubated for 1 h at 37°C in 50 µL, 8 µg mL⁻¹ protamine sulfate (110123, Sigma-Aldrich) in DMEM with or without chloroquine (C6628, Sigma-Aldrich, chloroquine diphosphate dissolved in ddH₂O) and retroviral stocks were pre-incubated for 30 min at 37°C with 5 × serum dilutions in PBS or chloroquine. 50 µL of the respective mix were then added to the pre-incubated cells and centrifuged for 90 min at 800 × g, at 32°C. After 48 h at 37°C, GFP expression was quantified by FC using a high throughput sampler on a LSR Fortessa instrument (Becton Dickinson).^[48]

5.2.10 Generation of VLPs and Engineered EVs*

To generate S⁺ VLPs containing appropriate levels of SARS-CoV-2 S(B.1, B.1.617.2 or B.1.1.529 BA.1), VSV-G⁺ EVs and control-EVs, HEK293T cells were seeded and transfected the next day, using PEI_{max} or TransIT-293 (MIR-2700, Mirus), according to the protocol described on page 77 with carefully adjusted ratios of codon-optimized expression vectors coding for S, VSV glycoprotein G (VSV-G), or mock together with CD63~HiBiT or CD63~BlaM and, optionally, M, N and E. For S⁺ VLPs *e.g.* plasmids for S, M, N, E and CD63~HiBiT or CD63~BlaM were transfected in DNA mass-ratios: 2:5:5:5:80 respectively. The expression plasmids are termed p7413.1 (S:B.1), p7487.IA1 (S:B.1.617.2), p7501.EA20

*As published by Roessler *et al.* 2022.^[48]

(S:B.1.1.529 BA.1), p5451 (VSV-G), p5025 (mock), p7447.SA11 (CD63~HiBiT), p7200.2 (CD63~BlaM), p7395.LA3 (M), p7396.NA9 (E), p7391.MA5 (N) and can be found in Table 5. Medium exchange was performed 6 h after the addition of the transfection mix to reduce a potential carry-over of plasmid DNA. After 72 h, S⁺ VLPs, VSV-G⁺ EVs or control EVs were harvested from conditioned cell culture supernatants (DMEM, 8% FBS, supplemented with Pen/Strep, Gibco, Thermo Fisher Scientific), low-speed centrifuged at 7°C for 10 min at 300 × g and 20 min at 4200 × g and generally used without further processing.^[48] For hACE2^{+/-}, CD63~LgBiT⁺ EVs, 4 × 10⁶ U251MG (CID4727 or CID4694) were seeded on a 130 mm cell culture dish (168381, Thermo Fisher Scientific) in 18 mL (DMEM, 8% FBS, Pen/Strep) and incubated for 72 h prior to harvest from conditioned media as described.

5.2.11 Purification of VLPs and Engineered EVs*

If necessary and as indicated, S⁺ VLP and EV supernatants were concentrated and further purified for some experiments. In these instances, EV depleted medium was utilized for S⁺ VLP and EV generation, to avoid enrichment of FBS EVs. Therefore, medium (DMEM, 20% FBS, Pen/Strep) was ultracentrifuged at 100 000 × g, 4°C for 16 h (Table 10), decanted, diluted to 8% FBS with DMEM (Pen/Strep) and sterile-filtered through a 0.22 μm filter (Techno Plastic Products) prior to usage. S⁺ VLP and EV supernatants were harvested from conditioned media as described and concentrated by centrifugal ultrafiltration with 100 kDa cutoff at 3000 × g or sedimented by ultracentrifugation at 100 000 × g, 4°C, 2 h. Further separation was achieved by floatation and fractionation in a carefully stacked discontinuous iodixanol (Optiprep, Sigma-Aldrich) density gradient (bottom to top: 1.75 mL sample with 34% final Optiprep concentration; 1.65 mL 30% Optiprep in PBS; 0.6 mL PBS) and ultracentrifugation at 160 000 × g, 4°C for 4 h. Collected fractions of 400 μL were washed with PBS by ultracentrifugation at 100 000 × g, 4°C for 2 h, and resuspended. Particle preparations were flash frozen in liquid nitrogen for storage at -80°C and subsequently characterized by WB, NTA, nano flow technology, ELISA, cryo-EM, Pierce BCA protein assay (23225, Thermo Fisher Scientific), VLPNT and cfVLPNT.^[48]

5.2.12 Western Blot*

Samples of S⁺ VLPs and other EVs from cell culture supernatants, concentrates or purified preparations were mixed with non-reducing 5× Laemmli buffer [10% (w/v) SDS, 300 mM Tris/HCl pH 6.8, 30 vol% glycerol and bromophenol blue] or reducing 5× Laemmli buffer [10% (w/v) SDS, 300 mM Tris/HCl pH 6.8, 30 vol% glycerol, 25 vol% 2-mercaptoethanol and bromophenol blue] and incubated at 95°C for 5 min, if indicated. For cell lysates, cells were washed with PBS, resuspended in RIPA buffer [150 mM NaCl, 50 mM Tris/HCl pH 7.4, 1 vol% NP-40 (IGEPAL CA-630, Sigma-Aldrich), 0.5% (w/v) sodium deoxycholate,

*As published by Roessler *et al.* 2022.^[48]

0.1% (w/v) SDS, supplemented with cOmplete EDTA-free protease inhibitor (Roche)], incubated for 30 min on ice and centrifuged for 30 min at $16\,000 \times g$. After discarding the pellet, lysates were normalized to protein concentration using Bradford reagent (Bio-Rad) and a photometer. Samples were separated by 4-12% or 10% SDS-PAGE, at 100 V for 2.5 h in Bis-Tris-glycin buffer (MOPS NuPAGE, Thermo Fisher Scientific), supplemented with 5 mM $\text{Na}_2\text{O}_5\text{S}_2$ for reducing blots. Proteins were transferred to nitrocellulose membranes (GE Healthcare Life Science) by semi-dry blotting (Trans-Blot turbo transfer system, Bio-Rad) at 18 V for 45 min in blotting buffer [0.3% (w/v) Tris, 200 mM glycine, 0.04 vol% SDS, 20 vol% MeOH] and blocked for 1 h in 5% (w/v) non-fat milk (Carl Roth) in ddH₂O at RT. Membranes were incubated at 7°C overnight with primary antibodies from Table 7 (43A11, rat IgG2b, COVEV; 1A9, mouse IgG, GeneTex; PA5-81795, polyclonal rabbit antibody, Invitrogen) at 1:2000 dilution in 5% (w/v) non-fat milk (Carl Roth) in ddH₂O, washed 3 times in TBST (Tris-buffered saline with 0.1% Tween-20) and incubated at RT for 1 h with HRP conjugated secondary antibody from Table 7 (1112-035-062, goat anti-rat IgG, Jackson Immuno Research Europe; 7076S, horse anti-mouse IgG, Cell Signaling; 7074S, goat anti rabbit IgG, Cell Signaling) at 1:20 000, 1:2000 and 1:2000 dilution respectively, in 5% (w/v) non-fat milk in PBST (PBS, 0.05% Tween-20). After $3 \times$ washing in TBST, blots were incubated with ECL reagent (GE Healthcare) and imaged using a Fusion FX (Vilber).^[48]

5.2.13 ELISA*

For the quantitation of spike in samples from various sources, a sandwich enzyme-linked immunosorbent assay (ELISA) was developed, using two anti-spike antibodies with non-overlapping epitopes. First, wells of a Nunc MaxiSorp 96-well plate (44-2404-21, Thermo Fisher Scientific) were coated at RT for 5 h with 100 μL $2 \mu\text{g mL}^{-1}$ anti-S capture antibody (55E10, rat IgG2b, COVEV) or isotype mAb (FLAG 4H3, rat IgG2b) in PBS. After washing ($4 \times 300 \mu\text{L}$) with PBST (PBS, 0.05 vol% Tween-20), free binding sites were blocked with 300 μL 5% (w/v) non-fat milk (Carl Roth) in PBS at RT for 2 h and the plate washed again ($4 \times 300 \mu\text{L}$ PBST). Samples of recombinant spike protein (S1+S2 extracellular domain, 40589-V08B1, Sino Biological), S⁺ VLPs, or controls were diluted as indicated in PBS and 100 μL incubated at 7°C for 16 h on the coated plate. After washing ($4 \times 300 \mu\text{L}$ PBST), 100 μL HRP conjugated anti-spike detection antibody (43A11_HRP, rat IgG2b, COVEV) diluted 1:500 in 5% (w/v) non-fat milk in PBS, were added at RT for 2 h. Upon repeated washing ($4 \times 300 \mu\text{L}$ PBST), the plate was incubated at RT with 100 μL TMB substrate reagent (BD555214, Becton Dickinson). The reaction was stopped after 12 min by adding 50 μL 1 M H₂SO₄ and absorbance was measured at 450 nm with 590 nm as reference wavelength in a CLARIOstar Plus (BMG Labtech). Upon subtraction of the reference OD, data analysis was performed with GraphPad Prism 9.2.^[48]

For the quantitation of spike from blood samples, human plasma and recombinant protein standard were diluted 1:10 in PBS, supplemented with 10 $\mu\text{g mL}^{-1}$ rat IgG2b (FLAG 4H3)

*As published by Roessler *et al.* 2022.^[48]

as scavenger, prior to the o/n incubation step on the coated plate. Thereby unspecific cross-binding of human antibodies to the capture rat antibody was quenched and assay interference reduced, as previously described by others.^[130]

5.2.14 NTA*

Nanoparticle tracking analysis (NTA) was performed with the ZetaView PMX110 instrument (Particle Metrix) and the corresponding software (ZetaView 8.04.02) was used to measure the number and the size distribution of S⁺ VLPs, virus stock and EV preparations. Samples were diluted in filtered PBS to achieve a vesicle concentration of approximately $1.0 \times 10^7 \text{ mL}^{-1}$. Pre-acquisition parameters were set to a sensitivity of 75, a shutter speed of 50, a frame rate of 30 frames per second and a trace length of 15. The post-acquisition parameters were set to a minimum brightness of 20, a minimum size of 5 pixels and a maximum size of 1000 pixels.^[48]

5.2.15 Nano Flow Technology*

Single S⁺ VLP, SARS-CoV-2 virions or EV particles were analyzed using a nano flow technology and a CytoFLEX LX cytometer (Beckman Coulter Life Science) with samples of S⁺ VLPs, SARS-CoV-2 stock and EVs pre-stained with CellTraceViolet (CTV, C34571, Thermo Fisher Scientific) at 37°C for 20 min and quenched with PBS with 1% (w/v) bovine serum albumin (BSA). Upon washing via a 100 kDa cutoff Amicon ultra filter, samples were stained with AlexaFluor488 conjugated anti-S antibody (43A11, rat IgG2b, COVEV), diluted and afterwards analyzed in the flow cytometer.^[48]

5.2.16 Negative Stain Electron Microscopy

For TEM with negative contrasting, aliquots of 20 μL from crude or purified S⁺ VLPs were deposited on EM grids coated with a perforated carbon film and incubated for 5 min. Upon draining excessive liquid with a filter paper, 20 μL 2% (w/v) phosphotungstic acid, $\text{H}_3[\text{P}(\text{W}_3\text{O}_{10})_4] \cdot n\text{H}_2\text{O}$, (79690, Sigma-Aldrich) in ddH₂O, were added on top of the grid and incubated for 1 min, before blotting excessive liquid with a filter paper and drying the sample in vacuum. For negative stain electron microscopy (nsEM), grids were mounted on a respective rack and analyzed in a Zeiss EM109/900 (Carl Zeiss) at 80 kV, with up to 140 000 \times magnification.

5.2.17 Cryo-Electron Microscopy*

Aliquots of 4 μL from crude or purified S⁺ VLPs were deposited on EM grids coated with a perforated carbon film. After draining the excess liquid with a filter paper, grids were

*As published by Roessler *et al.* 2022.^[48]

quickly plunged into liquid ethane cooled by liquid nitrogen, using a Leica EMCPD cryo-chamber, and stored in cryo-boxes under liquid nitrogen until use. For cryo-EM observation, grids were mounted onto a Gatan 626 cryoholder and transferred to a Tecnai F20 microscope (Field Electron and Ion Company, USA) operated at 200 kV. Images were recorded with an Eagle 2k CCD camera (Thermo Fisher Scientific).^[48]

5.2.18 EV Fusion Assay with BlaM Readout*

For EV fusion or EV neutralization assays with flow cytometry readout, 2×10^4 Vero, hACE2⁺ or U251MG, hACE2⁺ cells (CID4608, CID4663) in 100 μ L DMEM (8% FBS, Pen/Strep supplemented) were seeded per well in a 96-well plate (353072, Falcon) and incubated o/n at 37°C, 5% CO₂. Where indicated, the cells were then pre-incubated at 37°C for 1 h with chloroquine (C6628, Sigma-Aldrich, chloroquine diphosphate in ddH₂O) or were left without further treatment. The spent medium was replaced with up to 100 μ L concentrated CD63~BlaM⁺ EVs (S⁺, mock or VSV-G⁺) with or without prior pre-incubation with serum samples. After 4 h incubation at 37°C, 5% CO₂, the supernatant was removed, adherent cells were washed with PBS, trypsinized and moved to a V-bottom shaped 96-well plate (277143, Thermo Fisher Scientific) and sedimented by centrifugation. After washing the cells once in CO₂ independent medium (8% FBS, Pen/Strep supplemented, Gibco, Thermo Fisher Scientific), 50 μ L staining solution were added and cells incubated at RT in the dark o/n. The staining solution was composed of 2 μ L CCF4-AM, 8 μ L solution B (K1095, Thermo Fisher Scientific) and 10 μ L 250 mM probenecid (P8761, Sigma-Aldrich, in 300 mM NaOH_{aq.}) per 1 mL CO₂ independent medium (Thermo Fisher Scientific) supplemented with 8% FBS, Pen/Strep. After enzymatic turnover of CCF4, cells were washed once with PBS (3 vol% FBS) and analyzed by FC using an LSR Fortessa instrument (Becton Dickinson) with a high throughput auto sampler. The 409 nm wavelength laser (violet) was used for excitation of the fluorescence resonance energy transfer (FRET) substrate, resulting in emission of intact, non-cleaved CCF4 substrate at 520 nm (green), whereas emission of cleaved CCF4 substrate was detected at 447 nm (blue).^[48]

5.2.19 Confocal Fluorescence Microscopy

For LSCM, initially 7.5×10^4 U251MG hACE2^{+/-} cells (CID4697, CID4685) per well were seeded in 1 mL DMEM (8% FBS, Pen/Strep supplemented) on 12 mm glass coverslips (Carl Roth) in 12-well plates (150628, Thermo Fisher Scientific). After 20 h at 37°C, 5% CO₂, medium was removed and replaced with 1 mL S⁺ VLPs (CD63~BlaM⁺) or DMEM and incubated for further 7 h at 37°C. Upon removal of the medium, cells for BlaM readout were then incubated at RT overnight in the dark with 500 μ L staining solution, consisting of 2 μ L CCF4-AM, 8 μ L solution B (K1095, Thermo Fisher Scientific), 10 μ L 250 mM probenecid in 300 mM NaOH_{aq.} (P8761, Sigma-Aldrich) per 1 mL CO₂ independent medium (Thermo

*As published by Roessler *et al.* 2022.^[48]

Fisher Scientific), supplemented with 8%FBS, Pen/Strep. Cells for antibody staining, were treated with 500 μ L CO₂ independent medium (supplemented with 8% FBS, Pen/Strep) instead. After S⁺ VLP fusion and substrate turnover, medium was removed and cells carefully washed with 1 mL PBS, before fixation with 4 vol% paraformaldehyde (PFA) (50-980-487, Electron Microscopy Sciences) in PBS for 10 min at RT. Afterwards, cells for BlaM readout were washed with PBS. Cells for antibody staining were permeabilized with 0.3 vol% Tween-20 in PBS for 10 min at RT, blocked with 3% (w/v) BSA in PBS for 40 min at RT and stained for 1 h in the dark at RT with 1 μ g mL⁻¹ 43A11_AlexaFluor647, 1:3500 DAPI, 1% (w/v) BSA in PBS. Upon 3 \times washing with 1% (w/v) BSA, 0.1 vol% Tween-20 in PBS, and 3 \times washing with PBS, coverslips were dried by blotting, mounted upside down on glass slides with 7 μ L ProLong Diamond Antifade Mountant (Thermo Fischer Scientific) and let dry overnight at 4°C, before sealing the next day. Imaging by LSCM was conducted with a Leica DMI8 TCS SP8 confocal microscope (Leica Microsystems) and processed using ImageJ (NIH).

5.2.20 VLPNT with Nanouciferase Readout*

For VLPNTs, 2×10^4 U251MG (hACE2⁺, NM~LgBiT⁺) cells (CID4697) in 100 μ L DMEM (8% FBS, Pen/Strep supplemented) were seeded per well in a 96-well Lumitrac200 (655075, Greiner Bio-One) plate and incubated at 37°C, 5% CO₂ overnight. The following day, serial dilutions of serum samples by a factor of 2.1 starting at 1:2 to 1:360 were prepared in PBS in a 96-well plate. 12 μ L of the serial serum dilutions each were added to 48 μ L normalized S⁺ VLP (S, M, N, E, CD63~HiBiT) to obtain a series of final dilutions ranging from 1:10 to 1:1801. S⁺ VLPs and serum dilutions were incubated at 37°C for 30 min in a 96-well plate. Thereafter, 50 μ L were transferred to recipient cells after removal of their culture medium and the cells were incubated at 37°C, 5% CO₂ for 4 h. Prior to readout, the supernatant was removed and replaced with 25 μ L substrate mix (20 μ L OptiMEM, Gibco, Thermo Fisher Scientific, +5 μ L nano-Glo diluted 1:20 in LCS buffer, N2012, Promega). Bioluminescence was immediately quantified in a CLARIOstar Plus reader (BMG Labtech). Mean luminescence level of S⁺ VLPs, with PBS instead of serum, was set to 0% neutralization; while background luminescence obtained with Δ vFP EVs was set to 100% neutralization. For serum or antibody samples, the titers that corresponded to 50% neutralization were determined by modeling nonlinear, sigmoidal 4PL curves using Graphpad Prism 9.3.1 and calculating values that correspond to 50% absolute signal reduction after background correction. This value was termed 50% VLP neutralization titer (VLPN₅₀). The WHO international standard (NIBSC 20/136) was used as in-between runs and as within-run reference. For inhibitor experiments, cells were pre-incubated for 1 h at 37°C in 100 μ L DMEM (8% FBS, Pen/Strep supplemented) with chloroquine (C6628, Sigma-Aldrich, chloroquine diphosphate dissolved in ddH₂O) or camostat-mesylate (SML0057, Sigma-Aldrich, dissolved in DMSO) prior to incubation with S⁺ VLPs.^[48]

*As published by Roessler *et al.* 2022.^[48]

5.2.21 Cell-free VLPNT

For a cfVLPNT, serial dilutions of serum samples by a factor of 2.1 starting at 1:6 to 1:1081 were prepared in PBS in a 96-well plate. 7 μ L of the serial serum dilutions each were added to 28 μ L normalized S⁺ VLP (S, M, N, E, CD63~HiBiT) in a 96-well plate to obtain a series of final dilutions ranging from 1:30 to 1:5403. In parallel, 5 μ L of the serial serum dilution were added to 20 μ L ACE2⁺, CD63~LgBiT⁺ EV supernatant in a 96-well Lumitrac200 (655075, Greiner Bio-One) to obtain equal final serum dilutions ranging from 1:30 to 1:5403. Both mixtures were pre-incubated at 37°C for 30 min, before 25 μ L of the S⁺ VLP- serum mix were transferred to the 25 μ L ACE2⁺ EV - serum mix. The final mixture was then incubated at 37°C, 5% CO₂ for 4 h. Prior to readout, 6.6 μ L nano-Glo diluted 1:20 in LCS buffer (N2012, Promega) were added and bioluminescence was immediately quantified in a CLARIOstar Plus reader (BMG Labtech). VLPN₅₀ calculation of the cfVLPNT was performed similar as described for the VLPNT. For inhibitor experiments, S⁺ VLPs and ACE2⁺ EVs were pre-incubated separately for 30 min at 37°C with chloroquine (C6628, Sigma-Aldrich, chloroquine diphosphate dissolved in ddH₂O), camostat-mesyate (SML0057, Sigma-Aldrich, dissolved in DMSO) or BB94 (SML0041, Sigma-Aldrich, dissolved in DMSO) prior to mixing with each other and incubation.

5.2.22 Virus Stock Preparation*

CaCo-2 cells (American Type Culture Collection, ATCC, Virginia, USA) in cell culture medium (DMEM, 2% FBS) were challenged for 2 h with a clinical isolate of SARS-CoV-2 (GISAID EPI_ISL_2967222) previously obtained from a nasopharyngeal swab of a COVID-19 patient. Subsequently, cell culture medium was exchanged, and three days post infection supernatants were passaged on Vero-E6 cells (ATCC, Virginia, USA). Three days later, the cell culture supernatant was harvested and stored at -80°C. The virus stock was characterized by reverse transcription quantitative real-time PCR (RT-qPCR). Heat-inactivation of the virus stock was performed by incubating the sample for 30 min at 56°C.^[48]

5.2.23 SARS-CoV-2 Virus Neutralization Test*

Human sera were heat-inactivated at 56°C for 30 min and diluted in a series of two-fold dilution steps (1:4 to 1:512). 100 plaque-forming units (PFU) of SARS-CoV-2 stock (German isolate BavPat1/2020; European Virus Archive Global # 026 V-03883, GenBank: MZ558051.1) contained in 50 μ L was added to an equal volume of diluted serum. The mixture was incubated at 37°C and approximately 2×10^4 Vero C1008 cells (ATCC, Cat#CRL-1586) were added after 1 h. After a four-day incubation period, the CPE was evaluated by light microscopy. Virus neutralization was defined as the complete absence of CPE in a given serum dilution (VNT₁₀₀). The reciprocal geometric mean titer (GMT) was calculated from the

*As published by Roessler *et al.* 2022.^[48]

highest serum dilution without CPE based on three replicates. The lower detection limit of the assay was 1:8, corresponding to the first dilution of the serum tested. Two positive controls were used as inter-assay neutralization standards and quality control for each test. The WHO international standard (NIBSC 20/136) was tested seven times, resulting in a geometric mean titer (GMT) of 377 for 100% absence of CPE in this test.^[48,114]

5.2.24 Statistical Analysis*

Data and statistical analyses were performed using Prism 9.3.1 (GraphPad Software, California, USA). For main-, as well as supplementary figures, arithmetic mean values are displayed. Error bars for y-axes indicate standard deviation (SD) of at least three replicates or more if indicated. Prior to t-tests and one-way ANOVA, normal- or log₁₀-normal distribution according to Gaussian distribution was assured.^[48]

5.3 Patients and Specimens*

In this study, 80 serum specimens collected between April 6, 2020, and December 29, 2020, from 49 patients infected with SARS-CoV-2 and hospitalized at the LMU Klinikum, Munich, Germany were included. Patients are part of the COVID-19 Registry of the LMU Klinikum (CORKUM, WHO trial id DRKS00021225) and the study was approved on March 23, 2020 by the ethics committee (no. 20-245) of the Faculty of Medicine of the LMU (Ethik-Kommission bei der Medizinischen Fakultät der Ludwig-Maximilians-Universität München, Pettenkoferstr. 8a, 80336 München, Germany). Clinical data were obtained from health records and all patient data were anonymized for analysis. All patients were tested positive for SARS-CoV-2 by RT-qPCR in nasopharyngeal or oropharyngeal swabs. The median age of the 49 COVID-19 patients was 62 years (interquartile range 55 to 76 years), and 32.7% (16/49) of these individuals were female. Disease severity of the COVID-19 patients was categorized according to the WHO guideline ‘Clinical Management of COVID-19’:^[160] asymptomatic (no clinical signs of infection), mild (symptomatic patients without evidence of viral pneumonia or hypoxia), moderate (clinical signs of pneumonia, including fever, cough, dyspnoea), severe (clinical signs of pneumonia, plus one of the following: respiratory rate $>30 \text{ min}^{-1}$, severe respiratory distress, peripheral oxygen saturation (S_pO_2) $<90\%$ on room air), critical (one of the following: acute respiratory distress syndrome, sepsis, septic shock). Three patients were categorized as asymptomatic, 4 patients as mild, 12 patients as moderate, 15 patients as severe, and 15 patients as critical (Table 13).^[48]

Furthermore, serum samples of 12 healthy and naive donors were included as control group. These specimens were drawn from voluntary, according to their own statements, healthy donors, mostly laboratory staff, from October 2017 on, but no later than August

*As published by Roessler *et al.* 2022.^[48]

Table 13. Severity of COVID-19 patients.

Disease severity	Patients	Specimens
Asymptomatic	3	4
Mild disease	4	7
Moderate disease	12	17
Severe disease	15	25
Critical disease	15	27

Table 14. Vaccination scheme.

Prime	Boost	Vaccinees
BNT162b2	BNT162b2	5
mRNA-1273	mRNA-1273	2
AZD1222	BNT162b2	2
AZD1222	mRNA-1273	3
AZD1222	AZD1222	1
AZD1222		2
BNT162b2	2× BNT162b2	1
AZD1222	2× BNT162b2	2

2019. Therefore, the donors were by definition immunologically naive, with respect to SARS-CoV-2 infection. The median age of the 12 healthy and naive donors was 32 years (interquartile range 30 to 53 years), and 66.7% (8/12) of these individuals were female.

For test evaluation and VOC studies, serum samples of 13 COVID-19 vaccinees have been included in this study. They were drawn from voluntary donors, between February 2021 and September 2021 and mostly originate from laboratory personnel. According to their own statements, donors were healthy at the time of blood sampling and did not have a history of prior SARS-CoV-2 infection or COVID-19 until then. The median age of the 13 vaccinees was 60 years (interquartile range 45 to 67 years), and 53.8% (7/13) of these individuals were female. All fully vaccinated donors received two shots of the EMA authorized COVID-19 vaccines BNT162b2 (Comirnaty, BioNTech), mRNA-1273 (Spikevax, Moderna Biotech) or AZD1222 (Vaxzevria, AstraZeneca) either in a homologous or heterologous prime-boost scheme (Table 14). Vaccinations were attested for all donors by insight into the respective documentation. Blood sampling was conducted at least 13 days post second injection (median 19 days, interquartile range 14 to 33 days), to ensure seroconversion. From three of those donors, additional blood samples were drawn, after the first dose of vaccine, ~6 months post second injection and 1-3 months after a third shot (prime-boost-boost) for a small case study.

Data on all the individual titers, patients' clinical symptom severity, as well as all further information, from patients, vaccinees and naives can be found from page 103 on in Supplementary Table S2.

For the detection of spike protein in biological samples, 12 human blood plasma samples (with anticoagulant) of COVID-19 patients in an early stage with acute SARS-CoV-2 infection and 5 additional plasma samples of healthy donors were provided by Dr. Bastian Höchst, Institute of Molecular Immunology, Technische Universität München. Those specimens were exclusively used for ELISA and WB experiments and thus were not further specified within this work.

5.4 Contributions

All experiments shown in this dissertation were personally designed, executed and analyzed, except for the following contributions of others:

Prof. Dr. Wolfgang Hammerschmidt, HELMHOLTZ ZENTRUM MÜNCHEN, kindly cloned and provided most of the plasmids listed in Table 5 and Table 6 and helped experimentally to develop the formulation of SARS-CoV-2 S⁺ VLPs. Furthermore, he and **Dagmar Pich** generated and provided the cell lines CID4608, CID4684, CID4685, CID4693, CID4694 and CID4727 (Table 8) and conducted the sample preparation and acquisition for nano flow technology (Figure 10B).

Dr. Verena Krähling kindly performed cVNTs with replication competent SARS-CoV-2 in the BSL-4 laboratory of **Prof. Dr. Stephan Becker**, PHILIPPS UNIVERSITÄT MARBURG, at the Institute of Virology.

Prof. Dr. Oliver T. Keppler, MAX VON PETTENKOFER-INSTITUT, LUDWIG-MAXIMILIANS-UNIVERSITÄT MÜNCHEN, **Dr. Paul R. Wratil**, **Dr. Johannes C. Hellmuth**, department of medicine III, KLINIKUM DER UNIVERSITÄT MÜNCHEN, and others,^[48] kindly provided the 80 COVID-19 patient serum samples from the CORKUM registry of the LMU university hospital.

Prof. Dr. Alain Brisson, UMR-CBMN at CNRS-UNIVERSITY OF BORDEAUX-INP, Pessac, France, and **Sisareuth Tan** thankfully accomplished imaging of S⁺ VLPs by cryo-EM (Figure 7B).

Prof. Dr. Kaspar Matiasek, LUDWIG-MAXIMILIANS-UNIVERSITÄT MÜNCHEN and **Heidrun Schöl** kindly helped to perform negative staining of S⁺ VLP and TEM (Figure 7A) at the Institute of Veterinary Pathology.

Dr. Manuel Albanese, MAX VON PETTENKOFER-INSTITUT, gratefully conducted virus generation and inactivation in the BSL-3 laboratory of the TECHNISCHE UNIVERSITÄT MÜNCHEN.

Prof. Dr. Percy Knolle, KLINIKUM RECHTS DER ISAR der TECHNISCHE UNIVERSITÄT MÜNCHEN and **Dr. Bastian Höchst** kindly provided 12 COVID-19 patient plasma samples for the analysis of spike protein in human blood.

The **Monoclonal Antibody Core Facility** of the HELMHOLTZ ZENTRUM MÜNCHEN executed animal immunization, hybridoma generation and antibody production.

Dr. Markus Kellner, HELMHOLTZ ZENTRUM MÜNCHEN, kindly provided the purified antibodies REGN10987 and REGN10933.

Julia Hörmann, HELMHOLTZ ZENTRUM MÜNCHEN, thankfully acquired and processed confocal fluorescence microscopy images (Figure 12) of stained slides.

Bibliography

1. Mittal, A. *et al.* COVID-19 pandemic: Insights into structure, function, and hACE2 receptor recognition by SARS-CoV-2. *PLoS Pathog.* **16**, e1008762. doi:10.1371/journal.ppat.1008762 (2020).
2. De Wit, E., van Doremalen, N., Falzarano, D. & Munster, V. J. SARS and MERS: recent insights into emerging coronaviruses. *Nat. Rev. Microbiol.* **14**, 523–34. doi:10.1038/nrmicro.2016.81 (2016).
3. Wu, F. *et al.* A new coronavirus associated with human respiratory disease in China. *Nature* **579**, 265–269. doi:10.1038/s41586-020-2008-3 (2020).
4. Hu, B., Guo, H., Zhou, P. & Shi, Z. L. Characteristics of SARS-CoV-2 and COVID-19. *Nat. Rev. Microbiol.* **19**, 141–154. doi:10.1038/s41579-020-00459-7 (2021).
5. Yan, W., Zheng, Y., Zeng, X., He, B. & Cheng, W. Structural biology of SARS-CoV-2: open the door for novel therapies. *Signal Transduct. Target. Ther.* **7**, 26. doi:10.1038/s41392-022-00884-5 (2022).
6. Hofmann, H. & Pohlmann, S. Cellular entry of the SARS coronavirus. *Trends Microbiol.* **12**, 466–72. doi:10.1016/j.tim.2004.08.008 (2004).
7. Millet, J. K. & Whittaker, G. R. Host cell proteases: Critical determinants of coronavirus tropism and pathogenesis. *Virus Res.* **202**, 120–34. doi:10.1016/j.virusres.2014.11.021 (2015).
8. Shang, J. *et al.* Cell entry mechanisms of SARS-CoV-2. *Proc. Natl. Acad. Sci. USA* **117**, 11727–11734. doi:10.1073/pnas.2003138117 (2020).
9. Stevens, C. S., Oguntuyo, K. Y. & Lee, B. Proteases and variants: context matters for SARS-CoV-2 entry assays. *Curr. Opin. Virol.* **50**, 49–58. doi:10.1016/j.coviro.2021.07.004 (2021).
10. Papa, G. *et al.* Furin cleavage of SARS-CoV-2 Spike promotes but is not essential for infection and cell-cell fusion. *PLoS Pathog.* **17**, e1009246. doi:10.1371/journal.ppat.1009246 (2021).
11. Yan, R. *et al.* Structural basis for the recognition of SARS-CoV-2 by full-length human ACE2. *Science* **367**, 1444–1448. doi:10.1126/science.abb2762 (2020).
12. Wrapp, D. *et al.* Cryo-EM structure of the 2019-nCoV spike in the prefusion conformation. *Science* **367**, 1260–1263. doi:10.1126/science.abb2507 (2020).
13. Hoffmann, M. *et al.* SARS-CoV-2 Cell Entry Depends on ACE2 and TMPRSS2 and Is Blocked by a Clinically Proven Protease Inhibitor. *Cell* **181**, 271–280 e8. doi:10.1016/j.cell.2020.02.052 (2020).
14. Jackson, C. B., Farzan, M., Chen, B. & Choe, H. Mechanisms of SARS-CoV-2 entry into cells. *Nat. Rev. Mol. Cell Biol.* **23**, 3–20. doi:10.1038/s41580-021-00418-x (2022).
15. V'kovski, P., Kratzel, A., Steiner, S., Stalder, H. & Thiel, V. Coronavirus biology and replication: implications for SARS-CoV-2. *Nat. Rev. Microbiol.* **19**, 155–170. doi:10.1038/s41579-020-00468-6 (2021).

16. Pinto, D. *et al.* Cross-neutralization of SARS-CoV-2 by a human monoclonal SARS-CoV antibody. *Nature* **583**, 290–295. doi:10.1038/s41586-020-2349-y (2020).
17. Korber, B. *et al.* Tracking Changes in SARS-CoV-2 Spike: Evidence that D614G Increases Infectivity of the COVID-19 Virus. *Cell* **182**, 812–827 e19. doi:10.1016/j.cell.2020.06.043 (2020).
18. Davies, N. G. *et al.* Estimated transmissibility and impact of SARS-CoV-2 lineage B.1.1.7 in England. *Science* **372**. doi:10.1126/science.abg3055 (2021).
19. Zahradnik, J. *et al.* SARS-CoV-2 variant prediction and antiviral drug design are enabled by RBD in vitro evolution. *Nat. Microbiol.* **6**, 1188–1198. doi:10.1038/s41564-021-00954-4 (2021).
20. Burki, T. K. Lifting of COVID-19 restrictions in the UK and the Delta variant. *Lancet Respir. Med.* **9**, e85. doi:10.1016/S2213-2600(21)00328-3 (2021).
21. Liu, Y. & Rocklöv, J. The reproductive number of the Delta variant of SARS-CoV-2 is far higher compared to the ancestral SARS-CoV-2 virus. *J. Travel Med.* **28**. doi:10.1093/jtm/taab124 (2021).
22. Sheikh, A. *et al.* SARS-CoV-2 Delta VOC in Scotland: demographics, risk of hospital admission, and vaccine effectiveness. *Lancet* **397**, 2461–2462. doi:10.1016/S0140-6736(21)01358-1 (2021).
23. Karim, S. S. A. & Karim, Q. A. Omicron SARS-CoV-2 variant: a new chapter in the COVID-19 pandemic. *Lancet* **398**, 2126–2128. doi:10.1016/S0140-6736(21)02758-6 (2021).
24. Mohapatra, R. K. *et al.* Omicron (B.1.1.529 variant of SARS-CoV-2); an emerging threat: Current global scenario. *J. Med. Virol.* doi:10.1002/jmv.27561 (2021).
25. Zohar, T. & Alter, G. Dissecting antibody-mediated protection against SARS-CoV-2. *Nat. Rev. Immunol.* **20**, 392–394. doi:10.1038/s41577-020-0359-5 (2020).
26. Van de Veerdonk, F. L. *et al.* A guide to immunotherapy for COVID-19. *Nat. Med.* **28**, 39–50. doi:10.1038/s41591-021-01643-9 (2022).
27. Drożdżal, S. *et al.* An update on drugs with therapeutic potential for SARS-CoV-2 (COVID-19) treatment. *Drug Resist. Updat.* **59**, 100794. doi:10.1016/j.drug.2021.100794 (2021).
28. Chiu, M. N., Bhardwaj, M. & Sah, S. P. Safety profile of COVID-19 drugs in a real clinical setting. *Eur. J. Clin. Pharmacol.* **78**, 733–753. doi:10.1007/s00228-021-03270-2 (2022).
29. Okoli, G. N. *et al.* Antiviral drugs for coronavirus disease 2019 (COVID-19): a systematic review with network meta-analysis. *Expert Rev. Anti Infect. Ther.* **20**, 267–278. doi:10.1080/14787210.2021.1961579 (2022).
30. Abu-Raddad, L. J., Chemaitelly, H., Butt, A. A. & National Study Group for, C.-V. Effectiveness of the BNT162b2 Covid-19 Vaccine against the B.1.1.7 and B.1.351 Variants. *N. Engl. J. Med.* **385**, 187–189. doi:10.1056/NEJMc2104974 (2021).
31. Lopez Bernal, J. *et al.* Effectiveness of Covid-19 Vaccines against the B.1.617.2 (Delta) Variant. *N. Engl. J. Med.* **385**, 585–594. doi:10.1056/NEJMoa2108891 (2021).
32. Levine-Tiefenbrun, M. *et al.* Viral loads of Delta-variant SARS-CoV-2 breakthrough infections after vaccination and booster with BNT162b2. *Nat. Med.* doi:10.1038/s41591-021-01575-4 (2021).

33. Shanmugaraj, B., Siri wattananon, K., Wangkanont, K. & Phoolcharoen, W. Perspectives on monoclonal antibody therapy as potential therapeutic intervention for Coronavirus disease-19 (COVID-19). *Asian Pac. J. Allergy Immunol.* **38**, 10–18. doi:10.12932/AP-200220-0773 (2020).
34. Bar-On, Y. M. *et al.* Protection of BNT162b2 Vaccine Booster against Covid-19 in Israel. *N. Engl. J. Med.* **385**, 1393–1400. doi:10.1056/NEJMoa2114255 (2021).
35. Collie, S., Champion, J., Moultrie, H., Bekker, L. G. & Gray, G. Effectiveness of BNT162b2 Vaccine against Omicron Variant in South Africa. *N. Engl. J. Med.* **386**, 494–496. doi:10.1056/NEJMc2119270 (2022).
36. Simon-Loriere, E. & Schwartz, O. Towards SARS-CoV-2 serotypes? *Nat. Rev. Microbiol.* doi:10.1038/s41579-022-00708-x (2022).
37. Cohen, K. W. *et al.* Longitudinal analysis shows durable and broad immune memory after SARS-CoV-2 infection with persisting antibody responses and memory B and T cells. *Cell Rep. Med.* **2**, 100354. doi:10.1016/j.xcrm.2021.100354 (2021).
38. Niessl, J., Sekine, T. & Buggert, M. T cell immunity to SARS-CoV-2. *Semin. Immunol.*, 101505. doi:10.1016/j.smim.2021.101505 (2021).
39. DeFrancesco, L. COVID-19 antibodies on trial. *Nat. Biotechnol.* **38**, 1242–1252. doi:10.1038/s41587-020-0732-8 (2020).
40. Earle, K. A. *et al.* Evidence for antibody as a protective correlate for COVID-19 vaccines. *Vaccine* **39**, 4423–4428. doi:10.1016/j.vaccine.2021.05.063 (2021).
41. Feng, S. *et al.* Correlates of protection against symptomatic and asymptomatic SARS-CoV-2 infection. *Nat. Med.* **27**, 2032–2040. doi:10.1038/s41591-021-01540-1 (2021).
42. Khoury, D. S. *et al.* Neutralizing antibody levels are highly predictive of immune protection from symptomatic SARS-CoV-2 infection. *Nat. Med.* doi:10.1038/s41591-021-01377-8 (2021).
43. Krammer, F. A correlate of protection for SARS-CoV-2 vaccines is urgently needed. *Nat. Med.* **27**, 1147–1148. doi:10.1038/s41591-021-01432-4 (2021).
44. Khoury, D. S. *et al.* Measuring immunity to SARS-CoV-2 infection: comparing assays and animal models. *Nat. Rev. Immunol.* **20**, 727–738. doi:10.1038/s41577-020-00471-1 (2020).
45. Bewley, K. R. *et al.* Quantification of SARS-CoV-2 neutralizing antibody by wild-type plaque reduction neutralization, microneutralization and pseudotyped virus neutralization assays. *Nat. Protoc.* **16**, 3114–3140. doi:10.1038/s41596-021-00536-y (2021).
46. Von Rhein, C. *et al.* Comparison of potency assays to assess SARS-CoV-2 neutralizing antibody capacity in COVID-19 convalescent plasma. *J. Virol. Methods* **288**, 114031. doi:10.1016/j.jviromet.2020.114031 (2021).
47. Valcourt, E. J. *et al.* Evaluation of a commercially-available surrogate virus neutralization test for severe acute respiratory syndrome coronavirus-2 (SARS-CoV-2). *Diagn. Microbiol. Infect. Dis.* **99**, 115294. doi:10.1016/j.diagmicrobio.2020.115294 (2021).
48. Roessler, J. *et al.* Quantitation of SARS-CoV-2 neutralizing antibodies with a virus-free, authentic test. *PNAS Nexus* **1**. pgac045. doi:10.1093/pnasnexus/pgac045 (2022).

49. Laustsen, A. H., Greiff, V., Karatt-Vellatt, A., Muyldermans, S. & Jenkins, T. P. Animal Immunization, in Vitro Display Technologies, and Machine Learning for Antibody Discovery. *Trends Biotechnol.* **39**, 1263–1273. doi:10.1016/j.tibtech.2021.03.003 (2021).
50. González-Fernández, Á. *et al.* Non-animal-derived monoclonal antibodies are not ready to substitute current hybridoma technology. *Nat. Methods.* **17**, 1069–1070. doi:10.1038/s41592-020-00977-5 (2020).
51. Kalluri, R. & LeBleu, V. S. The biology, function, and biomedical applications of exosomes. *Science* **367**. doi:10.1126/science.aau6977 (2020).
52. Choi, S. J. *et al.* Active Immunization with Extracellular Vesicles Derived from *Staphylococcus aureus* Effectively Protects against Staphylococcal Lung Infections, Mainly via Th1 Cell-Mediated Immunity. *PLoS One* **10**, e0136021. doi:10.1371/journal.pone.0136021 (2015).
53. György, B., Hung, M. E., Breakefield, X. O. & Leonard, J. N. Therapeutic applications of extracellular vesicles: clinical promise and open questions. *Annu. Rev. Pharmacol. Toxicol.* **55**, 439–464. doi:10.1146/annurev-pharmtox-010814-124630 (2015).
54. Kellner, M. *et al.* A Novel Anti-CD73 Antibody That Selectively Inhibits Membrane CD73 Shows Antitumor Activity and Induces Tumor Immune Escape. *Biomedicines* **10**. doi:10.3390/biomedicines10040825 (2022).
55. Gärtner, K., Luckner, M., Wanner, G. & Zeidler, R. Engineering extracellular vesicles as novel treatment options: exploiting herpesviral immunity in CLL. *J. Extracell. Vesicles* **8**, 1573051. doi:10.1080/20013078.2019.1573051 (2019).
56. N.a. An EUA for casirivimab and imdevimab for COVID-19. *Med. Lett. Drugs Ther.* **62**, 201–202. doi:(PMID:33451174) (2020).
57. Baum, A. *et al.* Antibody cocktail to SARS-CoV-2 spike protein prevents rapid mutational escape seen with individual antibodies. *Science* **369**, 1014–1018. doi:10.1126/science.abd0831 (2020).
58. Hansen, J. *et al.* Studies in humanized mice and convalescent humans yield a SARS-CoV-2 antibody cocktail. *Science* **369**, 1010–1014. doi:10.1126/science.abd0827 (2020).
59. Nguyen, H., Lan, P. D., Nissley, D. A., O'Brien, E. P. & Li, M. S. Cocktail of REGN Antibodies Binds More Strongly to SARS-CoV-2 Than Its Components, but the Omicron Variant Reduces Its Neutralizing Ability. *J. Phys. Chem. B.* **126**, 2812–2823. doi:10.1021/acs.jpcc.2c00708 (2022).
60. Francino-Urdaniz, I. M. & Whitehead, T. A. An overview of methods for the structural and functional mapping of epitopes recognized by anti-SARS-CoV-2 antibodies. *RSC Chem. Biol.* **2**, 1580–1589. doi:10.1039/d1cb00169h (2021).
61. World Health Organization, . *International Nonproprietary Names (INN) for biological and biotechnological substances (a review) (2019)* Technical documents (2019).
62. Troyer, Z. *et al.* Extracellular vesicles carry SARS-CoV-2 spike protein and serve as decoys for neutralizing antibodies. *J. Extracell. Vesicles* **10**, e12112. doi:10.1002/jev2.12112 (2021).
63. Kuba, K. *et al.* A crucial role of angiotensin converting enzyme 2 (ACE2) in SARS coronavirus-induced lung injury. *Nat. Med.* **11**, 875–9. doi:10.1038/nm1267 (2005).
64. Yang, R. *et al.* Development and effectiveness of pseudotyped SARS-CoV-2 system as determined by neutralizing efficiency and entry inhibition test in vitro. *Biosaf. Health* **2**, 226–231. doi:10.1016/j.bsheal.2020.08.004 (2020).

65. Hoffmann, M. *et al.* Chloroquine does not inhibit infection of human lung cells with SARS-CoV-2. *Nature* **585**, 588–590. doi:10.1038/s41586-020-2575-3 (2020).
66. Rolain, J. M., Colson, P. & Raoult, D. Recycling of chloroquine and its hydroxyl analogue to face bacterial, fungal and viral infections in the 21st century. *Int. J. Antimicrob. Agents* **30**, 297–308. doi:10.1016/j.ijantimicag.2007.05.015 (2007).
67. Giroglou, T. *et al.* Retroviral vectors pseudotyped with severe acute respiratory syndrome coronavirus S protein. *J. Virol.* **78**, 9007–15. doi:10.1128/JVI.78.17.9007-9015.2004 (2004).
68. Nolte-'t Hoen, E., Cremer, T., Gallo, R. C. & Margolis, L. B. Extracellular vesicles and viruses: Are they close relatives? *Proc. Natl. Acad. Sci. USA* **113**, 9155–61. doi:10.1073/pnas.1605146113 (2016).
69. Hsieh, P. K. *et al.* Assembly of severe acute respiratory syndrome coronavirus RNA packaging signal into virus-like particles is nucleocapsid dependent. *J. Virol.* **79**, 13848–55. doi:10.1128/JVI.79.22.13848-13855.2005 (2005).
70. Siu, Y. L. *et al.* The M, E, and N structural proteins of the severe acute respiratory syndrome coronavirus are required for efficient assembly, trafficking, and release of virus-like particles. *J. Virol.* **82**, 11318–30. doi:10.1128/JVI.01052-08 (2008).
71. Ujike, M., Huang, C., Shirato, K., Makino, S. & Taguchi, F. The contribution of the cytoplasmic retrieval signal of severe acute respiratory syndrome coronavirus to intracellular accumulation of S proteins and incorporation of S protein into virus-like particles. *J. Gen. Virol.* **97**, 1853–1864. doi:10.1099/jgv.0.000494 (2016).
72. Ujike, M. & Taguchi, F. Incorporation of spike and membrane glycoproteins into coronavirus virions. *Viruses* **7**, 1700–25. doi:10.3390/v7041700 (2015).
73. Boson, B. *et al.* The SARS-CoV-2 envelope and membrane proteins modulate maturation and retention of the spike protein, allowing assembly of virus-like particles. *J. Biol. Chem.* **296**, 100111. doi:10.1074/jbc.RA120.016175 (2021).
74. Gheysen, D. *et al.* Assembly and release of HIV-1 precursor Pr55gag virus-like particles from recombinant baculovirus-infected insect cells. *Cell* **59**, 103–12. doi:10.1016/0092-8674(89)90873-8 (1989).
75. Gonelli, C. A., Khoury, G., Center, R. J. & Purcell, D. F. J. HIV-1-based Virus-like Particles that Morphologically Resemble Mature, Infectious HIV-1 Virions. *Viruses* **11**. doi:10.3390/v11060507 (2019).
76. Ruiss, R. *et al.* A virus-like particle-based Epstein-Barr virus vaccine. *J. Virol.* **85**, 13105–13. doi:10.1128/JVI.05598-11 (2011).
77. Lopez-Macias, C. Virus-like particle (VLP)-based vaccines for pandemic influenza: performance of a VLP vaccine during the 2009 influenza pandemic. *Hum. Vaccin. Immunother.* **8**, 411–4. doi:10.4161/hv.18757 (2012).
78. Tariq, H., Batool, S., Asif, S., Ali, M. & Abbasi, B. H. Virus-Like Particles: Revolutionary Platforms for Developing Vaccines Against Emerging Infectious Diseases. *Front. Microbiol.* **12**, 790121. doi:10.3389/fmicb.2021.790121 (2021).
79. Richert-Pöggeler, K. R., Franzke, K., Hipp, K. & Kleespies, R. G. Electron Microscopy Methods for Virus Diagnosis and High Resolution Analysis of Viruses. *Front. Microbiol.* **9**, 3255. doi:10.3389/fmicb.2018.03255 (2018).
80. Ritchie, A. E., Deshmukh, D. R., Larsen, C. T. & Pomeroy, B. S. Electron microscopy of coronavirus-like particles characteristic of turkey bluecomb disease. *Avian Dis.* **17**, 546–58 (1973).

81. Zhu, N. *et al.* A Novel Coronavirus from Patients with Pneumonia in China, 2019. *N. Engl. J. Med.* **382**, 727–733. doi:10.1056/NEJMoa2001017 (2020).
82. Ke, Z. *et al.* Structures and distributions of SARS-CoV-2 spike proteins on intact virions. *Nature* **588**, 498–502. doi:10.1038/s41586-020-2665-2 (2020).
83. Liu, C. *et al.* The Architecture of Inactivated SARS-CoV-2 with Postfusion Spikes Revealed by Cryo-EM and Cryo-ET. *Structure* **28**, 1218–1224 e4. doi:10.1016/j.str.2020.10.001 (2020).
84. Yao, H. *et al.* Molecular Architecture of the SARS-CoV-2 Virus. *Cell* **183**, 730–738 e13. doi:10.1016/j.cell.2020.09.018 (2020).
85. Zhang, L. *et al.* SARS-CoV-2 spike-protein D614G mutation increases virion spike density and infectivity. *Nat. Commun.* **11**, 6013. doi:10.1038/s41467-020-19808-4 (2020).
86. Ou, X. *et al.* Characterization of spike glycoprotein of SARS-CoV-2 on virus entry and its immune cross-reactivity with SARS-CoV. *Nat. Commun.* **11**, 1620. doi:10.1038/s41467-020-15562-9 (2020).
87. Walls, A. C. *et al.* Structure, Function, and Antigenicity of the SARS-CoV-2 Spike Glycoprotein. *Cell* **181**, 281–292.e6. doi:10.1016/j.cell.2020.02.058 (2020).
88. Turonova, B. *et al.* In situ structural analysis of SARS-CoV-2 spike reveals flexibility mediated by three hinges. *Science* **370**, 203–208. doi:10.1126/science.abd5223 (2020).
89. Filby, A., Begum, J., Jalal, M. & Day, W. Appraising the suitability of succinimidyl and lipophilic fluorescent dyes to track proliferation in non-quiescent cells by dye dilution. *Methods* **82**, 29–37. doi:10.1016/j.ymeth.2015.02.016 (2015).
90. Chu, H. *et al.* Comparative tropism, replication kinetics, and cell damage profiling of SARS-CoV-2 and SARS-CoV with implications for clinical manifestations, transmissibility, and laboratory studies of COVID-19: an observational study. *Lancet Microbe.* **1**, e14–e23. doi:10.1016/S2666-5247(20)30004-5 (2020).
91. Albanese, M. *et al.* MicroRNAs are minor constituents of extracellular vesicles that are rarely delivered to target cells. *PLoS Genet.* **17**, e1009951. doi:10.1371/journal.pgen.1009951 (2021).
92. Cavrois, M., De Noronha, C. & Greene, W. C. A sensitive and specific enzyme-based assay detecting HIV-1 virion fusion in primary T lymphocytes. *Nat. Biotechnol.* **20**, 1151–4. doi:10.1038/nbt745 (2002).
93. Carlon-Andres, I. & Padilla-Parra, S. Quantitative FRET-FLIM-BlaM to Assess the Extent of HIV-1 Fusion in Live Cells. *Viruses* **12**. doi:10.3390/v12020206 (2020).
94. Cavrois, M., Neidleman, J. & Greene, W. C. HIV-1 Fusion Assay. *Bio Protoc.* **4**. doi:10.21769/bioprotoc.1212 (2014).
95. Desai, T. M., Marin, M., Mason, C. & Melikyan, G. B. pH regulation in early endosomes and interferon-inducible transmembrane proteins control avian retrovirus fusion. *J. Biol. Chem.* **292**, 7817–7827. doi:10.1074/jbc.M117.783878 (2017).
96. Feeley, E. M. *et al.* IFITM3 inhibits influenza A virus infection by preventing cytosolic entry. *PLoS Pathog.* **7**, e1002337. doi:10.1371/journal.ppat.1002337 (2011).
97. Jones, D. M. & Padilla-Parra, S. The beta-Lactamase Assay: Harnessing a FRET Biosensor to Analyse Viral Fusion Mechanisms. *Sensors (Basel)* **16**. doi:10.3390/s16070950 (2016).

98. Dixon, A. S. *et al.* NanoLuc Complementation Reporter Optimized for Accurate Measurement of Protein Interactions in Cells. *ACS Chem. Biol.* **11**, 400–8. doi:10.1021/acscchembio.5b00753 (2016).
99. Miyakawa, K. *et al.* Rapid quantitative screening assay for SARS-CoV-2 neutralizing antibodies using HiBiT-tagged virus-like particles. *J. Mol. Cell Biol.* **12**, 987–990. doi:10.1093/jmcb/mjaa047 (2020).
100. Yamamoto, M. *et al.* Cell-cell and virus-cell fusion assay-based analyses of alanine insertion mutants in the distal alpha9 portion of the JRFL gp41 subunit from HIV-1. *J. Biol. Chem.* **294**, 5677–5687. doi:10.1074/jbc.RA118.004579 (2019).
101. Somiya, M. & Kuroda, S. Real-Time Luminescence Assay for Cytoplasmic Cargo Delivery of Extracellular Vesicles. *Anal. Chem.* **93**, 5612–5620. doi:10.1021/acs.analchem.1c00339 (2021).
102. Kawase, M., Shirato, K., van der Hoek, L., Taguchi, F. & Matsuyama, S. Simultaneous treatment of human bronchial epithelial cells with serine and cysteine protease inhibitors prevents severe acute respiratory syndrome coronavirus entry. *J. Virol.* **86**, 6537–45. doi:10.1128/JVI.00094-12 (2012).
103. Jocher, G. *et al.* ADAM10 and ADAM17 promote SARS-CoV-2 cell entry and spike protein-mediated lung cell fusion. *EMBO Rep.* **23**, e54305. doi:10.15252/embr.202154305 (2022).
104. Callaway, E. & Ledford, H. How bad is Omicron? What scientists know so far. *Nature* **600**, 197–199. doi:10.1038/d41586-021-03614-z (2021).
105. Cui, Z. *et al.* Structural and functional characterizations of infectivity and immune evasion of SARS-CoV-2 Omicron. *Cell* **185**, 860–871.e13. doi:10.1016/j.cell.2022.01.019 (2022).
106. Planas, D. *et al.* Considerable escape of SARS-CoV-2 Omicron to antibody neutralization. *Nature* **602**, 671–675. doi:10.1038/s41586-021-04389-z (2022).
107. Niu, L., Wittrock, K. N., Clabaugh, G. C., Srivastava, V. & Cho, M. W. A Structural Landscape of Neutralizing Antibodies Against SARS-CoV-2 Receptor Binding Domain. *Front. Immunol.* **12**, 647934. doi:10.3389/fimmu.2021.647934 (2021).
108. Piccoli, L. *et al.* Mapping Neutralizing and Immunodominant Sites on the SARS-CoV-2 Spike Receptor-Binding Domain by Structure-Guided High-Resolution Serology. *Cell* **183**, 1024–1042 e21. doi:10.1016/j.cell.2020.09.037 (2020).
109. Tortorici, M. A. *et al.* Ultrapotent human antibodies protect against SARS-CoV-2 challenge via multiple mechanisms. *Science* **370**, 950–957. doi:10.1126/science.abe3354 (2020).
110. Brouwer, P. J. M. *et al.* Potent neutralizing antibodies from COVID-19 patients define multiple targets of vulnerability. *Science* **369**, 643–650. doi:10.1126/science.abc5902 (2020).
111. Keng, C. T. *et al.* Amino acids 1055 to 1192 in the S2 region of severe acute respiratory syndrome coronavirus S protein induce neutralizing antibodies: implications for the development of vaccines and antiviral agents. *J. Virol.* **79**, 3289–96. doi:10.1128/JVI.79.6.3289-3296.2005 (2005).
112. Kristiansen, P. A. *et al.* WHO International Standard for anti-SARS-CoV-2 immunoglobulin. *Lancet* **397**, 1347–1348. doi:10.1016/S0140-6736(21)00527-4 (2021).
113. Chesher, D. Evaluating assay precision. *Clin. Biochem. Rev.* **29 Suppl 1**, S23–6 (2008).

114. Romero-Olmedo, A. J. *et al.* Induction of robust cellular and humoral immunity against SARS-CoV-2 after a third dose of BNT162b2 vaccine in previously unresponsive older adults. *Nat. Microbiol.* **7**, 195–199. doi:10.1038/s41564-021-01046-z (2022).
115. Liu, C. *et al.* Reduced neutralization of SARS-CoV-2 B.1.617 by vaccine and convalescent serum. *Cell* **184**, 4220–4236 e13. doi:10.1016/j.cell.2021.06.020 (2021).
116. Planas, D. *et al.* Reduced sensitivity of SARS-CoV-2 variant Delta to antibody neutralization. *Nature* **596**, 276–280. doi:10.1038/s41586-021-03777-9 (2021).
117. Dejnirattisai, W. *et al.* SARS-CoV-2 Omicron-B.1.1.529 leads to widespread escape from neutralizing antibody responses. *Cell* **185**, 467–484 e15. doi:10.1016/j.cell.2021.12.046 (2022).
118. El-Shennawy, L. *et al.* Circulating ACE2-expressing extracellular vesicles block broad strains of SARS-CoV-2. *Nat. Commun.* **13**, 405. doi:10.1038/s41467-021-27893-2 (2022).
119. Sengar, A., Bondalapati, S. T. & Kasson, P. M. Single-virus fusion measurements yield an opportunistic model for SARS-CoV-2 fusion. *bioRxiv*. doi:10.1101/2021.05.04.442634. eprint: <https://www.biorxiv.org/content/early/2021/05/06/2021.05.04.442634.full.pdf> (2021).
120. Harrison, S. C. Viral membrane fusion. *Virology* **479–480**, 498–507. doi:10.1016/j.virol.2015.03.043 (2015).
121. Más, V. & Melero, J. A. Entry of enveloped viruses into host cells: membrane fusion. *Subcell. Biochem.* **68**, 467–87. doi:10.1007/978-94-007-6552-8_16 (2013).
122. Wojtowicz-Praga, S. M., Dickson, R. B. & Hawkins, M. J. Matrix metalloproteinase inhibitors. *Invest. New Drugs* **15**, 61–75. doi:10.1023/a:1005722729132 (1997).
123. Sasaki, M. *et al.* SARS-CoV-2 variants with mutations at the S1/S2 cleavage site are generated in vitro during propagation in TMPRSS2-deficient cells. *PLoS Pathog.* **17**, e1009233. doi:10.1371/journal.ppat.1009233 (2021).
124. Wang, C. *et al.* A human monoclonal antibody blocking SARS-CoV-2 infection. *Nat. Commun.* **11**, 2251. doi:10.1038/s41467-020-16256-y (2020).
125. Li, W. *et al.* Rapid identification of a human antibody with high prophylactic and therapeutic efficacy in three animal models of SARS-CoV-2 infection. *Proc. Natl. Acad. Sci. USA* **117**, 29832–29838. doi:10.1073/pnas.2010197117 (2020).
126. Starr, T. N. *et al.* Prospective mapping of viral mutations that escape antibodies used to treat COVID-19. *Science* **371**, 850–854. doi:10.1126/science.abf9302 (2021).
127. Kuate, S., Cinatl, J., Doerr, H. W. & Uberla, K. Exosomal vaccines containing the S protein of the SARS coronavirus induce high levels of neutralizing antibodies. *Virology* **362**, 26–37. doi:10.1016/j.virol.2006.12.011 (2007).
128. Sun, Y., Kobe, B. & Qi, J. Targeting multiple epitopes on the spike protein: a new hope for COVID-19 antibody therapy. *Signal Transduct. Target. Ther.* **5**, 208. doi:10.1038/s41392-020-00320-6 (2020).
129. Liu, L. *et al.* Potent neutralizing antibodies against multiple epitopes on SARS-CoV-2 spike. *Nature* **584**, 450–456. doi:10.1038/s41586-020-2571-7 (2020).
130. Degn, S. E., Andersen, S. H., Jensen, L., Thiel, S. & Jensenius, J. C. Assay interference caused by antibodies reacting with rat kappa light-chain in human sera. *J. Immunol. Methods* **372**, 204–8. doi:10.1016/j.jim.2011.06.030 (2011).

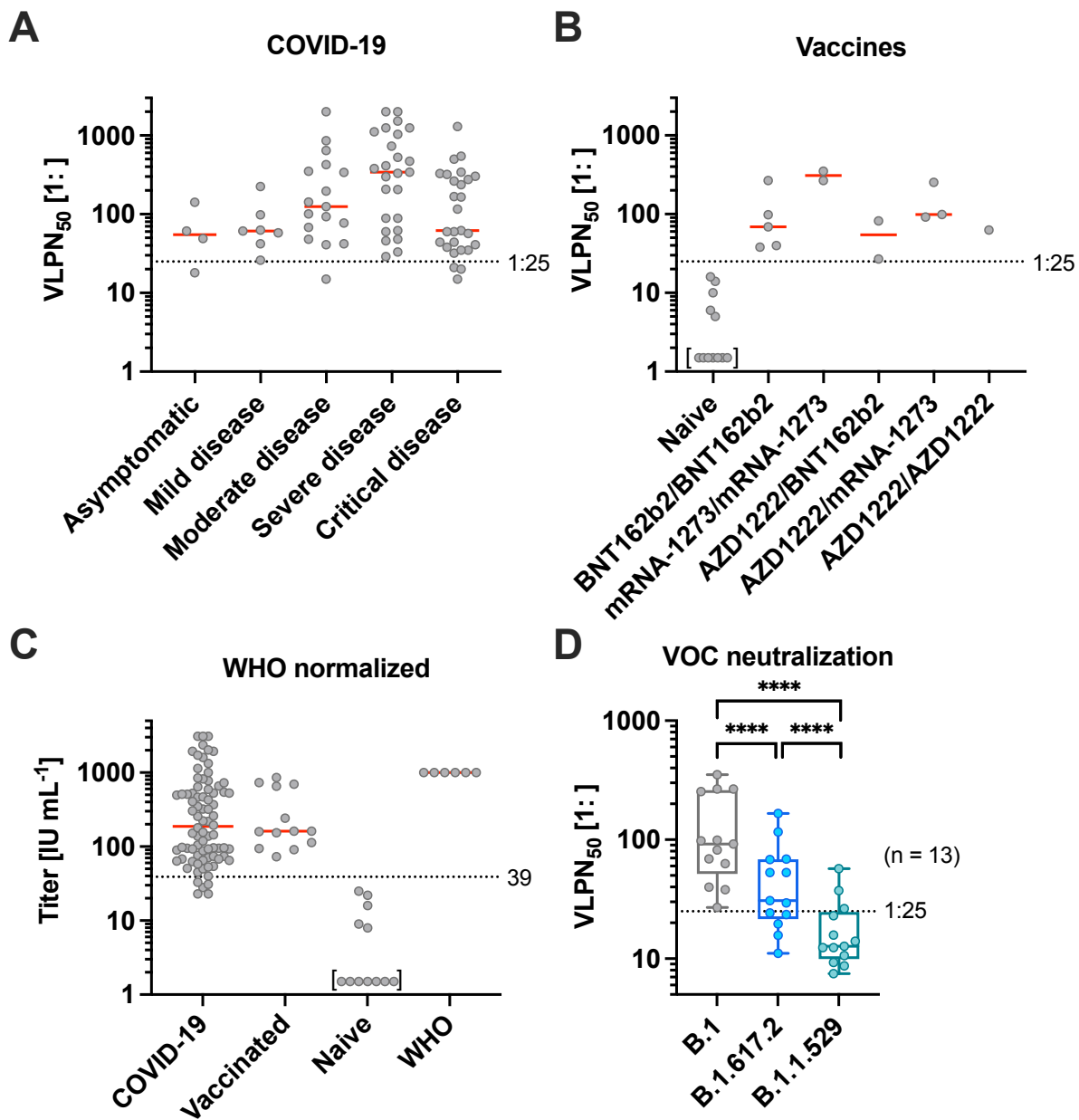
131. Taylor, P. C. *et al.* Neutralizing monoclonal antibodies for treatment of COVID-19. *Nat. Rev. Immunol.* **21**, 382–393. doi:10.1038/s41577-021-00542-x (2021).
132. Kumar, S., Chandele, A. & Sharma, A. Current status of therapeutic monoclonal antibodies against SARS-CoV-2. *PLoS Pathog.* **17**, e1009885. doi:10.1371/journal.ppat.1009885 (2021).
133. VanBlargan, L. A. *et al.* An infectious SARS-CoV-2 B.1.1.529 Omicron virus escapes neutralization by therapeutic monoclonal antibodies. *Nat. Med.* **28**, 490–495. doi:10.1038/s41591-021-01678-y (2022).
134. Cameroni, E. *et al.* Broadly neutralizing antibodies overcome SARS-CoV-2 Omicron antigenic shift. *Nature* **602**, 664–670. doi:10.1038/s41586-021-04386-2 (2022).
135. Suthar, M. S. *et al.* Rapid Generation of Neutralizing Antibody Responses in COVID-19 Patients. *Cell Rep. Med.* **1**, 100040. doi:10.1016/j.xcrm.2020.100040 (2020).
136. Vanderheiden, A. *et al.* Development of a Rapid Focus Reduction Neutralization Test Assay for Measuring SARS-CoV-2 Neutralizing Antibodies. *Curr. Protoc. Immunol.* **131**, e116. doi:10.1002/cpim.116 (2020).
137. Meng, B. *et al.* Altered TMPRSS2 usage by SARS-CoV-2 Omicron impacts infectivity and fusogenicity. *Nature* **603**, 706–714. doi:10.1038/s41586-022-04474-x (2022).
138. Syed, A. M. *et al.* Rapid assessment of SARS-CoV-2 evolved variants using virus-like particles. *Science*, eabl6184. doi:10.1126/science.abl6184 (2021).
139. Fukushi, S. *et al.* Evaluation of a novel vesicular stomatitis virus pseudotype-based assay for detection of neutralizing antibody responses to SARS-CoV. *J. Med. Virol.* **78**, 1509–12. doi:10.1002/jmv.20732 (2006).
140. Temperton, N. J. *et al.* Longitudinally profiling neutralizing antibody response to SARS coronavirus with pseudotypes. *Emerg. Infect. Dis.* **11**, 411–6. doi:10.3201/eid1103.040906 (2005).
141. Xu, J. *et al.* Antibodies and vaccines against Middle East respiratory syndrome coronavirus. *Emerg. Microbes Infect.* **8**, 841–856. doi:10.1080/22221751.2019.1624482 (2019).
142. Chi, X. *et al.* A neutralizing human antibody binds to the N-terminal domain of the Spike protein of SARS-CoV-2. *Science* **369**, 650–655. doi:10.1126/science.abc6952 (2020).
143. Tan, C. W. *et al.* A SARS-CoV-2 surrogate virus neutralization test based on antibody-mediated blockage of ACE2-spike protein-protein interaction. *Nat. Biotechnol.* **38**, 1073–1078. doi:10.1038/s41587-020-0631-z (2020).
144. Shirato, K., Kawase, M. & Matsuyama, S. Wild-type human coronaviruses prefer cell-surface TMPRSS2 to endosomal cathepsins for cell entry. *Virology* **517**, 9–15. doi:10.1016/j.virol.2017.11.012 (2018).
145. Shirato, K., Kanou, K., Kawase, M. & Matsuyama, S. Clinical Isolates of Human Coronavirus 229E Bypass the Endosome for Cell Entry. *J. Virol.* **91**. doi:10.1128/JVI.01387-16 (2017).
146. Zhou, Y. *et al.* Protease inhibitors targeting coronavirus and filovirus entry. *Antiviral Res.* **116**, 76–84. doi:10.1016/j.antiviral.2015.01.011 (2015).
147. Iwata-Yoshikawa, N. *et al.* TMPRSS2 Contributes to Virus Spread and Immunopathology in the Airways of Murine Models after Coronavirus Infection. *J. Virol.* **93**. doi:10.1128/JVI.01815-18 (2019).

148. Shuai, H. *et al.* Attenuated replication and pathogenicity of SARS-CoV-2 B.1.1.529 Omicron. *Nature* **603**, 693–699. doi:10.1038/s41586-022-04442-5 (2022).
149. Zhao, H. *et al.* SARS-CoV-2 Omicron variant shows less efficient replication and fusion activity when compared with Delta variant in TMPRSS2-expressed cells. *Emerg. Microbes Infect.* **11**, 277–283. doi:10.1080/22221751.2021.2023329 (2022).
150. Carreno, J. M. *et al.* Activity of convalescent and vaccine serum against SARS-CoV-2 Omicron. *Nature* **602**, 682–688. doi:10.1038/s41586-022-04399-5 (2022).
151. Marot, S. *et al.* Rapid decline of neutralizing antibodies against SARS-CoV-2 among infected healthcare workers. *Nat. Commun.* **12**, 844. doi:10.1038/s41467-021-21111-9 (2021).
152. Wratil, P. R. *et al.* Three exposures to the spike protein of SARS-CoV-2 by either infection or vaccination elicit superior neutralizing immunity to all variants of concern. *Nat. Med.* **28**, 496–503. doi:10.1038/s41591-022-01715-4 (2022).
153. Gaebler, C. *et al.* Evolution of antibody immunity to SARS-CoV-2. *Nature* **591**, 639–644. doi:10.1038/s41586-021-03207-w (2021).
154. Andrews, N. *et al.* Covid-19 Vaccine Effectiveness against the Omicron (B.1.1.529) Variant. *N. Engl. J. Med.* **386**, 1532–1546. doi:10.1056/NEJMoa2119451 (2022).
155. Liu, Y. *et al.* An infectivity-enhancing site on the SARS-CoV-2 spike protein targeted by antibodies. *Cell* **184**, 3452–3466 e18. doi:10.1016/j.cell.2021.05.032 (2021).
156. Scully, E. P., Haverfield, J., Ursin, R. L., Tannenbaum, C. & Klein, S. L. Considering how biological sex impacts immune responses and COVID-19 outcomes. *Nat. Rev. Immunol.* **20**, 442–447. doi:10.1038/s41577-020-0348-8 (2020).
157. Cornetta, K. & Anderson, W. F. Protamine sulfate as an effective alternative to polybrene in retroviral-mediated gene-transfer- implications for human gene therapy. *J. Virol. Methods* **23**, 187–94. doi:10.1016/0166-0934(89)90132-8 (1989).
158. Frohman, M. A. Rapid amplification of complementary DNA ends for generation of full-length complementary DNAs: thermal RACE. *Methods Enzymol.* **218**, 340–56. doi:10.1016/0076-6879(93)18026-9 (1993).
159. Engels, B. *et al.* Retroviral vectors for high-level transgene expression in T lymphocytes. *Hum. Gene Ther.* **14**, 1155–68. doi:10.1089/104303403322167993 (2003).
160. World Health Organization, . *Clinical management of COVID-19: interim guidance, 27 May 2020* Technical documents (2020), 62 p.

Appendix

Supplementary Table S1. Relevant segments of COVEV rat antibody sequences with CDRs highlighted.

mAb	Chain	Amino acid sequence
43A11	V _H	QVTLKESGPGILQPSQTL SLTCTFSGFSLKTYGLGVVWIRQPSGKGLEWLANIWDDDKH YNPFLKNRLTISKDTSKSQAFLKITNVGTGDTATYYCARMGYYGFKFYALYAWGQGTS VTSP
	V _L	NIQLTXSPSLLSASVGD RVTLSCKGSQSLNNDLAWYQQKLGEAPKLLIYDTHSLQTGIPS RFSGSGSGSDYTLTINSLQPEDVATYFCYQYNNGWTFGGGSKLELKRA
55E10	V _H	EVKLLES GGGLVQPGGSLSLSCAASGFTFTDFYMSWIRQPPGKAPEWLGVIRNKANSYTI EYNPSVKGRFTISRDN TQNLLYLQMNTLRAEDTAIYYCASGYYYSTSPDYWGQGMVTVS S
	V _L	DIQMTQSPSSLPASLGD RVTITCRASQDIGSYLRWFQLKAGKSPRLMIYGVINLAVGVPS RFSGCRSGSDYSLTIKSLESEDMAIYYCLQHNEY PFTFGSGTKLEIKRA
35B12	V _H	QVQLQQSGAELTKPGSSVKISCKPSGYTFTNYDISWMKQRPGQALEWIGTINPGSGGTGY NEKFKGKATLTVDKSSSTAFMQLSSLT PPDDTAVYYCARDYDTPYYFDYWGQGMVTVSS
	V _L	DTVLTQSPALAVSPGERVTISCRASESVNSRMHWYQQKSGQQPKVLIYGT SNLESGVPAR FSGSGSGTDFTLTIDPVEADDSATYFCQ QSWNDPNTFGAGTKLELKRA



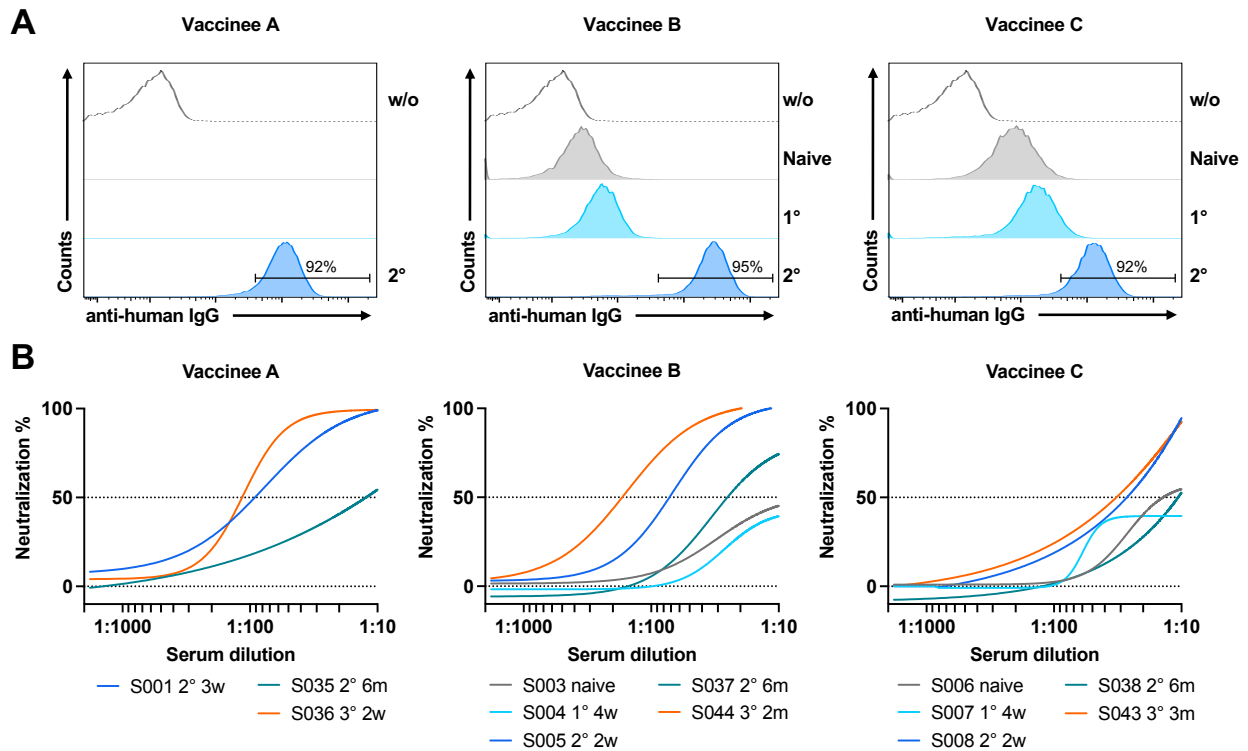
Supplementary Figure S1. VLPNT titers of COVID-19 and vaccinee sera.

(A) VLPN₅₀ titers of 80 COVID-19 sera are sorted according to their patient's clinical disease course. Red bars indicate median values of grouped data.

(B) VLPN₅₀ serum titers of 12 healthy naive donors and 13 vaccinees are shown according to their prime-boost scheme of different COVID-19 vaccines received. Red bars indicate median values of the groups. Values in square brackets indicate serum samples with VLPN₅₀ below the LOD.

(C) The chart shows the data from Figure 16B, normalized to international units (IU), according to the WHO standard (NIBSC 20/136).

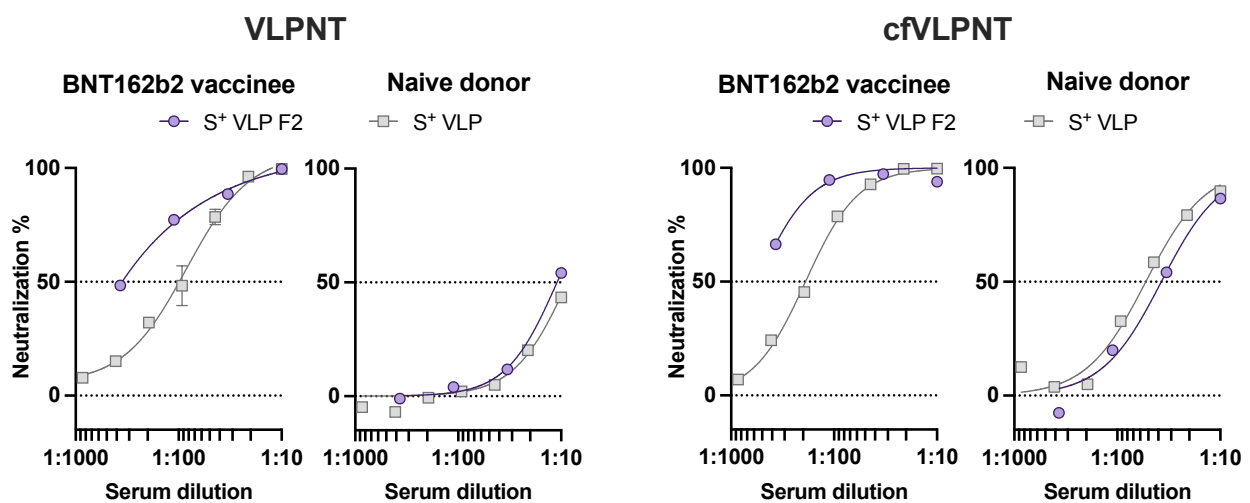
(D) Similar to Figure 16E, VLPN₅₀ results of sera from 13 COVID-19 vaccinees are shown individually and as box plots for SARS-CoV-2 VOCs B.1, B.1.617.2 and B.1.1.529 (BA.1). Boxes show median and 25th to 75th percentiles. Data were analyzed using a matched one-way ANOVA, with Tukey's multi comparison test and a single pooled variance. Results are indicated: **** $p \leq 0.0001$. Parts of this figure were adapted from Roessler *et al.*,^[48] under CC BY 4.0.



Supplementary Figure S2. Case reports of three vaccinees.

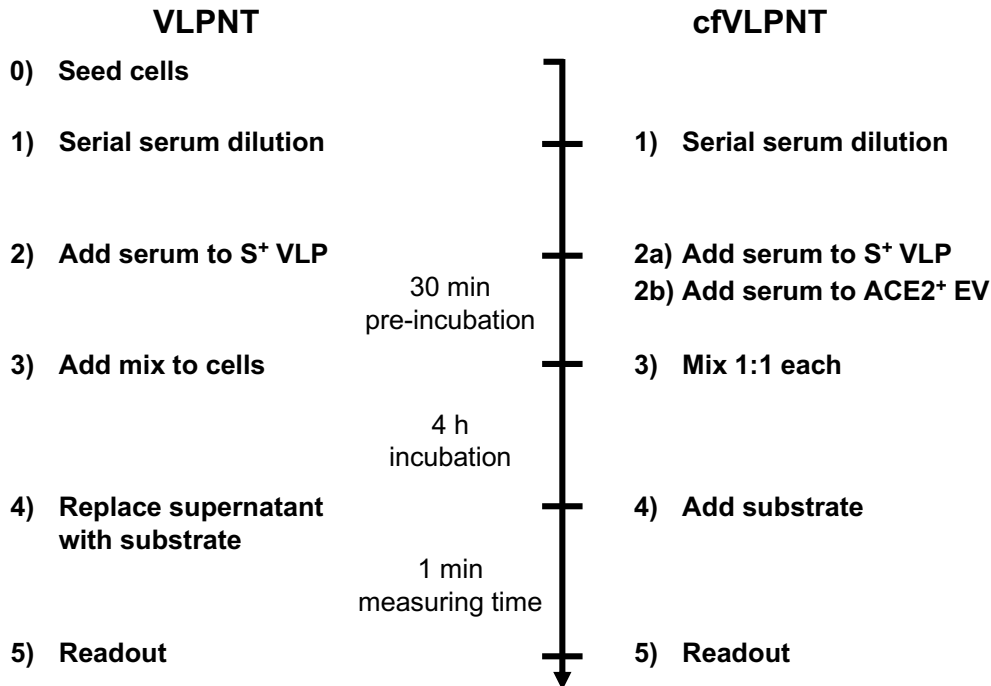
(A) Sera from three donors A-C were analyzed before and after vaccination in flow cytometry on a S⁺ HEK293 cell line with a fluorescently labeled anti-human IgG secondary antibody for seroconversion. Control samples without human serum are indicated w/o and show the background of the secondary antibody.

(B) Matching sera of various points of time from the three prime-boost-boost vaccinees A-C were analyzed in the VLPNT with B.1 S⁺ VLP. If available, naive serum, drawn before mid 2019, was compared to serum drawn several weeks (w) or months (m) after primary (1°), secondary (2°) or third (3°) vaccination with a licensed COVID-19 vaccine.



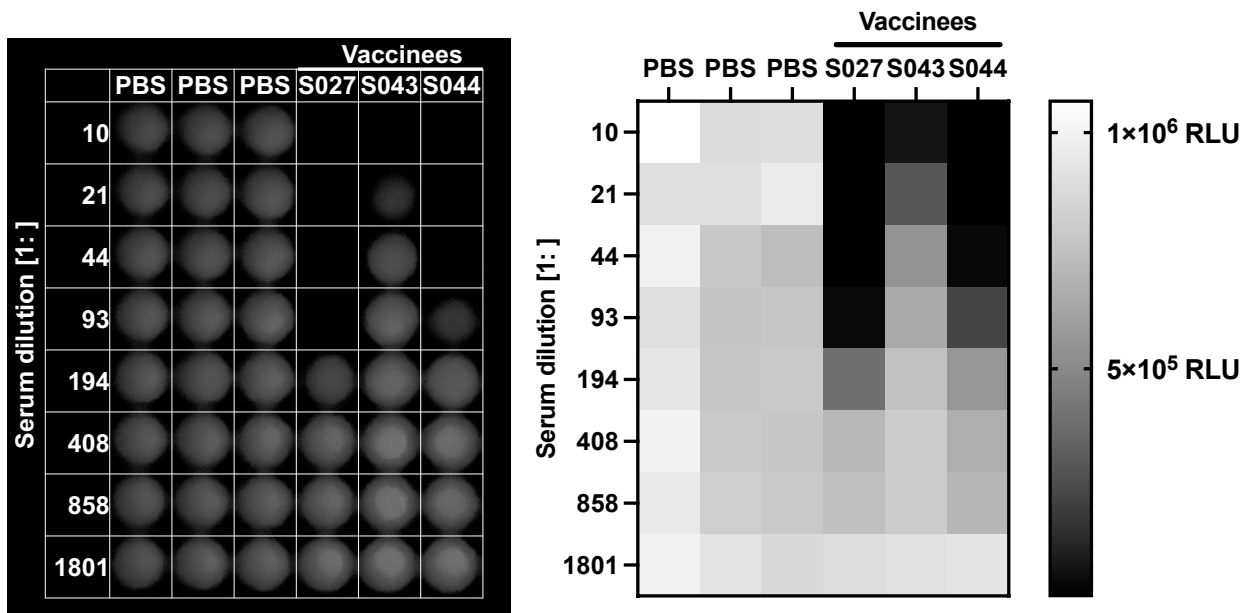
Supplementary Figure S3. VLPNT and cfVLPNT with purified S⁺ VLP preparations.

As described in Figure 21F, S⁺ VLP from a density gradient's fraction F2 and raw S⁺ VLP preparations were used for a VLPNT and a cell-free VLP neutralization test (cfVLPNT). Use of purified, S1 subunit free, F2 S⁺ VLP increased specific neutralization capacity in both assays for a neutralizing sample of a vaccinee, while non-specific neutralization from a naive specimen, was barely affected.



Supplementary Figure S4. Schematic workflow of VLPNT and cfVLPNT.

In the scheme above, the working steps for a VLP neutralization test (VLPNT) and a cell-free VLP neutralization test (cfVLPNT) are compared, as described in the methods section from page 83 on.



Supplementary Figure S5. Photographic readout of the VLPNT.

A microtiter plate of a VLPNT with controls and sera of three COVID-19 vaccinees was analyzed in a luminometer, as described, giving relative light units (RLU), depicted in a heatmap on the right. Afterwards, the plate was evaluated by photography and bulb exposure in the dark, with a standard smartphone camera (iPhone13, Apple) for 30 s. Resulting blue circles on the left side are accumulated luminescence signals from the respective well. This unsophisticated approach demonstrates that the readout can be simplified for a poorly equipped laboratory, if needed, while retaining at least semi-quantitative outcomes.

Supplementary Table S2. Individual data of analyzed human serum samples.

ID	Sex	Age	Sampling	COVID-19 severity	RT-qPCR	Vaccination scheme			VLPNT				cfVLPNT		cVNT				
						Prime	Boost	d p. PCR ^a	d p. Boost ^b	B.1		B.1.617.2		B.1.1.529		B.1	B.1	VNT ₁₀₀ ^d	Titer ₁₀₀
										VLPN ₅₀ [1:]	Titer ₅₀ ^c [IU mL ⁻¹]	VLPN ₅₀ [1:]	VLPN ₅₀ [1:]	VLPN ₅₀ [1:]	VLPN ₅₀ [1:]				
A01	f	31	Jun 2020	asymptomatic	+				104	49	76				8	21			
A02	f	62	Jun 2020	moderate dis.	+				54	352	546				81	215			
A03	m	60	Jun 2020	asymptomatic	+				79	18	28				8	21			
A04	m	32	Jun 2020	severe dis.	+				76	>2000	>3101				≥1024	≥2716			
A05	m	57	May 2020	mild dis.	+				17	26	40				†4	†11			
A06	m	36	May 2020	mild dis.	+				70	61	95				16	42			
A07	m	51	May 2020	severe dis.	+				4	89	138				†4	†11			
A08	m	51	May 2020	moderate dis.	+				57	>2000	>3101				≥1024	≥2716			
A09	m	84	May 2020	severe dis.	+				53	89	138				25	66			
A10	m	57	May 2020	mild dis.	+				11	58	90				†4	†11			
A11	m	58	May 2020	moderate dis.	+				38	340	527				102	271			
A12	m	73	May 2020	critical dis.	+				13	329	510				203	538			
B01	m	62	May 2020	asymptomatic	+				15	142	220				81	215			
B02	m	54	May 2020	moderate dis.	+				26	645	1000				≥1024	≥2716			
B03	m	86	Apr 2020	moderate dis.	+				9	426	660				323	857			
B04	f	31	May 2020	asymptomatic	+				54	61	95				†4	†11			
B05	m	84	Apr 2020	severe dis.	+				22	46	71				40	106			
B06	m	84	Apr 2020	severe dis.	+				18	29	45				10	27			
B07	m	59	Apr 2020	severe dis.	+				12	1527	2367				512	1358			
B08	m	88	Apr 2020	severe dis.	+				2	48	74				†4	†11			
B09	m	86	Apr 2020	critical dis.	+				2	44	68				†4	†11			
B10	m	59	Apr 2020	severe dis.	+				8	1250	1938				645	1711			
B11	m	29	Apr 2020	moderate dis.	+				1	125	194				81	215			
C01	f	71	Apr 2020	moderate dis.	+				17	143	222				228	427			
C02	f	69	Apr 2020	critical dis.	+				28	62	96				†4	†11			
C03	f	69	Apr 2020	critical dis.	+				30	60	93				†4	†11			
C04	f	31	Apr 2020	mild dis.	+				50	42	65				†4	†11			
C05	m	62	Apr 2020	critical dis.	+				15	21	33				51	8			
C06	m	36	May 2020	mild dis.	+				21	98	152				81	215			
C07	m	54	May 2020	moderate dis.	+				23	857	1329				≥1024	≥2716			
C08	f	67	May 2020	severe dis.	+				30	62	96				20	53			
C09	f	69	May 2020	critical dis.	+				48	20	31				†4	†11			
C10	m	56	May 2020	moderate dis.	+				44	42	65				59	27			

Continued on next page

ID	Sex	Age	Sampling	COVID-19 severity	RT-qPCR	Vaccination scheme			VLPNT				cfVLPNT		cVNT			
						Prime	Boost	d p. PCR ^a	d p. Boost ^b	VLPN ₅₀ [1:]	Titer ₅₀ ^c [IU mL ⁻¹]	B.1.617.2		B.1.1.529		VLPN ₅₀ [1:]	VNT ₁₀₀ ^d [1:]	Titer ₁₀₀ [IU mL ⁻¹]
												VLPN ₅₀ [1:]	VLPN ₅₀ [1:]	VLPN ₅₀ [1:]	VLPN ₅₀ [1:]			
C47	f	77	Oct 2020	critical dis.	+				22		546	847			645	1711		
C48	f	76	Oct 2020	severe dis.	+			20		60	93			10	27			
C49	m	82	Oct 2020	critical dis.	+			23		165	256			128	340			
C50	f	78	Nov 2020	critical dis.	+			15		35	53			13	34			
C51	f	76	Oct 2020	severe dis.	+			23		381	591			645	1711			
C52	f	77	Oct 2020	critical dis.	+			36		320	495			512	1358			
C53	f	61	Apr 2020	severe dis.	+			16		330	512			645	1711			
C54	m	77	Apr 2020	severe dis.	+			17		413	640			203	538			
C55	m	77	Apr 2020	severe dis.	+			21		732	1135			256	679			
C56	m	88	May 2020	severe dis.	+			22		470	728			256	679			
C57	f	62	Jun 2020	moderate dis.	+			47		197	305			161	427			
S001	f	93	Feb 2021			BNT162b2	BNT162b2		24	100	155	24	12	267				
S005	m	26	May 2021			AZD1222	BNT162b2		13	82	113	31	9	182				
S008	m	60	May 2021			AZD1222	BNT162b2		14	27	73	16	11					
S011	f	28	Jul 2021			mRNA-1273	mRNA-1273		19	352	860	116	57	556				
S012	m	66	Jul 2021			AZD1222	mRNA-1273		15	99	242	53	16					
S014	m	70	Jul 2021			AZD1222	AZD1222		37	63	154	29	12					
S015	f	32	Jul 2021			mRNA-1273	mRNA-1273		13	267	654	166	23	513				
S016	f	59	Jul 2021			BNT162b2	BNT162b2		56	38	91	20	8					
S025	f	68	Aug 2021			AZD1222	mRNA-1273		22	254	697	68	26					
S026	m	66	Aug 2021			AZD1222	mRNA-1273		15	92	162	53	37					
S027	f	58	Aug 2021			BNT162b2	BNT162b2		14	267	734	69	13					
S033	f	60	Sep 2021			BNT162b2	BNT162b2		29	69	162	24	14					
S034	m	59	Sep 2021			BNT162b2	BNT162b2		90	40	94	11	9					
S004	m	25	Mar 2021			AZD1222			28	†0	†0							
S007	m	60	Mar 2021			AZD1222			27	†0	†0							
S035	f	93	Aug 2021			BNT162b2	BNT162b2		204	12	19							
S037	m	26	Oct 2021			AZD1222	BNT162b2		173	25	39							
S038	m	60	Nov 2021			AZD1222	BNT162b2		189	11	17							
S036	f	94	Sep 2021			BNT162b2	2×BNT162b2		17	115	178							
S043	m	60	Feb 2022			AZD1222	2×BNT162b2		98	32	50							
S044	m	26	Feb 2022			AZD1222	2×BNT162b2		77	169	262							

Continued on next page

ID	Sex	Age	Sampling	COVID-19 severity	RT-qPCR	Vaccination scheme		d p. PCR ^a	d p. Boost ^b	VLPNT			cfVLPNT		cVNT	
						Prime	Boost			B.1	B.1.617.2	B.1.1.529	B.1	B.1	VLPN ₅₀	VNT ₁₀₀ ^d
										VLPN ₅₀ [1:]	VLPN ₅₀ [1:]	VLPN ₅₀ [1:]	VLPN ₅₀ [1:]	VLPN ₅₀ [1:]	VNT ₁₀₀ [1:]	Titer ₁₀₀ [IU mL ⁻¹]
S003	m	24	Aug 2019							5	8				68	
S006	m	56	Oct 2017							14	22				68	
S009	f	26	May 2019							†0	†0				58	
S018	f	30	Oct 2017							16	25				35	
S019	f	69	Nov 2017							†0	†0				57	
S020	f	35	Nov 2017							†0	†0				60	
S021	f	43	Dec 2017							†0	†0				56	
S022	f	53	Dec 2017							†0	†0				38	
S023	f	31	Oct 2017							†0	†0				47	
S024	m	na	Dec 2017							6	9				55	
S028	m	30	Mar 2019							†0	†0				†0	
S029	f	32	Mar 2019							10	16				40	
WHO	na	na	2020							645	*1000	257	42		377	*1000
WHO	na	na	2020							409	*1000	422	43			
WHO	na	na	2020							417	*1000					
WHO	na	na	2020							364	*1000					
WHO	na	na	2020							567	*1000					
WHO	na	na	2020							426	*1000					

m, male; f, female; na, not available; dis., disease; d, days; p., post; *, per WHO definition; †, below limit of detection

^aDays between first positive SARS-CoV-2 RT-qPCR report and sampling

^bDays between booster dose and sampling

^cVLPN₅₀ titer normalized to the WHO reference serum's within-run performance

^dReciprocal geometric mean titer (GMT) from the highest serum dilution displaying 100% reduction of CPE based on three replicates

List of Figures

1	SARS-CoV-2, structure, replication cycle and immune response.	3
2	Molecular structure of the spike protein.	5
3	Anti-spike antibody generation.	11
4	Anti-spike antibody characterization.	13
5	Evaluation of spike protein in plasma samples.	16
6	Pseudotyped virus neutralization test.	19
7	Electron microscopy images of SARS-CoV-2 VLPs.	21
8	WB of protein lysates from S ⁺ VLPs and SARS-CoV-2.	23
9	ELISA and particle analysis of S ⁺ VLP and SARS-CoV-2 preparations.	25
10	Nano flow technology of S ⁺ VLPs and SARS-CoV-2 virions.	26
11	Fusion analysis of S ⁺ EVs with single-cell BlaM readout.	28
12	Confocal fluorescence microscopy with S ⁺ VLPs.	30
13	Scheme of S ⁺ VLP fusion mechanism and neutralization test, VLPNT.	32
14	Characterization of the VLP and spike EV fusion assay.	34
15	Tropism and specificity of S ⁺ VLPs.	35
16	VLP neutralization test validation.	38
17	Neutralization capacity of monoclonal antibodies.	41
18	Scheme of cell-free fusion of a S ⁺ VLP with an ACE2 ⁺ EV.	43
19	Tropism and specificity of cell-free S ⁺ VLP and ACE2 ⁺ EV fusion.	43
20	Characterization of the cell-free fusion assay.	45
21	Fractionation of donor and acceptor particles and cell-free fusion assay.	46
22	Cell-free VLP neutralization test validation.	50
S1	VLPNT titers of COVID-19 and vaccinee sera.	100
S2	Case reports of three vaccinees.	101
S3	VLPNT and cfVLPNT with purified S ⁺ VLP preparations.	101
S4	Schematic workflow of VLPNT and cfVLPNT.	102
S5	Photographic readout of the VLPNT.	102

List of Tables

1	Comparison of Vero and U251MG cells as recipients for BlaM ⁺ EVs.	29
2	Characteristics of the novel monoclonal anti-spike antibodies.	57
3	Comparison of various types of virus neutralization tests.	60
4	Drugs and compounds.	69
5	Expression plasmids.	70
6	Viral vectors for transductions.	71
7	Primary and secondary antibodies.	72
8	Cell lines.	73
9	Primer for rat antibody sequencing.	73
10	Ultracentrifugation equipment.	73
11	Software aids.	74
12	RACE PCR protocol.	77
13	Severity of COVID-19 patients.	86
14	Vaccination scheme.	86
S1	COVEV antibody sequences.	99
S2	Individual data of analyzed human serum samples.	103

Danksagung

Eine Dissertation ist Voraussetzung für die Befähigung zum selbständigen wissenschaftlichen Arbeiten und ist dennoch nicht das Werk eines einzelnen. Daher gilt mein Dank all denjenigen, die diese Doktorarbeit erst ermöglicht und zu deren Gelingen beigetragen haben:

Prof. Reinhard Zeidler danke ich zuallererst für die umfassende Betreuung als Doktorand, sowohl vor als auch während der COVID-19 Pandemie, für die zahlreichen Ideen, wie u. a. die Fusion von VLPs mit EVs, für die wissenschaftliche Freiheit mehreren Projekten und Kollaborationen teils gleichzeitig nachzugehen, die immer offene Tür, seine ermutigende Art, sein Interesse an neuen Ergebnissen und den dennoch stets kritischen Blick auf diese.

Prof. Wolfgang Hammerschmidt danke ich für die intensive Zusammenarbeit und die Betreuung dieses spannenden Projekts, sowie seine Ideen, experimentellen Beiträge und die umfassenden Klonierungsarbeiten, die all dies erst ermöglicht haben. Darüber hinaus schätze ich seine fachliche Expertise in der Virologie und die zahlreichen anspruchsvollen Diskussionen sehr, die mich als Wissenschaftler geprägt und bereichert haben. Sowohl Wolfgang als auch Reinhard danke ich ausdrücklich für das entgegengebrachte Vertrauen in meine Arbeit.

Prof. Karl-Klaus Conzelmann danke ich für die Bereitschaft als Zweitgutachter dieser Arbeit zu fungieren.

Außerdem möchte ich mich bedanken bei:

Dagmar Pich für ihre Hilfe und den unermüdlichen Einsatz in der Zellkultur, der maßgeblich zum Erfolg des Projekts beigetragen hat.

Verena Krähling für die fruchtbare Kollaboration und die Durchführung des Virusneutralisationstest mit SARS-CoV-2 in Marburg.

Prof. Oliver T. Keppler, Robin Wratil und **Manuel Albanese** für die Bereitstellung der COVID-19 Serumproben und ihre Aufgeschlossenheit gegenüber dem Projekt.

Allen **COVID-19 Patienten** und deren Angehörigen, für die Teilnahme an der CORKUM Studie des LMU Klinikums, sowie allen weiteren **Blutspendern**.

Prof. Alain Brisson, Prof. Kaspar Matiasek und **Heidrun Schöl** für ihren ausdauernden Einsatz am Elektronenmikroskop und die eindrucksvollen Aufnahmen der VLPs.

Prof. Percy Knolle für seine Beiträge im Thesis Advisory Comitee und zusammen mit **Bastian Höchst** für die Kollaboration und das Interesse an den Spike Antikörpern.

Regina Feederle und dem gesamten Team der **Monoclonal Antibody Core Facility** für die durchgeführten Immunisierungen und die hervorragende Versorgung mit Antikörpern.

Allen Laborkollegen der **Arbeitsgruppe Zeidler** und Mitgliedern der **AGV** (Abteilung Genvektoren), insbesondere jedoch **Markus Kellner** für die Bereitstellung rekombinanter Antikörper, **Julia Hörmann** für ihre Expertise und Hilfe bei der konfokalen Fluoreszenzmikroskopie, sowie **Kathrin Gärtner**, **Judith Dünzkofer** und **Susanne Fackler** für deren umfassende Hilfsbereitschaft im Laboralltag. Ihnen allen möchte ich für die freundschaftliche Atmosphäre und den Zusammenhalt danken.

Ein herzlicher Dank gilt auch meinen langjährigen **Freunden**, die mich mit Sport, Spaß und Frohsinn durch all die Jahre des Studiums und als Doktorand begleitet haben und egal ob in der Turnhalle, den Bergen oder dem Hörsaal immer für mich da waren.

Ein besonderer Dank gilt meiner ganzen **Familie** und meiner **Freundin**, die mir mit ihrem Rückhalt immer bedingungslos und liebevoll zur Seite standen.

Zu guter Letzt möchte ich meine **Eltern** hervorheben, ihnen bin ich für ihre grenzenlose Unterstützung schlichtweg unendlich dankbar.

Eidesstattliche Versicherung

Rößler, Johannes

Name, Vorname

Ich erkläre hiermit an Eides statt, dass ich die vorliegende Dissertation mit dem Titel:

Quantitation of SARS-CoV-2 Neutralizing Antibodies Using Virus-Like Particles

selbständig verfasst, mich außer der angegebenen keiner weiteren Hilfsmittel bedient und alle Erkenntnisse, die aus dem Schrifttum ganz oder annähernd übernommen sind, als solche kenntlich gemacht und nach ihrer Herkunft unter Bezeichnung der Fundstelle einzeln nachgewiesen habe.

Ich erkläre des Weiteren, dass die hier vorgelegte Dissertation nicht in gleicher oder in ähnlicher Form bei einer anderen Stelle zur Erlangung eines akademischen Grades eingereicht wurde.

München, 15.03.2023

Ort, Datum

Johannes Rößler

Unterschrift Doktorand

Lebenslauf

Johannes Rößler, geboren in München

Ausbildung

- 2005 - 2013 GYMNASIUM GRAFING
Allgemeine Hochschulreife
- 2013 - 2016 TECHNISCHE UNIVERSITÄT MÜNCHEN, TUM
Studium der Chemie, B.sc.
- 2016 - 2018 Studium der Chemie, M.sc.
- 2019 - 2022 LUDWIG-MAXIMILIANS-UNIVERSITÄT MÜNCHEN, LMU
Medizinische Fakultät, Promotionsstudium Dr. rer. nat.,
Dissertation: „Quantitation of SARS-CoV-2 Neutralizing Antibodies
Using Virus-Like Particles“, betreut durch Prof. R. Zeidler

Tätigkeiten

- 2016 TUM, Lehrstuhl für Pharmazeutische Radiochemie
Bachelor Thesis: „¹⁸F-Labelled CXCR4-Ligands via Chemoselective
Conjugation Strategies“, Prof. H.J. Wester
- 2018 TUM, Lehrstuhl für Organische Chemie II
Master Thesis: „Investigation of pArg-Mimics as Degradation Tags for
the ClpCP Protease“, Prof. S.A. Sieber
- 2018 - 2019 MAX-PLANCK INSTITUT FÜR BIOCHEMIE, MPI
Department Molecular Machines and Signaling „Ubiquitination of
GPCRs by HECT E3 Ligases“, Prof. B.A. Schulman
- 2019 - 2022 KLINIKUM DER UNIVERSITÄT MÜNCHEN
HNO Klinik und Poliklinik - Forschung, Prof. R. Zeidler
- HELMHOLTZ ZENTRUM MÜNCHEN
Abteilung Genvektoren, AGV, Prof. W. Hammerschmidt
- DEUTSCHES ZENTRUM FÜR INFektionsFORSCHUNG, DZIF
Standort München

Sonstiges

- 2015 - 2018 MAX WEBER PROGRAMM
Stipendium der Studienstiftung des deutschen Volkes e. V. und des
Elitenetzwerks Bayern
- 2017 NORWEGIAN UNIVERSITY OF SCIENCE AND TECHNOLOGY, NTNU
Auslandssemester in Trondheim, Norwegen